Simulation Study Investigating the Novel use of Drive Torque Vectoring for Dynamic Post-Impact Vehicle Control

P S Delves

PhD   2015

Simulation Study Investigating the Novel use of Drive Torque Vectoring for Dynamic Post-Impact Vehicle Control

Peter Samuel Delves

A thesis submitted in partial fulfilment of the requirements of the Manchester Metropolitan University for the degree Doctor of Philosophy

School of Engineering

Manchester Metropolitan University

2015

Peter Samuel Delves

Declaration

I hereby declare that the work has been done by myself and no portion of the work contained in this thesis has been submitted in support of any application for any other degree or qualification at this or any other university or institution of learning.

Peter Samuel Delves

Peter Samuel Delves

Acknowledgements

Peter Samuel Delves

Abstract

The work presented here investigates the use of drive torque vectoring as a method of post-impact vehicle control.

Crash statistics show a high number of serious injuries occurring on British roads, with 46% of the 1713 fatalities in 2013 being car occupants. In total there were 21657 serious injuries sustained across all road users in the same time period. Research has highlighted that people involved in multiple impact crashes have an increased risk of sustaining serious injury compared to those involved in a single impact event (Transport 2013). This highlights post-impact control, as a means to avoid secondary impacts, as an important area of study, an area that is still in its infancy. Work carried out so far that aims to control a vehicle after impact makes use of the braking and/or steering systems. This work has produced reasonable levels of success, however the use of drive torque vectoring control has received little attention.

To this end, a non-linear 8 Degree of Freedom model is developed that is capable of simulating a vehicle's behaviour and trajectory during a crash instigated by an impulse disturbance. These crash impulse disturbances are calculated using momentum theory, taking into account energy loss during the impact. They are used to simulate two vehicle crash scenarios: a rear impact, and a side swipe impact. Simulation of these crash scenarios is carried out on the vehicle model before drive torque vectoring control is implemented to produce a benchmark set of results against which the controlled system is evaluated.

The control system presented is a six-phase switched PID controller scheme using a set of 'Settling' and 'Holding' controllers. The control objective is to settle the vehicle at a heading angle that is parallel to the original (e.g. 0^0, 180^0 or 360^0), such that the final trajectory re-aligns the main crash structures of the vehicle with the carriageway so as not to expose the side of the vehicle to a secondary collision. Re-aligning the vehicle with the carriageway before it has come to a stop has the additional benefit of reducing lateral displacement when compared with the benchmark results. This control action results in a reduced risk of a secondary impact and thus of serious injury. This system resulted in safe heading angles for all simulations compared with the current work in the field, leading to safer outcomes for occupants.

Peter Samuel Delves

Table of Contents

Peter Samuel Delves

Peter Samuel Delves

Peter Samuel Delves

Peter Samuel Delves

Peter Samuel Delves

List of Figures

Peter Samuel Delves

Peter Samuel Delves

Peter Samuel Delves

Peter Samuel Delves

List of Tables

Peter Samuel Delves

Peter Samuel Delves

Peter Samuel Delves

Nomenclature

A list of symbols and abbreviations that are used throughout the thesis are presented below.

Symbols

a	Distance from front axle to centre of gravity
B	Tyre model stiffness factor
b	Distance from rear axle to centre of gravity
C	Tyre model lateral shape factor
C_d	Co-efficient of drag
C_f	Front tyre stiffness
C_r	Rear tyre stiffness
c_r	Roll damping
D	Tyre model peak force
E	Tyre model curvature factor
e	Co-efficient of restitution
F_{areo}	Force from aerodynamic drag
F_{xd}	Longitudinal crash impulse force
F_{xF}	Longitudinal tyre force (front wheels)
F_{xR}	Longitudinal tyre force (Rear wheels)
F_{yd}	Lateral crash impulse force
F_{yF}	Lateral tyre force (front wheels)
F_{yR}	Lateral tyre force (Rear wheels)
F_z	Vertical tyre load
F_{z0}	Vertical tyre test force
F_{zpitch}	Vertical tyre load transfer due to pitch
F_{zFroll}	Vertical tyre load transfer due to roll (front wheels)
F_{zRroll}	Vertical tyre load transfer due to roll (rear wheels)
h_{cg}	Centre of gravity height
h_r	Roll centre height
I_{wF}	Inertia of front wheel

Peter Samuel Delves

I_{wR}	Inertia of rear wheel
I_{xx}	Roll inertia
I_{xz}	Coupled roll and yaw inertia
I_{zz}	Yaw inertia
k_r	Roll stiffness
L_{xd}	Longitudinal impact position from centre of gravity
L_{yd}	Lateral impact position from centre of gravity
L_{zd}	Vertical impact position from centre of gravity
l	Wheel base $(a + b)$
M	Momentum
Mo_{xd}	Momentum exchange between vehicles during crash (Longitudinal)
Mo_{yd}	Momentum exchange between vehicles during crash (Lateral)
m	Total mass of vehicle
m_b	Mass of vehicle body (sprung mass)
m_{bF}	Vehicle body mass on front wheel
m_{bR}	Vehicle body mass on rear wheel
m_1	Mass of impactor vehicle
m_2	Mass of target vehicle
r_{wF}	Radius of front wheel
r_{wR}	Radius of rear wheel
S	Frontal area of vehicle
S_H	Tyre model horizontal shift factor
S_V	Tyre model vertical shift factor
T_{wF}	Torque on front wheel
T_{wR}	Torque on rear wheel
t	Track width
u	Longitudinal velocity
$\dot{u}$	Longitudinal acceleration
V_d	Velocity difference of vehicles pre-crash
V_{xd}	Longitudinal component of pre-crash velocity difference
V_{x1}	Longitudinal velocity of target vehicle pre-impact

Peter Samuel Delves

V_{x2}	Longitudinal velocity of target vehicle post-impact
V_{yd}	Lateral component of pre-crash velocity difference
V_{y1}	Lateral velocity of target vehicle pre-impact
V_{y2}	Lateral velocity of target vehicle post-impact
v	Lateral velocity
$\dot{v}$	Lateral acceleration
x	Longitudinal displacement
y	Lateral displacement
α_f	Front lateral tyre slip angle
α_r	Rear lateral tyre slip angle
δ_f	Front wheel steer angle
κ	Longitudinal slip ratio
μ	Co-efficient of friction
ρ_a	Air density
$\ddot{\phi}$	Roll acceleration (Rotational acceleration about x axis)
$\dot{\phi}$	Roll rate (Rotational velocity about x axis)
ϕ	Roll angle
$\dot{\Psi}$	Yaw acceleration (Rotational acceleration about z axis)
Ψ	Yaw rate (Rotational velocity about z axis)
ψ	Yaw displacement (Heading angle)
$\dot{\omega}_{wF}$	Rotational acceleration of front wheel
ω_{wF}	Rotational velocity of front wheel
$\dot{\omega}_{wR}$	Rotational acceleration of rear wheel
ω_{wR}	Rotational velocity of rear wheel

Abbreviations

ABS	Anti-lock Braking System
ACC	Adaptive Cruise Control
ADAS	Advanced Driver Assistance Systems
AEB	Automatic Emergency Braking
CA	Collision Avoidance
CW	Collision Warning

Peter Samuel Delves

DOF   Degree of Freedom
DYC   Dynamic Yaw Control
ECU   Electronic Control Unit
ESC   Electronic Stability Control
EV   Electric Vehicle
FCV   Fuel Cell Vehicle
HEV   Hybrid Electric Vehicle
HGV   Heavy Goods Vehicle
ICE   Internal Combustion Engine
ICV   Internal Combustion Vehicle
LQG   Linear Quadratic Gaussian
LT   Lane Tracking
MBS   Multi Body Simulation
MIMO   Multi Input Multi Output
PID   Proportional Integral Derivation
PSD   Power Spectral Density
QLOC   Quasi-Linear Optimal Control
TCS   Traction Control System
TTR   Through the Road

Peter Samuel Delves

1. Chapter One: Introduction

1.1. Introduction and Background

Vehicle control research into improving driver safety and thus reducing serious injuries occurring in traffic accidents has been ongoing since the 90's. The first major step in driver safety came about with the introduction of unintelligent occupant protection systems such as seat belts, crumple zones and air-bags. The first steps of intelligent vehicle control to enhance driver safety came about in the form of driver assistance systems that extended the operating range of a vehicle. Systems such as anti-lock braking, traction control and stability control are unobtrusive under normal driving conditions and only activate during more extreme situations so that the vehicle is stable and controllable for longer. The next step has seen the development of pre-crash systems such as automatic emergency braking, collision warning and collision avoidance systems, which automatically intervene if they sense a collision is imminent to reduce the severity of incident by reducing speed or attempting to avoid a collision altogether. However, work concerning the control of a vehicle in the post-impact phase is still in its infancy. Schemes that use the braking and/or steering systems have been studied/developed with reasonable levels of success. However, the use of drive torque vectoring, which appears to be an ideal candidate, has received little attention.

Crash statistics still show a high number of serious injuries occurring on roads with 46% of the 1713 fatalities on British roads in 2013 being car occupants. There were also 21,657 serious injuries sustained across all road users in the same time period (Transport 2013). (Digges and Bahouth 2003) study into crash statistics in North America highlights the severity of multiple impact crashes showing that people involved in multiple impact crashes have an increased risk of sustaining serious injury compared to those exposed to a single impact event. The data revealed that 24% of all crashes involved multiple impacts, that is, the vehicle was subject to at least one more impact after the original crash pulse. However these multiple impact incidents accounted for 42% of all serious injuries. The study showed that the worst sequences of impacts leading to serious injuries were: 1) side impact followed by a second side impact, 2) front impact followed by a side impact, and 3) front impact followed by a subsequent front impact. These statistics imply that a reduction in multiple impact

Peter Samuel Delves

incidents would reduce the chance of serious injuries and that any form of side impact is most likely to result in serious injury. This, amongst other factors, has led to extensive research over the past two decades into occupant protection systems and dynamic control systems that improve handling behaviour close to the limit of stability.

Electronic Stability Control (ESC), Anti-Lock Braking Systems (ABS) and Traction Control Systems (TCS) all extend the region in which a vehicle is stable allowing the driver more control during scenarios where the vehicle is operating around its stability region. These systems do not take control of the vehicle, but instead modify driver input when required to keep the vehicle stable and controllable. Another field of vehicle safety research focuses on systems that take more authority over vehicle control in pre-crash situations otherwise known as Advanced Driver Assistance Systems (ADAS). These investigate predominantly pre-crash and crash evasion control, including systems such as Advanced Cruise Control (ACC), Collision Warning (CW), and Collision Avoidance (CA). Advanced vehicular control strategies focussing on post-impact control are currently an underdeveloped area of research. Simulation studies investigating the use of the steering system (Ching-Yao and Han-Shu 1999) have shown potential at highway speeds, but a shift in technique has occurred in recent years towards using the braking system with Yang et al and Kim and Peng (Yang, Gordon et al. 2011, Byung-joo Kim and Peng 2012, Yang, Gordon et al. 2012, Byung-joo Kim and Peng 2014, Yang, Jacobson et al. 2014) leading the development of this approach. However, an area that has received little attention is if drive torque vectoring is or is not a viable candidate for post-impact control. However, there is much work concerning the potential that motor torque vectoring has in limit handling manoeuvres such as its application for improving established systems such as TCS (Ilic-Spong, Miller et al. 1987, Hori, Toyoda et al. 1998, Hori 2001, Hori 2004).

1.2. Thesis Statement

Investigate the viability of using drive torque vectoring for dynamic post-impact control.

Peter Samuel Delves

1.3. Thesis Objectives

1. Produce a critical literature review, which highlights the critical areas of research and development within the areas of vehicle safety, dynamic vehicle control and advanced driver assistance systems.

2. Develop a non-linear vehicle model, which allows the simulation of various crash scenarios to be carried out and has the capacity to control torque at the wheels.

3. Implement a drive torque vectoring control scheme to analyse the potential it has to stabilise a vehicle after an initial impact.

1.4. Scheme of work

To investigate torque vectoring potential for post-impact dynamic control this thesis developed a vehicle model that was capable of simulating post-impact dynamics which could control torque at the wheels directly.

The vehicle model was generated over three phases generating a linear 2 Degree of Freedom (2-DOF), non-linear 7-DOF and non-linear 8-DOF vehicle models. The linear model used a set tyre stiffness, in Newtons per degree of slip, to transmit force and the non-linear models uses an empirical curve-fitting method developed by Pacejka known as the 'magic tyre formula'. These three models were then simulated through two steady state manoeuvres at velocities from 10-40m/s to assess the variation in model behaviour as extra DOF are added and verify the accuracy of the 8-DOF model. The manoeuvres used were steady-state cornering and lane change manoeuvres. It was observed that at higher simulated velocities the results between linear and non-linear models varied by up to 12%. This demonstrated that at lower velocities the linear model's performance is comparable and could be used for testing but as test velocities increased the vehicle enters its non-linear region and results diverged. Taking into account that the crash simulation study involved high velocities and large lateral accelerations, where the vehicle entered the non-linear region, the 8-DOF model was used for the rest of the study.

Vector analysis was then carried out to calculate crash force impulses in lateral and longitudinal directions at velocity differences of 2.5 and 5m/s at angles of incidence

4

of 10^0, 20^0 and 30^0 producing six sets of crash impulses. These crash impulses were then used to simulate two different crash scenarios: a rear impact and side-swipe impact. Simulations were carried out on the vehicle model before control was applied to produce a benchmark set of 12 results.

Once the vehicle model was verified and comparison data had been collected the post-impact control system was developed. The main objective of the control system was to re-stabilise the vehicle traveling parallel with the main carriageway re-aligning the main crash structures with the direction of travel. This meant that the vehicle could end up either traveling forwards or backwards. This resulted in heading angle being selected as the control state. This study assumed that the vehicle was on a straight and flat section of road leading to final target angles of 0^0, 180^0 or 360^0 of original heading being set. As the control objective need to be switched depending on current heading angle and yaw rate a single Proportional, Integrator, Derivative (PID) was not sufficient to achieve the desired control. This led to the development of a six-phase switching PID control schema using a set of 'Settling' and 'Holding' controllers. The settling controllers used very aggressive high gains that reduced yaw rate quickly in an attempt to settle the vehicle at the target heading. The holding controllers were lower gain and activated at various heading angle thresholds to sustain yaw rate so that the vehicle would reach the next settling point threshold whereupon the next settling controller was activated. Once this system was implemented on the 8-DOF vehicle model, simulation was carried out using the same crash impulses and two crash scenarios. It was found that the switching control system was able to re-align and stabilise all of the 12 simulations with the carriageway. It also reduced the lateral displacement of all of the vehicles and thus lowered the chance of a secondary collision with another vehicle or roadside object occurring. These results demonstrate that torque vectoring can be used to control a vehicle during a crash.

1.5. Outline of Thesis

Chapter 2 reviews literature for vehicle modelling, and advance dynamic control strategies. Chapter 3 details the construction of the base 8-DOF vehicle model with non-linear tyre dynamics and compares performance against a 2-DOF linear and 7-

DOF non-linear models to analyse the difference in behaviour between them. Chapter 4 introduces a global transformation matrix so that vehicle trajectories can be analysed during the simulations and uses vector analysis to calculate crash force impulses at two velocities acting at three angles of incidence. Crash simulation is then carried out using two scenarios: a side-swipe and rear impact. These are used to analyse crash trajectories before any control intervention is applied and allows comparison to be carried out in later. Chapter 5 details the PID switching controller construction. It then simulates the vehicle with control intervention comparing results with the uncontrolled vehicle results in chapter 4. Chapter 6 collates the main conclusions of the work together and suggests further work.

2. Chapter Two: Literature Review

Chapter 2 looks at current research relating to the areas of Advanced Driver Assistance Systems (ADAS) and dynamic control systems, vehicle modelling and drivetrains.

2.1. Introduction to Literature Areas

2.1.1. Advanced Driver Assistance Systems (ADAS)

The literature review has highlighted the increasing attention paid to vehicle dynamics control research over the past 20 years. There have seen advances in active control systems to improve stability with many inexpensive cars taking advantage of Anti-lock Braking Systems (ABS), and Traction Control Systems (TCS), as well as high end vehicles using Dynamic Yaw Control (DYC) and Electronic Stability Control (ESC). All these systems work as an active 'safety net' and aim to be unobtrusive in day to day driving. These systems have advanced limit handling stability thus improving vehicle safety but they have a limited working region of medium-low speed manoeuvres. They also require large amounts of computational resource to monitor all their sensors and actuators and can result in complex control strategies. As with ADAS systems, complex control strategies seem to be unavoidable if a robust system is to be produced.

Cabin occupant protective systems have also seen rapid development in tandem with dynamic control. Mercedes have lead the way with their Pre-Safe systems (Schoeneburg and Breitling 2005). These systems consist of smart airbags, pre-tensioning seat belts (Mahmud, 1995), and active interior (seats and trim). These systems, coupled with smart crumple zones, have brought in an era of ultra-safe vehicles where drivers and passengers can walk away from the majority of incidents.

Advanced control systems have been developed and are just starting to emerge from the laboratory into production. Some of the advanced control systems in the literature frequently discuss are: lateral control, longitudinal control & avoidance, reversing & parking aids, vision enhancement, intelligent speed adaption, driver monitoring, pre-crash systems and road surface monitoring(Pietzsch, Trung Dung et al. 2009).

Future ADAS technologies are also discussed in (Lindgren and Chan 2006). These include autonomous systems, perception of vehicles surroundings, smart highways and driver health monitoring.

The literature survey shows that the majority of research is developing pre-crash systems with little work investigating dynamic post-impact control.

Brake vectoring and/or steering control have shown some promise in the area of post-impact control (Byung-joo Kim and Peng 2012, Yang, Gordon et al. 2012, Byung-joo Kim and Peng 2014, Yang, Jacobson et al. 2014). However there appears to be little to no research being conducted on what potential the powertrain systems of a vehicle could bring to the field.

2.1.2. Vehicle Modelling

As can be seen from the literature there are multiple vehicle models from 2-13-DOF with varying levels of complexity. This highlights how important it is to consider model selection when it comes to dynamic simulation. Factors to consider are: What problem is being addressed and the complexity of the problem

This leads to the consideration of: Level of model accuracy required, the complexity of the required model and the level of computational intensity generated by the model

These are important considerations as the model has to have a certain level of complexity to generate reliable results in accordance with the dynamic intensity of the simulation. However this has to be weighed with the computational expense of the model, as models with high complexity can take hours if not days run simulations (Kondo and Makino 2008).

2.1.3. Control Schemes

The literature suggests that the development of a control scheme is an evolutionary process starting off with basic systems and building in complexity. (Yang, Gordon et al. 2011) shows the usual path of development starts off with Proportional-Integral-Derivative (PID) control to prove the concept and developing into Linear Quadratic Gaussian (LQG) to provide improved robustness to modelling uncertainties.

(Milehins, Cheng et al. 2010) use a yaw gain map based yaw controller. This method requires a lot of data to be gathered on a particular vehicle, either through physical prototype testing or by using an accurate vehicle model, and plotting this over a map.

Peter Samuel Delves

This map can then be referenced to read a desired input value for the desired behaviour. The problem with this method is that it is a very labour intensive process to get a good detailed map or, if a lower resolution map is used it can be inaccurate, as some values will need to be interpolated.

Either LQG or H-infinity control can provide more advanced control since the control system is a Multi Input Multi Output (MIMO) system with potentially high levels of modelling uncertainty. LQG requires a Kalman filter to reduce unwanted sensor noise and aid system stability. However as this study is investigating the initial application of drive torque vectoring an expanded PID configuration will be appropriate.

2.1.4. Drivetrains

It was important to consider architectural layouts to see what sort of control schemes will be plausible. The literature shows that the move towards hybrid and electric vehicles is permitting the development of more flexible architectural layouts than were previously possible with conventional Internal Combustion Engines (ICE). Milehins, Cheng et al. (2010) have investigated the use of DYC in a "Through The Road" (TTR) hybrid architecture and presented some promising results. This research shows the potential for torque vectoring control. Although this thesis is not primarily concerned with pure electrical architecture research, it is important to understand that the control system being proposed would be very hard to implement in the real world without understanding the potential architectural flexibility electric vehicles deliver.

Electric vehicle powertrain layouts allow greater flexibility then ICE vehicles as batteries can be placed anywhere within the vehicle and run cables to motors which can be directly mounted into wheels. However, majority of EV's available follow traditional powertrain layouts with power electronics and battery mounted in the engine bay with a single motor connected to a conventional differential. Some may mount motors to each wheel and generate a form of differential by varying torque output between the two sides of the vehicle. This can be done in either forward or rear wheel drive configurations.

Peter Samuel Delves

The flexibility of EV powertrains would also make it easier to build a four wheel drive vehicle as there is no need for complicated transfer boxes and multiple differentials as mounting motors in each wheel and controlling each wheel independently.

2.2. Dynamic Vehicle Control

2.2.1. Introduction

Dynamic vehicle control is a broad term which refers to any system that can be used to alter a vehicle's lateral, longitudinal, or vertical dynamic behaviour through manipulation of the dynamic systems on the vehicle; (e.g. braking, steering, suspension or powertrain,) using computationally controlled 'active' systems or mechanical passive systems. This study is focused on the use of active and semi-active systems.

Dynamic vehicle control systems, otherwise known as Advanced Driver Assistance Systems (ADAS), have gone through some rapid development in the last couple of decades. Control strategies for body, steering, and braking systems are now standard on many modern day vehicles with Mercedes-Benz leading the technological advances with their pre-safe systems (Schoeneburg and Breitling 2005, Breitling, Schöneburg et al. 2009). Commonly seen systems are designed to make general day-to-day driving safer (e.g. ESC, ABS, and TCS). These constantly monitor vehicle parameters to improve handling behaviour consistency and act as a safe-guard when the vehicle is being driven on the edge of the vehicle's dynamic capabilities. There are also systems designed to improve vehicle limit handling performance (DYC).

ESC, ABS, and TCS are standard on many modern vehicles and further developments in active control are still ongoing. These developments are moving from systems that act as an electronic safety net looking after the vehicle on the edge of its performance to more elaborate systems that push the vehicle's dynamics to perform better and even to strategies that can autonomously drive the vehicle. For example Advanced Cruise Control (ACC), Collision Warning (CW), Collision Avoidance (CA), Automatic Emergency Braking (AEB), and Lane Tracking (LT) use cameras, sensors and image processing to track other vehicles, lane markings and identify potential hazards and then communicate with motors and actuators attached to steering and braking

systems to steer and brake the car autonomously in normal driving (Pomerleau 1995, McCall and Trivedi 2004, Tideman, van der Voort et al. 2010) and in emergency situations (Hernandez and Chen Yuan 2004, Sugimoto and Sauer 2005).

Advanced control systems are also being investigated that make extreme use of vehicles mechanical systems for use in post-impact dynamic vehicle control(Byung-joo Kim and Peng 2014, Yang, Jacobson et al. 2014). Automated steering and torque vectoring (using both brakes and drivetrain) capabilities for vehicle control have been developed from systems that have already been proven such as TCS, ABS, ESC and DYC (Tideman, van der Voort et al. 2010, Tchamna and Youn 2013).

2.2.2. Stability Control Systems

Stability control systems are designed to aid the driver by keeping the vehicle in a region of stability and should not be intrusive in day to day driving. They mainly make use of traction and braking systems.

2.2.2.1. Electronic Stability Control Systems (ESC)

These systems are mainly seen on high specification vehicles. Each manufacturer has its own name but these systems perform the same function, allowing a driver to keep control of a vehicle when performing manoeuvres near the limit of handling. The system is generally composed of the braking system, sensors, and Engine Control Unit (ECU) to monitor drivers' steering input and reference these against how the vehicle is responding (Farmer 2004). The system responds to the sensor readings of vehicle trajectory and if the vehicle is judged to be deviating from its intended path the system actuates the brakes to correct its path.

Farmer (2004) looked at what effect ESC had on road traffic accidents and injuries over 7 states in America since it started to appear in the late 90s. The results showed that a person who had a vehicle equipped with "ESC had a single-vehicle crash risk approximately 41 percent lower than a vehicle without ESC" (Farmer 2004). A single vehicle crash is a crash where the vehicle has lost control and collided with another object or rolled over. There are systems that are being designed especially to reduce the chance of rollover (Odenthal, Bünte et al. 1999). Farmer (2004) showed that there was a reduction of a few percent in multiple vehicle incidents but it was not

statistically significant. This could be down to the fact that a vehicle does not have to be in an unstable state to be in an accident with another vehicle.

The literature shows that ESC is generally effective at stabilising a vehicle during manoeuvres and provides assistance when excessive speed leads a vehicle to become unstable. Although it appears that there is no major gain in accident mitigation, these systems do allow a driver to stay in control of a vehicle for longer, reducing accident risk in certain scenarios.

2.2.2.2. Anti-Lock Braking Systems (ABS)

Anti-lock Braking Systems (ABS) allow the driver to apply maximum braking force without locking wheels during hard braking and in icy conditions. There are two reasons for this system: Reducing the stopping distance and keeping the driver in control of the vehicle.

ABS improves stopping distance by stopping the wheels from locking. This is because whilst a wheel is still rotating, it can apply the maximum braking force to the tyres (they can only apply a finite amount of force) before the wheels lock up resulting in a reduction in the available braking force. This improvement in available force also allows the driver to retain some lateral control of the vehicle making it possible to take evasive action if needed.

(Hogan 2008) shows that when a vehicle locks its wheels the maximum tyre force available is reduced to the detriment of stopping distances and lateral control. ABS highlights the importance of tyre force utilisation within crash mitigation.

2.2.2.3. Traction Control Systems (TCS)

Traction Control Systems (TCS) control longitudinal slip during acceleration by monitoring longitudinal wheel slip and adjusting power and torque accordingly. During hard acceleration and in slippery conditions they are of particular use for stopping a vehicle from spinning its wheels and applying its power efficiently. In doing so, these systems increase the time that the vehicle is stable, allowing the driver to be in control for a longer period of time.

Peter Samuel Delves

One of the main safety features of this system is that it stops vehicles from losing control in corners by applying too much torque and overloading the tyres. (Hori, Toyoda et al. 1998) show the development of a TCS for their experimental electric vehicle using model-following control and optimal slip ratio control. They provided conclusive results that an optimal slip ratio control was most effective, and concluded that vehicles powered by electric motors (with their quick precise torque response) were effective candidates for this type of system.

2.2.2.4. Dynamic Yaw Control (DYC)

More complex systems can precisely distribute engine torque and braking forces to give the vehicle Dynamic Yaw Control (DYC). DYC is a system that allows more precise and extreme cornering as it can increase a vehicle's rotational (yaw) speed by independently braking the inside set of wheels round a corner to increase the speed differential between the left and right side of the vehicle. As it is difficult and complicated to use torque vectoring with an ICE vehicle, requiring a mechanical differential, they generally use braking systems, whereas with an electrical set up with independent wheel motors it is possible to use torque vectoring through the motors as described in the "Through the Road" hybrid set up (Milehins, Cheng et al. 2010). One of the other advantages of electric motors is that they can be used to quickly apply braking torque as well as accelerating torque.

As is shown from the literature DYC has great potential and is in use today in some production vehicles (Manning and Crolla 2007). (Hori 2004) has shown with their experimental electric vehicle that is possible to enhance DYC with the use of torque vectoring between the 4 independently driven wheels for greater precision control.

2.2.3. Post-Impact Control Systems

Post-impact control systems aim to reduce the severity of an impending accident.

This is still a relatively young area of study with the majority of research carried out so far primarily investigating the use of the steering and/or braking systems on a vehicle. Yang, Gordon et al. (2011), Yang, Gordon et al. (2012) earlier work investigates a brake vectoring system which uses Quasi-Linear Optimal Control (QLOC) for path-trajectory control. The system aims to minimise path deviation from

the vehicle's original trajectory and shows initial potential. Yang, Jacobson et al. (2014) most recent work combines the original brake vectoring control with steering control. The addition of steering control provided some additional control benefit though not for all post-impact situations. Byung-joo Kim and Peng (2012) shows the use of brake vectoring for combined heading and lateral displacement control after an impact. It shows that a delicate balance is needed between the final heading and reduction in lateral displacement control objectives so that the side of the vehicle is not left exposed to potential secondary impact. Later work by Byung-joo Kim and Peng (2014) is more focused on how a combined pre-crash steering and combined post-impact steering and braking control system can improve post-impact trajectory control. The system relies on initial sensors recognising that an impact is imminent to allow the pre-emptive pre-crash system to activate. The amount of pre-crash steering application is dependent on a collision strength estimation so that an opposing yaw rate is applied to the vehicle before impact. The system sees a reduction in peak yaw rates during the impact and a reduction in overall lateral displacement. These systems aim to reduce the severity of secondary impact by reducing velocity quickly but at times they left the vehicle stopped with its side exposed which could potential result in a serious secondary impact. There are some limitations to this work such as: It can only apply a retarding force; if braking system is damaged could cause failure of such a system; hydraulic actuation is not instantaneous leading to a lag in brake application. Both authors use simulation models which do not use wheel DOF and just apply the desired braking force to model directly.

As shown steering and/or braking systems are demonstrating some promise in this area. However, the use of the drivetrain to perform control appears to have received little to no attention as a post-impact control system. This may be because the nature of the ICE means that power and torque vectoring is difficult and requires very complex control systems as well as heavy and complex drive lines, clutches and differentials to vector power. However with the proliferation of electric motor usage in drivetrains this could be a viable solution. Electric Vehicles (EV) have the distinct advantage that torque and power outputs from motors is very predictable, meaning

Peter Samuel Delves

that precise torque control is achievable with simple controller strategies (De Novellis, Sorniotti et al. 2012). This, combined with driveline flexibility and the possibility of removing heavy cumbersome mechanical linkages and drivelines from the system, has the potential to improve vehicle dynamic response and emergency control.

2.2.3.1. Steering Control

There have been numerous studies investigating the effectiveness of automated steering systems in both normal driving and post-impact handling conditions (Pomerleau 1995, Ching-Yao and Han-Shue 2001) (Chan and Tan 1999). These systems consist of a motorised steering system where the steering wheel is linked to the steering rack by an electric motor. The motor on the steering column monitors driver input and actuates the motor on the rack accordingly. This is a manner in which manufacturers implement power assisted and variable rate steering but also comes with the advantage of using it to automate the steering.

There are two levels to this work: fully automated driving systems and post-impact systems. The former (Pomerleau 1995) has been proven with over 3000 miles of road testing with minimal human interaction. This is as part of a larger control architecture with vision systems. The post-impact system is designed to actuate during an incident to re-stabilise the vehicle so that the driver can regain control. (Ching-Yao and Han-Shue 2001) present a convincing proof of concept but the work is yet to make it onto production vehicles.

2.2.3.2. Rollover Avoidance

Vehicle rollover is mainly an issue for high sided and short wheel base vehicles. It can be caused by a few situations: high side winds (mainly an issue for high sided vehicles), excessive cornering speeds and in collisions. The main dynamic cause of rollovers is that as the lateral acceleration increases, a vehicle's body roll increases. This results in a shift in weight from side to side reducing the load on the inner wheels and increasing load on the outer wheels. This causes an issue as tyres can only transmit a limited amount of force based on their vertical loading before they become 'saturated'. At this point the transmitted force then starts to reduce, thus

Peter Samuel Delves

the net overall tyre force reduces as the inner tyres are unloaded and the outer tyres are overloaded. Rollover avoidance systems work by analysing vehicle wheel loads so that when one side unloads the system activates to restore stability through brake and steering controllers (Odenthal, et al.1999).

2.2.3.3. Torque vectoring (Brake and Drive)

The literature highlights the potential that torque vectoring (through braking and traction systems) has to manipulate post-impact dynamics. Whilst much research has focused on brake vectoring for use in post-impact control, drive vectoring has been primarily used to enhance vehicle stability and handling. There seems to be no detailed study into systems which combined the two systems.

(Yang, Gordon et al. 2011) show that lateral deviation can be reduced significantly after an initial impact with the use of brake vectoring alone. However, this sort of system can only apply decelerating forces to the vehicle and the use of conventional hydraulic systems means there is some lag in actuation time.

Drive vectoring has been the subject of numerous investigations into improving vehicle handling and stability in DYC systems as well as being implemented in high performance vehicles. (Hori 2004) highlights the potential electric vehicles have with their flexible drivetrain architecture and the superior torque response of electric motors. However, there are no comprehensive studies investigating the impact drive vectoring has on post-impact control.

The literature highlights torque vectoring control as significant in bringing improvements in vehicle handling and stability (De Novellis, Sorniotti et al. 2012), and is showing promise for post-impact control. Research into torque vectoring in post-impact control still seems to be in its infancy and is an area requiring further investigation.

2.2.4.3. Human Machine Interaction (HMI)

This is a difficult part of the controller tuning process as it is a highly subjective area which looks at how people interact with the vehicles as well as different manufacture's handling philosophies. Using automated assistance and control

Peter Samuel Delves

systems like ESC and ACC is a very difficult area to judge. The issue is that systems have to have a safety threshold where they start working, but it should not be so low that drivers do not feel like they are in total control of the vehicle. On the other end of the scale this threshold should not be set so high that it's too close to the vehicle's dynamic stability limit, resulting in loss of control. One paper within the literature by Odenthal, et al (1999) on steering and braking control for rollover avoidance shows this problem. They set the threshold for when the system actuates at a value of 0.9 (where 1 indicates when the outside tyres of the vehicle are carrying no load and starting to lift off the road). A value of 0.9 should give the system time to react, but a safety margin of only 10% seems very small when a value of 0.75 or 0.8 would give a higher safety margin without creating too much interference with normal driving. This is especially the case as the study is mainly focused on high-sided vehicles which are not designed primarily for cornering performance. This shows the need to think about what the vehicle is for initially and then a relevant threshold can be applied.

2.3. Simulation and Modelling

2.3.1. Introduction

In the field of vehicle dynamics it has become ever increasingly important to create accurate virtual models for use in simulation and testing. In both industry and research, simulation and modelling is a powerful tool used both independently and alongside conventional prototype testing. The advantage that virtual modelling has over physical testing is it reduces the expense of testing, equipment and prototyping with a high level of repeatability and customisation (e.g. change of conditions, materials, scenarios…). It also allows testing in environments not easily replicated physically on earth (e.g. space, other planets).

Modelling has its positives and negatives when you take into account the complexity of some of the problems dealt with in vehicle dynamics. The model needs to have a high enough level of detail to replicate the dynamics of the vehicle appropriately but also not be so complex that it becomes computationally intensive (Kondo and Makino 2008).

Peter Samuel Delves

Thus it is important to consider what level of fidelity the model requires so as to give realistic and accurate results but not take hours or even days to produce results.

There are five parts to consider when modelling vehicle dynamics. These fields are vehicle characteristics, tyres, road, drivetrain and controller modelling.

2.3.2. Modelling Approaches

There are several approaches to modelling vehicle dynamics. There is pure mathematical modelling which formulates equations of motion and applies them in programs such as MatLab/Simulink. This approach increases complexity of the model as it incorporates more DOF. Mistakes can easily occur if care is not taken when inputting equations. Also to the untrained eye it can initially be difficult to decipher results as they are purely graphical but it does have the advantage that they are generally stable and once validated they are accurate. It is also straightforward to integrate control algorithms.

Another approach is Multi Body Systems (MBS) modelling using software packages such as ADAMS. The model is built up of multiple bodies which have geometry, mass, position and inertia connected by constraining joints. Joint selection is important as it dictates what DOF each part has. MBS modelling programs use this geometric information to formulate the equations of motion for the model. Motions can be applied to joints in the DOF they possess and external forces can also be applied to affect the model dynamics. These software packages are also often capable of animating the simulation to give a visual representation of system behaviour. This is especially useful for simulation validation and analysis, as any irregularities are easily identified. Post processors in these packages also allow a high level of data processing and feature extraction. A key issue with this form of simulation is that complex systems can be extremely computationally expensive to simulate, especially when running online animation.

An alternative to pure mathematical modelling or pure MBS modelling is to combine the two approaches through Co-simulation. This allows the physical suspension components and vehicle bodies to be modelled in MBS with control architecture implementation performed through a mathematical modelling package. This

Peter Samuel Delves

combination is a powerful tool allowing integration of geometric modelling with complex control.

Table 2.1: Vehicle model comparison matrix

Model	Degrees of Freedom	Notes
2-DOF (Bicycle model)	Yaw, Lateral	Fixed longitudinal speed. Good for analysing low to moderate handling situations (Cornering, lane change). Accuracy is good up to 0.3G
8-DOF	Body: Yaw, Lateral, Longitudinal, roll, Tyres: Longitudinal slip at each wheel	This model is commonly used in studies primarily focused on lateral vehicle dynamics where your more interested in roll induced weight transfer rather than longitudinal.
9-DOF (Ride)	Body: Yaw, Lateral, Longitudinal, Roll, Pitch Suspension: 4 Vertical	Introduces the effects of suspension displacement into the model. More commonly used for ride modelling
9-DOF (Handling)	Body: Yaw, Lateral, Longitudinal, Roll, Pitch Tyres: Longitudinal slip at each wheel.	Introduces Longitudinal slip at the wheels. This allows individual wheels to be modelled as rotating independently. Good model to use when looking into torque manipulation.
13-DOF	Body: Yaw, Lateral, Longitudinal, Roll, Pitch Suspension: 4 Vertical Tyres: Longitudinal slip at each wheel	Adding complexity combining ride and handling which have typically been looked at separately in dynamic research but are intrinsically linked in the real world and important to consider it final product development.

Peter Samuel Delves

2.3.3. Vehicle Characteristics Modelling

The dynamic model is the vehicle base which all the other models are integrated with to build up the full model. It is designed to replicate the vehicle's body and suspension dynamics. The complexity of the dynamic scenario and the aim of the simulation, is the study most interested in ride or handling behaviour, dictates which direction the model takes.

Table 2.1 show a selection of models to highlight the different levels of complexity that can be achieved. It illustrates the importance of assessing the complexity of the research problem in the model selection process.

2.3.4. Tyre Modelling

Tyre modelling is a very important aspect of vehicle modelling as it can introduce much complexity and non-linearity into the dynamic tyre behaviour. The complexities of tyre modelling can be illustrated by considering the multiple physical effects that the vehicles weight distribution, drivetrain, and suspension have on its behaviour.

Tyres have a 'saturation' point where they reach the maximum force they can transmit relating to vertical load, slip angles (both lateral and longitudinal), caster angle and toe. There are also external factors such as coefficient of friction and road spectral density. Also it is important to consider how complex the tyre model needs to be for the given research problem.

There are two main ways of modelling tyres: empirical and physical. The former requires collecting data sets by running tests on tyres at set vertical loads and side slip angles measuring the lateral and longitudinal forces produced. For a simple linear tyre model a reduced data set can be used in an interpolation based model, which estimates the tyre force between known measured points. When the problem being addressed is more complex this model can become inaccurate, this is solved by increasing the amount of data points. Whilst initially being expensive (running tests and processing the data), once all the data has been processed and placed in a look-up table it is a computationally inexpensive method. It is more common to see functional methods. Pacejka and I.J.M. (1997) has developed a formula from the

measured data to represent the tyre force curve. This method does increase the computational expense of the model but allows the introduction of more complex physical vehicle phenomena like self-aligning torque moments and the effects of camber. The simplest method uses a linear formula defining the initial slope of the tyre curve. This formula works well when small slip angles are involved but is not accurate at higher slip angles. The most commonly used empirical curve fitting method is Pacejka's 'Magic Formula'. This is as follows:

$$F_{xo} = D_x sin[C_x \arctan\{B_x \kappa_x - E_x(B_x \kappa_x - \arctan(B_x \kappa_x))\}] + S_{Vx}$$

The coefficients B-E are all shaping factors which are dependent on vertical load, camber angle and friction and are calculated through the combination of 11 equations with multiple coefficients and parameters gathered through physical tests performed. This model can handle weight transfers across the vehicle which makes it very useful when it comes to dealing with non-linear handling problems.

The other type of model is a physical based model which represents the tyre mechanics as a set of multi body elements. This approach to modelling involves representing the tyre in terms of springs or elastic beams. These include: Taut string model, beam on an elastic foundation, brush model, radial spoke model,

The radial spoke model defined by (Sharp and Limebeer 2001) models the tyre as a collection of elastic beams. It is modelled by splitting the tyre into a large number of spokes (the more spokes the more detailed the model) which can deform radially, laterally and circumferentially but independent of each other. Each of the perimeters is associated with their own stiffness. Spokes that are within the contact patch are given a displacement relating to slip angle, camber and vertical load. This deformation is then used with their corresponding stiffness values to calculate the force generated at that point before advancing time and recalculating. The advantage of this type of model is that it requires only seven parameters compared to what can be 100s with the Pacejka model.

Empirical modelling frequently requires expensive testing to develop accurate data sets and can be computationally expensive once implemented. Physical models are

22

less computationally complex, require less data to produce an accurate model and are in good agreement with Pacejka's model which, although complex is well established and proven in industry as well as being used in a large body of the literature.

2.3.5. Road Modelling

The ideal road surface is a flat and smooth one with no imperfections. Unfortunately the only road surfaces close to this are race circuits and they are still not perfect. The reason for these imperfections is the nature of the constituent parts in tarmac. A solid aggregate mixed with flexible oil (tar) allows the surface to be spread flat and set hard. As environmental conditions change, the flexibility of the surface will also change, leading to cracking or creeping. This results in a surface with multiple frequencies which can be transformed into a Power Spectral Density (PSD) (i.e. translating these frequencies into displacement power). These values are dependent on surface roughness. Surface roughness has different coefficients relating to a particular type of road (for example, a smooth motorway may have a lower roughness coefficient than a minor road which is less well kept).

There are not many handling dynamics papers in the literature which mention road modelling. The main value related to road conditions used is the coefficient of friction µ which is dealt with through the tyre model.

2.3.6. Drivetrain Modelling

This is an area that has become more important as research considers optimising power management and consumption for hybrid vehicles. It is also used to study the interaction between the ICE and electrical motor systems. Drivetrain modelling consists of representing the drive systems as torque inputs into the wheels in a similar way to how brake torques are applied to the vehicle. This can be either through the use of a torque map, or lookup table, which represents how the drivetrain behaves or by modelling the system mathematically to represent how it functions. This can be performed by taking into account throttle positions and speed to work out at which points the vehicle drive systems are operating including gears and engine speeds. Both approaches require a lot of information about engine

Peter Samuel Delves

operation (e.g. speed, engine speed, gear selection, torque/power curves) to produce an accurate model.

The main body of the research appears to apply torque directly to the vehicle model through the wheel DOF (the order in which the forces are generated in the real world). This shows the importance of having an accurate tyre model when studying drivetrain behaviour.

2.3.7. Model Selection

Before modelling begins it is important to assess what level of performance and accuracy is required for the research scenario. There are conflicts when considering the level of complexity needed for the research problem as a very accurate but complex model becomes very computationally expensive (potentially taking hours or even days to complete one simulation (Kondo and Makino 2008)).

2.4. Drivetrains

2.4.1. Introduction

With environmental pressures growing on reducing pollution the motor industry needs to find ways to improve efficiency and reduce emissions. Alternative propulsion is the way forward and will most likely lead to all road vehicles being at least partially propelled by electric motors. This trend can already be seen in the major increase in Hybrid Electric Vehicles (HEV) across all vehicle manufactures. Even in top level motorsport it can be seen in Formula 1 with the introduction of full hybrid powertrains from 2014 and les Mans 24 hour race being won by a hybrid vehicle since 2012. Manufactures are also pushing forward with the development of pure electric vehicles such as the Nissan leaf, Renault Zoe, BMW i3 and the high performance Tesla.

As can be seen by recent developments in the motor industry, drivetrain technology is going through major changes. This section outlines the key current drivetrain technologies research both looking at the advantages and disadvantages of various drive system/layouts in relation to normal driving and safety and crash control potential.

Peter Samuel Delves

2.4.2. Driveline Layouts

Drivetrain layout is the term used to describe how a vehicle's mechanical and electrical systems are laid out to transfer drive to the tyres. In the modern supermini the drivetrain layout is composed of an ICE which transfers its power through a gearbox and differential to the front wheels. Other layouts power rear wheels or all wheels in a similar way, with engines mounted in the front, middle or rear of the vehicle depending upon the manufacturer's design philosophy for vehicle handling, balance and comfort. Hybrid architectures are a little more complex than the standard layout as they incorporate electric motors into a fairly standard Internal Combustion Vehicle (ICV) layout. Chan (2002), Chan (2007), Chan, Bouscayrol et al. (2010) have written review papers outlining the various Electric Vehicle (EV), Hybrid Electric Vehicle (HEV) and Fuel Cell Vehicle's (FCV) layouts and how they operate.

2.4.3. Hybrid Electric Vehicles (HEV)

HEV are going to fill the gap between ICV and EV until battery technologies have developed far enough to bring parity with ICVs range and performance. The reason for this is that HEVs can deliver the performance and range of a standard ICV as well as improving fuel consumption by 50% or more (Burke 2007). Chan (2007) introduces the three basic Hybrid drivetrain layouts: series, parallel, and series-parallel.

A series hybrid only uses an electric motor to drive the vehicle and the ICE to drive a second motor generator unit to produce power for the driving motor. This power is either used drive the motor directly or stored in batteries for later. This allows the ICE to be run at optimum efficiency in order to balance economy with torque and power and allows the vehicle to burn less fuel. The system does not couple the ICE to the wheels, this means that the transmission can be simplified to either: a single gear differential transferring power from the motor or a motor mounted on each driven wheel to create an electric differential. The controllability of electric motors would makes it a simple system to implement more advanced torque vectoring control schemas on.

Parallel hybrids couple the ICE and a single electric motor to the transmission allowing power to be drawn from the ICE only, the electric motor only, or both

Peter Samuel Delves

combined for extra acceleration. Battery power is restored via regenerative braking and storage of excess energy produced by the engine. It can deliver similar dynamic performance to that of a vehicle with a large engine through the combination of a small engine assisted by an electric motor which can reduce fuel consumption. One issue raised is that the whole system is mechanically coupled so the ICE cannot always work in its optimum range and cannot run under full electric motor propulsion. The use of clutches is also needed to couple the motor and ICE together, reducing system efficiency through clutch slippage and requiring a traditional architectural layout.

Series-parallel layout is the most complex of all the hybrid drivetrains. It has all its parts linked by a planetary gear set coupled to the transmission. This allows the vehicle to work as either a series or parallel hybrid. What is engaged to the transmission depends on what system is driving the vehicle. It may be the most versatile system, but with that versatility and flexibility comes complexity and expense. This system also demands a traditional architectural layout so the engine and electric motor can drive the wheels.

2.4.4. Hybrid Vehicle Review

All of these systems have advantages and disadvantages and lend themselves to different applications. Series systems are ideal for use in buses and Heavy Goods Vehicles (HGVs) which, by nature, are stop-start vehicles which do not need particularly high acceleration rates and generally do not travel at high speed. Series systems allow the ICE to be run in the optimum range for power and efficiency, and the high torque capability of electric motors from a stand-still is ideal for heavy, slow travelling vehicles.

Parallel hybrids are mainly used in performance vehicles where the electric motor can be used to give a power boost under hard acceleration and be used to start the engine if it is equipped with a stop-start system.

The series-parallel system delivers the greatest propulsion flexibility as it allows variation between a full electric configuration, full ICE system and combined. The

Peter Samuel Delves

main problem with this configuration is that it has a very complex architecture and requires many control systems to run at its optimum.

It is obvious from literature that no one layout stands out as the best for all driving applications.

2.4.5. Electric Vehicle Review (EV)

The move to a fully electric drivetrain brings opportunities for the development of fresh vehicle layouts because the amount of mechanical linkages is reduced and the electronic systems can be placed anywhere. However, there are also some packaging disadvantages (for example, where the heavy and the often-large battery packs should be placed). Multiple architectures have been mentioned such as: single motor coupled to a conventional gearbox, differential and drive shaft systems; and independent motors mounted in each wheel using motor control to implement a differential. As with the hybrid system each have advantages and disadvantages. But EV architectures appear to lend themselves to better overall vehicle dynamic control because of the predictable nature of the electric motor power and torque delivery (Sakai, Sado et al. 1999).

Peter Samuel Delves

3. Chapter Three: Vehicle Modelling and Validation

The vehicle model selection, derivation and validation process is detailed in this chapter. It discusses the need to analyse the dynamic intensity of the scenarios in the study so that the model is valid for the required dynamic operating region. To demonstrate the dynamic variations that can occur in various models an eight degree of freedom (DOF) model was constructed in three phases; firstly, a linear 2-DOF bicycle model was created. The model was then extended to 7-DOF with the inclusion of the wheel rotational dynamics and longitudinal DOF introducing non-linear tyre dynamics through the implementation of a Pacejka model. Finally roll dynamics and quasi-static weight distribution were added to the model. A steady state cornering and a lane change manoeuvre were used to analyse the variation in dynamic behaviour of the three different models at velocities between 10 and 40m/s.

Peter Samuel Delves

3.1. Introduction

A vehicle-handling model was constructed to allow observation of a vehicle's behaviour during a crash scenario, with the capability to implement a control system that manipulates wheel torque. The model allows simulations to be carried out to ascertain if drive torque vectoring is a plausible candidate for stabilisation of a vehicle after an impact. As discussed in the literature review, the dynamic intensity of the problem is important. For example if low intensity 0-0.3g steady state manoeuvres are involved a linear 2-DOF model will be sufficient. At what is referred to as high dynamic intensity scenarios, where body accelerations are in the range of 0.3-0.8g, the vehicle's behaviour becomes non-linear in nature and the linear models simulation results will no longer be valid, as it will be able to produce much higher accelerations than are physically possible.

This thesis investigates control of a vehicle, which has been subject to a crash impulse, where accelerations in excess of 1g are produced. The current literature justifies the use of a 3-DOF model with simplified tyre dynamics to investigate these scenarios as it is less computationally intensive, but this could be said to be inadequate considering the large accelerations produced in an incident. To test this assertion, simulations were performed to compare the dynamic response of a linear 2-DOF model and non-linear 7-DOF model with the proposed non-linear 8-DOF model to investigate if a higher fidelity model is required.

The simulation study was performed using two manoeuvres, steady state cornering and a lane change with constant forward velocities of 10, 20, 30 and 40m/s. It showed that at 10 m/s the results for the manoeuvres for all three models correlated closely with each other for yaw rate and lateral acceleration, but did start to diverge from 30 m/s. This is because when accelerations are low the vehicle is within its linear region and it is reasonable to use the linear model but, as accelerations increase these models become inaccurate as they can generate far higher accelerations than are physically possible resulting in the divergence in results from the linear to non-linear models. The non-linearity was introduced to the model using a Pacejka tyre model, which is an empirical curve-fitting model, which limits force at high angles of slip. For the final crash control simulations, the crash scenarios cause the vehicle to

29

spin, which required alteration to the small lateral slip assumption. Alterations were made to the lateral slip angle equations to solve computational issues present when the vehicle is facing backwards to its original heading direction.

This view appears to be the same view throughout the current dynamic crash control research by Kim and Peng (2011, 2012, 2014) and Yang et al (2011, 2011, 2012, 2014). They use 3-DOF and 4-DOF models, with non-linear tyre dynamics respectively, approaching their tyre modelling differently. They both use Pacejka models but Yang et al. use the pure lateral slip equation but simplify their longitudinal component to be a function of torque applied to the wheel and wheel radius. Kim and Peng (2011, 2012, 2014) use the combined slip tyre model, which is just as easy to implement as the previous method but generates force based on the longitudinal slip of the tyre. The combined tyre slip has saturation points which limit maximum force avalible for both longitudinal and lateral force built into them, whereas the Yang et al (2011, 2011, 2012, 2014) model includes an additional function to limit longitudinal force based on vertical load, road friction coefficient and lateral slip angle.

Results for the 8-DOF model were validated against and were visually similar to the results presented by Milehins, Cheng et al. (2010).

3.2. Vehicle Model Construction

The 8-DOF vehicle model was constructed using the Matlab&Simulink environment. The model was derived from 1st principles equations of motion for each DOF (lateral, longitudinal, yaw, roll and the four individual wheel rotations). Tyre forces were represented by a combined slip Pacejka model.

Modelling was carried out in five steps: Firstly a 2-DOF bicycle model was built with Lateral and Yaw DOF. Next the addition of the longitudinal DOF and four wheel DOF expanded the model to 7-DOF. A Pacejka tyre model was then introduced to add non-linear tyre mechanics. The final 8-DOF incorporated roll accelerations and finally quasi-static weight distribution for both pitch and roll were added.

The development phases are important as they allowed comparative studies to be carried out between models to observe the variations in behaviour. These models

were compared to determine how the non-linear and linear results diverge at high dynamic intensities and thus require a non-linear model.

3.2.1. Two Degree of Freedom model

The linear 2-DOF handling model, also known as the bicycle model, simplifies a vehicle from two tracks with four wheels into a single track lumping the front and rear wheels into a single front and rear wheel. As it is a pure handling model the suspension is solid and therefor there is no weight transfer from front to back or side to side. In the literature it has been argued that a linear bicycle model should be used rather than a non-linear model because it reduces model complexity and thus simulation time (Kondo and Makino 2008). This is reasonable when studying low level dynamic behaviour, but the lack of two tracks means that yaw behaviour generated by a speed differential between left and right sides of the vehicle is not possible. However, it is an integral part of the full vehicle models as it is used as a base for both lateral and yaw DOF within them.

The bicycle model free body diagram is displayed in Figure 3.1 showing the single track made up of two wheels, which are used to generate lateral and yaw DOF.
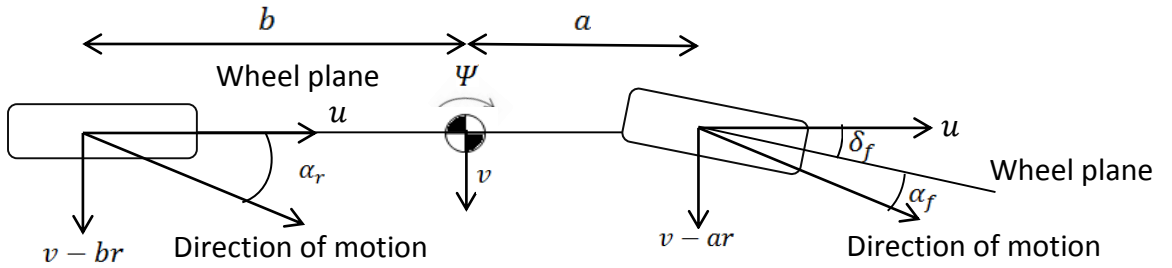
Figure 3.1: Single-track Bicycle model free-body diagram showing how front and rear wheel sets are combined into one single front and one rear wheel (hence bicycle)

Front α_f and rear α_r tyre slip angles are described by the following relationship:

$$\alpha_f = \frac{v - a\Psi}{u} - \delta_f \tag{3.1}$$

$$\alpha_r = \frac{v - b\Psi}{u} \tag{3.2}$$

31

Peter Samuel Delves

Where v is lateral velocity, u is longitudinal velocity of the wheel, a and b are distance from centre of gravity to front and rear axles respectively, Ψ is yaw rate and δ_f is front wheel steer angle.

α_f and α_r are then used in the following equations to represent front and rear lateral tyre forces.

$$F_{yf} = -C_f \alpha_f \qquad (3.3)$$

$$F_{yr} = -C_r \alpha_r \qquad (3.4)$$

Where C_f and C_r are front and rear cornering stiffness.

These are combined with the dynamic equations that represent the Yaw acceleration $\dot{\Psi}$ and lateral acceleration $(\dot{v} + u\Psi)$ DOF:

$$m(\dot{v} + u\Psi) = F_{yF} + F_{yR} \qquad (3.5)$$

$$I_{zz}\dot{\Psi} = aF_{yF} - bF_{yR} \qquad (3.6)$$

Where m is the mass of the vehicle and I_{zz} is the yaw inertia of the vehicle.

A model with cornering stiffness can only represent linear behaviour but represents a vehicle's behaviour well for simulations involving low dynamic intensity manoeuvres and as a reference model when performing control on a non-linear system. To introduce non-linearities into this model the cornering stiffness components can be replaced by a Pacejka tyre model, which will be discussed in section 3.3.

3.2.2. Seven Degree of Freedom Vehicle Modelling

The 7-DOF model uses the bicycle model as its base to build adding the four wheel rotational DOF to the vehicle, which when combined with a tyre model produce lateral F_y and longitudinal F_x forces. The lateral forces are combined with the lateral and yaw components of the bicycle model inducing moments about the centre of gravity creating the two tracks of the vehicle. Likewise the longitudinal forces, which

Peter Samuel Delves

consist of tyres and aerodynamic drag forces, are combined to create the longitudinal DOF of the model.

3.2.2.1. Model construction for 7-DOF
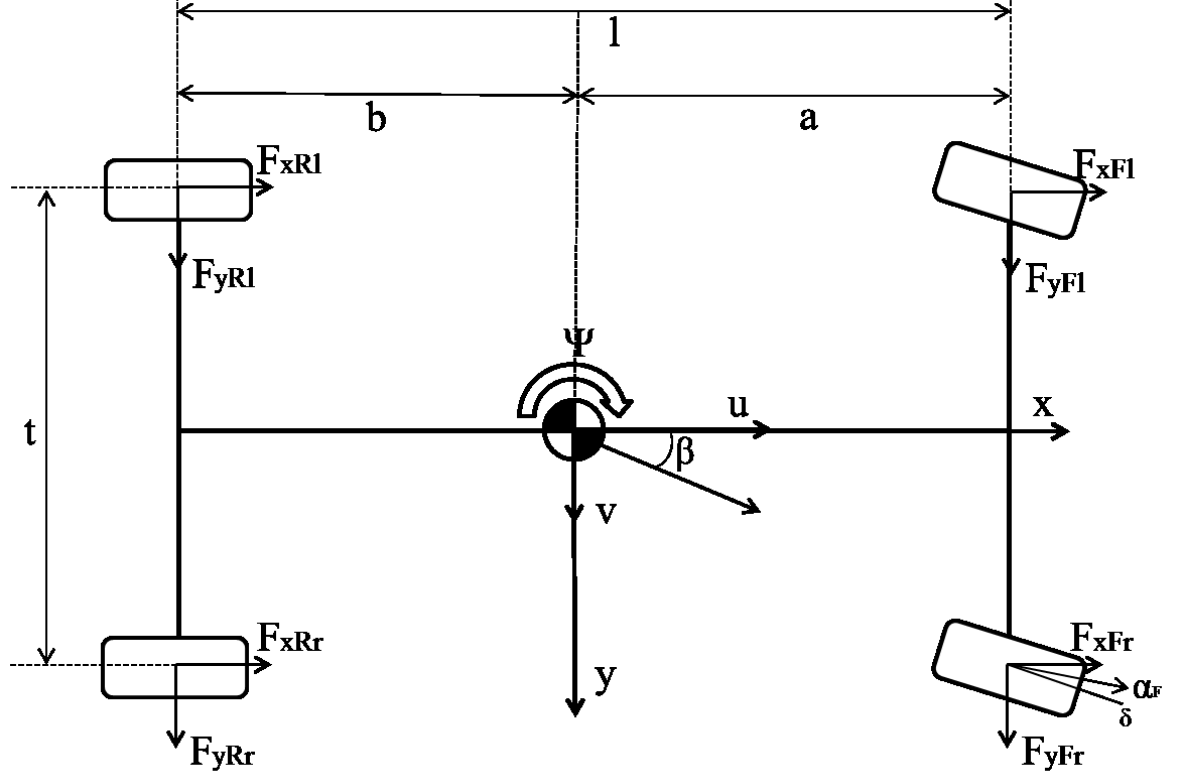
The addition of a second track, as shown in Figure 3.2, required minor alterations to the original lateral and yaw DOF equations of motion to incorporate the lateral forces from all four tyres, and in the case of the yaw DOF longitudinal tyre forces also were included:

$$m(\dot{v} + u\Psi) = F_{yFl} + F_{yFr} + F_{yRl} + F_{yRr} \tag{3.7}$$

$$I_{zz}\dot{\Psi} = a\left(F_{yFl} + F_{yFr}\right) - b\left(F_{yRl} + F_{yRr}\right) + \frac{t}{2}\left(F_{xFl} + F_{xRl}\right)$$
$$- \frac{t}{2}\left(F_{xFr} + F_{xRr}\right) \tag{3.8}$$

Where t is the track width between wheels. F_x at each wheel is generated through longitudinal slip κ which is calculated through:

33

Peter Samuel Delves

$$\kappa = \frac{\omega_w - u}{u} \tag{3.9}$$

Where ω_w is the rotational velocity of the wheel. To calculate this value the wheel rotational DOF. are introduced using the following:

$$I_{wF}\dot{\omega}_{wFl} = T_{wFl} - F_{xFl}r_{wF} \tag{3.10}$$

$$I_{wF}\dot{\omega}_{wFr} = T_{wFr} - F_{xFr}r_{wF} \tag{3.11}$$

$$I_{wR}\dot{\omega}_{wRl} = T_{wRl} - F_{xRl}r_{wR} \tag{3.12}$$

$$I_{wR}\dot{\omega}_{wRr} = T_{wRr} - F_{xRr}r_{wR} \tag{3.13}$$

These are derived from the wheel free-body diagram in Figure 3.3 below where, I_w is the inertia of the wheel, $\dot{\omega}_w$ is rotational acceleration, T_w is the torque applied on the wheel, and r_w is the radius of the wheel.
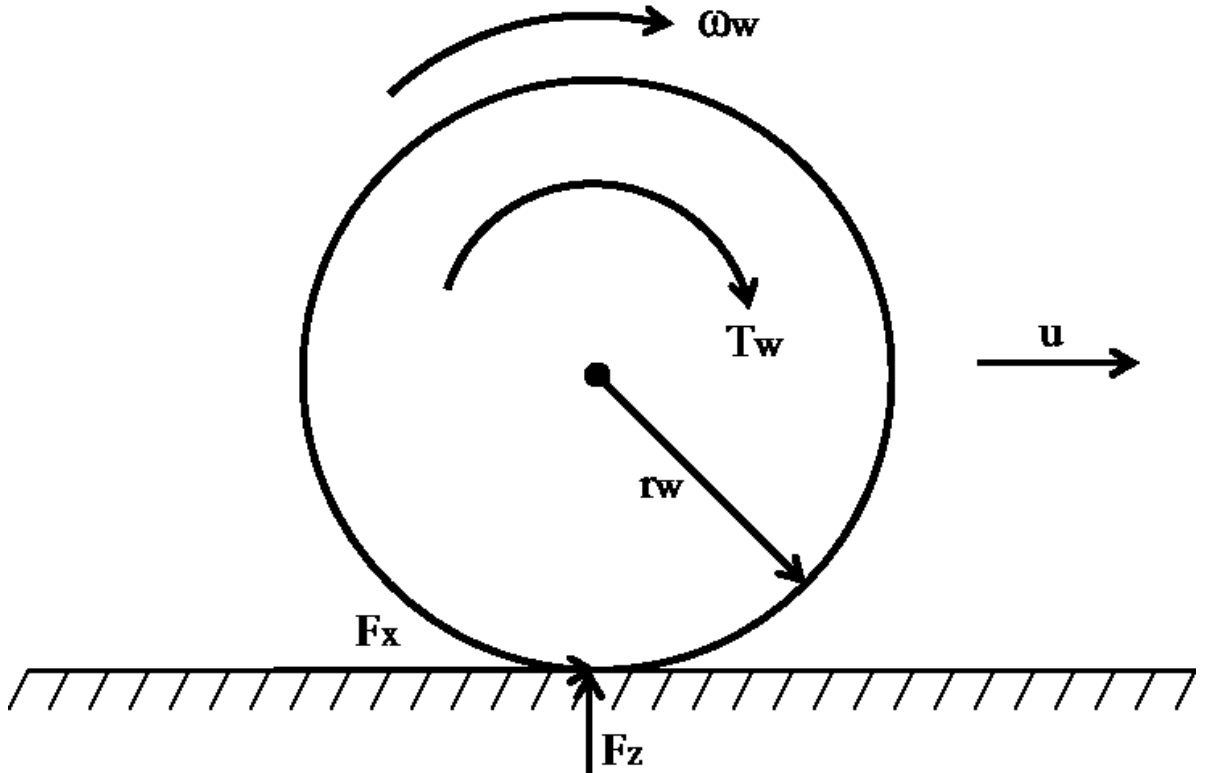
Figure 3.3: Freebody diagram of wheel dynamics

Peter Samuel Delves

These equations are combined to generate the longitudinal forces used for the Longitudinal DOF:

$$m(\dot{u} - v\Psi) = F_{xFl} + F_{xFr} + F_{xRl} + F_{xRr} - F_{areo} \qquad (3.14)$$

Where F_{areo} is aerodynamic drag represented by:

$$F_{areo} = \frac{\rho_a u^2 C_d S}{2} \qquad (3.15)$$

Where ρ_a is air density, C_d is the vehicle drag coefficient and S is the frontal area of the vehicle.

3.2.3. Eight Degree of Freedom Model Expansion (Addition of Roll Dynamics)

The large lateral accelerations associated with a crash scenario requires the addition of roll accelerations and resultant weight transfer to the model. These lateral accelerations will shift weight from one side of the vehicle as it rolls. As the maximum force developed by a tyre is dependent on the vertical load, net available force will be reduced at large roll angles. The roll free-body diagram is as shown below in Figure 3.4:

35
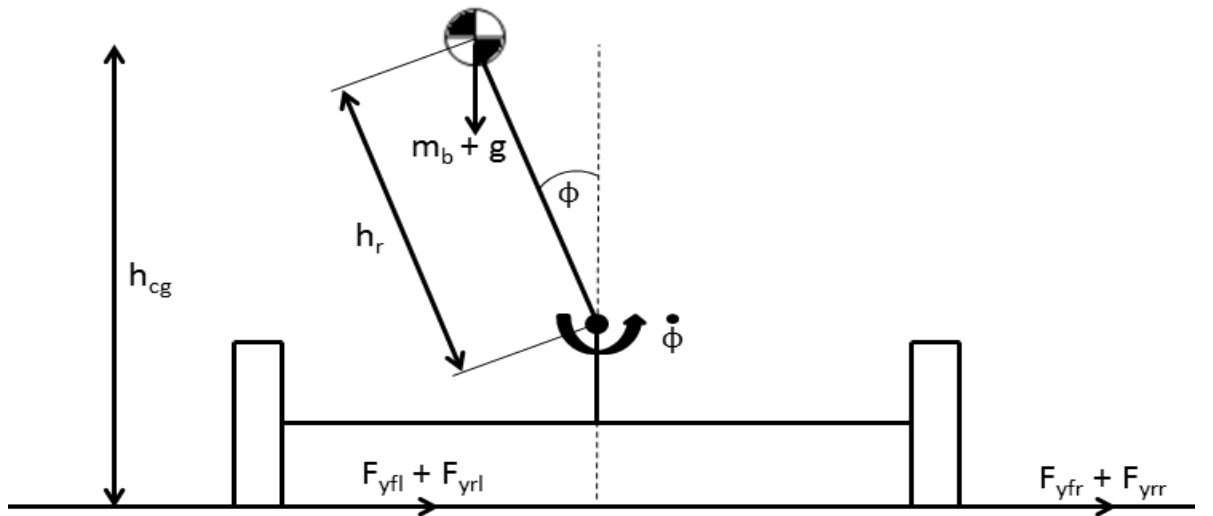
Where $\dot{\phi}$ is roll velocity, ϕ is roll angle, m_b is the mass of the vehicle body, h_r is the roll centre in relation to the centre of gravity height h_{cg}.

The addition of the roll DOF effects the equations of motion as follows:

$$m(\dot{v} + u\Psi) = F_{yFl} + F_{yFr} + F_{yRl} + F_{yRr} + m_b h_r \ddot{\phi} \tag{3.16}$$

$$m(\dot{u} - v\Psi) = F_{xFl} + F_{xFr} + F_{xRl} + F_{xRr} - F_{areo} \tag{3.17}$$

$$I_{zz}\dot{\Psi} + I_{xz}\ddot{\phi} = a(F_{yFl} + F_{yFr}) - b(F_{yRl} + F_{yRr}) + \frac{t}{2}(F_{xFl}$$
$$+ F_{xRl}) - \frac{t}{2}(F_{xFr} + F_{xRr}) \tag{3.18}$$

$$I_{xx}\ddot{\phi} + I_{xz}\dot{\Psi} + m_t(\dot{v} + u\Psi) = (m_b g h_r - k_r)\phi - c_r \dot{\phi} \tag{3.19}$$

Where $\ddot{\phi}$ is roll acceleration, m_t is the total mass of the vehicle including suspension and wheel mass, I_{xz} is the coupled inertia of the yaw and roll of the vehicle, I_{xx} is the roll inertia of the vehicle, k_r is the lumped roll stiffness of the suspension and c_r is the lumped roll damping of the vehicle.

3.2.4. Quasi-Static Weight Distribution

The lateral and longitudinal accelerations induced in a crash will cause weight to shift from front to back and left to right of the vehicle. The shift in weight laterally and longitudinally is calculated quasi-statically by taking the current lateral and longitudinal accelerations and multiplying them by roll and gravity centres respectively. The two equations that dictate the load change due to lateral acceleration for the front and rear of axles are:

$$F_{zFroll} = \frac{hr \ (\dot{v} + u\Psi) \ m_{bF}}{t} \tag{3.20}$$

$$F_{zRroll} = \frac{hr \ (\dot{v} + u\Psi) \ m_{bR}}{t} \tag{3.21}$$

Where $m_{bF/R}$ is the mass of the vehicle body on the Front/Rear wheels

Peter Samuel Delves

These values are then added or subtracted, depending on cornering direction, from the static vertical loads to give the instantaneous vertical load on each tyre.

The load transfer between the front and a rear axles under longitudinal acceleration is as follows:

$$F_{zpitch} = \frac{h_{cg}(\dot{u} - v\Psi)m_b}{l} \qquad (3.22)$$

Where l is total wheel base.

The result is the total weight transfer between the front and rear axles so to calculate the actual change in load for each wheel required this value to be divided by two.

3.3. Tyre Modelling

All of the forces that the driver has control over are produced through the tyres therefore the choice of tyre model is just as important to the overall fidelity of the model as the number of DOF. This is also true for all the ADAS systems the driver has access to such as, steering, braking and powertrain control systems. It is also where the majority of the non-linear behaviour of the vehicle is introduced.

A combined slip Pacejka tyre model was used, as the two DOF model linear tyre forces are represented as front and rear cornering stiffness. This is a simplified idealised method which applies a given force for each degree of later slip that is applied to the wheel. When investigating low intensity manoeuvres it is common practise as it does not add unnecessary complexity to the model whilst still producing comparable results to non-linear methods. However for this study high intensity dynamics are being investigated so using cornering stiffness would be too simplistic an approach. This can be observed in the results section 3.5 of this chapter where the linear model's results diverge as dynamic intensity increases.

3.3.1. The Pacejka 'Magic Formula' Tyre Model

The variant used in this study is the combined slip model, because during an incident where a spin is induced slip is generated in both lateral and longitudinal directions of the tyre which are intrinsically linked and can only transmit a total finite force

Peter Samuel Delves

between them. This results in little force being available in one direction when large slips are produced in the other direction.

Construction of the Pacejka model was performed in 3 steps: Build the pure lateral slip model; Construct the pure longitudinal slip model; Combine these two models to form the combined slip model.

Each phase was validated against the Pacejka data sets to reduce the potential for modelling error.

3.3.2. Pure Lateral Slip Model Construction

The lateral model was constructed in the Simulink modelling environment from Pacejka's(1997) paper to implement the following pure lateral slip 'magic formula' equation:

$$F_{yo} = D_y sin\left[C_y \arctan\{B_y\alpha_y - E_y\left(B_y\alpha_y - \arctan\left(B_y\alpha_y\right)\right)\}\right] + S_{Vy} \quad (3.23)$$

Where:

F_{yo}: Lateral Force

α_y: Lateral Slip Angle

B_y: Stiffness Factor (Determines the slope from the origin)

C_y: Lateral Shape Factor (Determines the shape of the curve)

D_y: Peak Factor (Determines the maximum lateral force produced. Dependent on coefficient of friction μ)

E_y: Curvature Factor (Controls the curvature and position of the peak value)

S_{Vy}: Vertical shift factor (Offsets the curve vertically from the origin)

3.3.2.1. Pure Lateral Slip Model Validation

The validation test was carried out by running a lateral slip (α) sweep test at the three vertical loads F_z use by Pacejka (2002)of 2000, 4500 and 7000 Newtons. All three data sets where generated simultaneously using the magic formula Simulink

model sweeping α from -15° to 15° and Coefficient of friction μ = 1 as performed by Pacejka (2002).

Figure 3.5 plots all three curves on the same graph, which correlate with the baseline results produced by Pacejka (2002) himself. It shows the model has an initial linear region at low slip angles, demonstrating why at low slip angles tyre force can be represented by cornering stiffness; however, as the tyre approaches the force saturation point values plateau where linear values would continue to increase. It was observed that the gradient of the initial slope gets steeper as F_z is increased so a single cornering stiffness is only valid for one value of F_z.

Table 3.1 highlights points of interest from Figure 3.5. It demonstrates how there is not a linear increase in maximum tyre force as F_z is increased, with a significant drop in maximum tyre force produced from 2000N-7500N. Slip angles when the tyres reach 99% of their maximum value, which can be considered as the start of its saturation region, are also shown. It was observed that as vertical load increases the point at which this occurs increases. This is due to the way that the curvature factor E_y is linked to the ratio of the vertical tyre load F_z and the test load F_{zo} used to generate all of the tyre model parameters. One result of the tyre model is that negative and positive peak forces are not the same, this is due to the vertical shift factor S_{Vy} applied in the equation to stop singularity occurring at 0° slip. For a list of all Pacejka tyre model parameters and coefficients see appendix 1.

Peter Samuel Delves
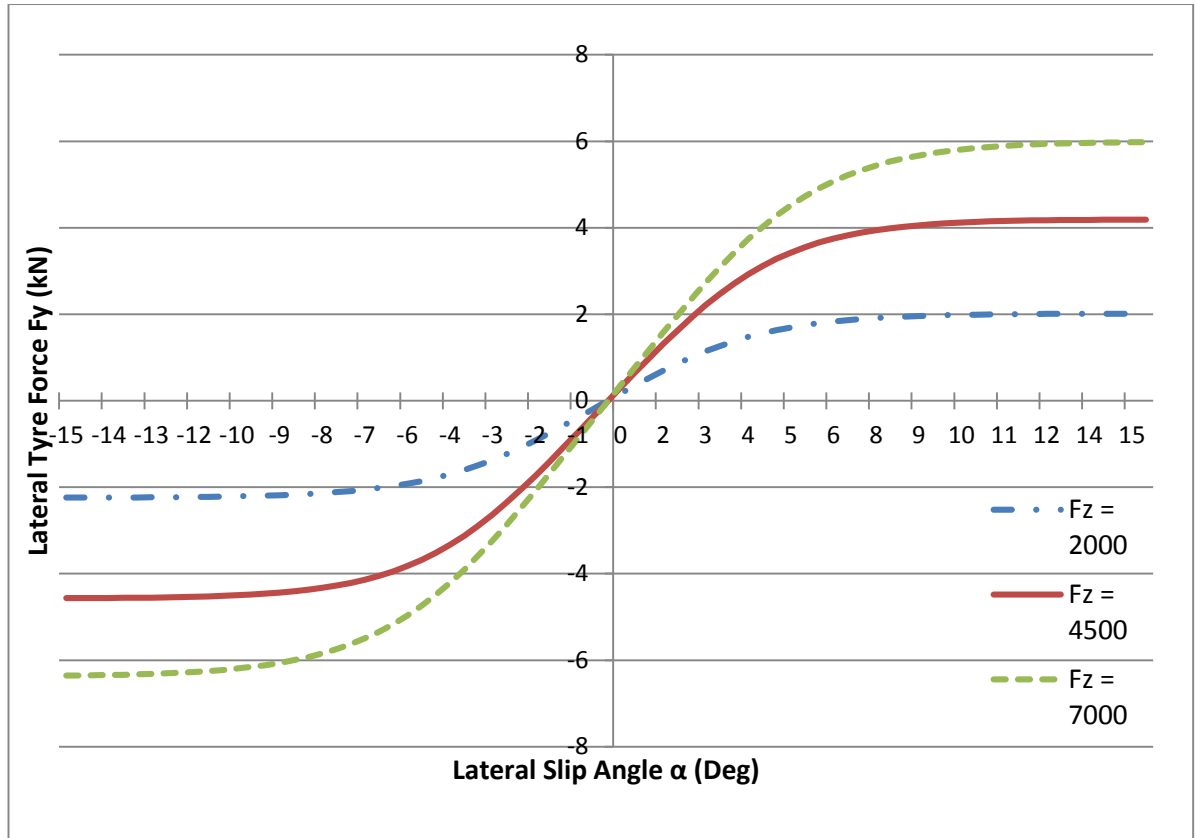
Figure 3.5: Graph showing the pure lateral slip 'magic formula' tyre model. It plots lateral tyre force Fy from -15 to 15 degrees of lateral slip (α) to demonstrate how transmitted force alters with slip and how it plateaus at high slip angles

Table 3.1: Table showing the peak forces generated in both negative and positive directions and at what slip angle peak force reaches 99% of this peak for the pure lateral slip model.

Fz (N)	Peak positive force (N)	Peak α (^{0})	α at 99% peak force (^{0})	Peak negative force (N)	Peak α (^{0})	α at 99% peak force (^{0})
2000	2010	15	10	-2239	-15	-10.8
4500	4184	15	10.8	-4569	-15	-11.2
7000	5978	15	11.6	-6352	-15	-11.6

3.3.3. Pure Longitudinal Slip Model Construction

Just as with the lateral force model, the longitudinal model was constructed in Matlab's Simulink environment implementing Pacejka's magic formula equation for the pure longitudinal slip. The equation is as follows:

$$F_{xo} = D_x sin[C_x \arctan\{B_x\kappa_x - E_x(B_x\kappa_x - \arctan(B_x\kappa_x))\}] + S_{Vx} \quad (3.24)$$

Peter Samuel Delves

Where:

F_{xo}: Longitudinal Force

κ_x: Longitudinal slip (0 = No Slip, 1= Full Slip (Wheel Spin))

B_x: Stiffness Factor (Determines the slope from the origin)

C_x: Lateral Shape Factor (Determines the shape of the curve)

D_x: Peak Factor (Determines the maximum lateral force produced. Dependent on coefficient of friction μ)

E_x: Curvature Factor (Controls the curvature and position of the peak value)

S_{Vx}: Vertical shift factor (Offsets the curve vertically from the origin)

3.3.3.1. Pure Longitudinal Slip Model Validation

The same F_z and μ perimeters used for the lateral model were used for the longitudinal model. A sweep of longitudinal slip κ was performed from 0 to -100%, 0 denoting no slip with 100% representing full wheel lock up as is data used by Pacejka.

As with the lateral tyre model, the initial slope is linear until it approaches the saturation point, where it starts to curve towards its maximum point, shown in figure-3.6. Maximum force is developed at slip rates of 12-18%. As tyres are stiffer in their longitudinal plane, higher peak forces are generated then in the lateral direction but there is a more severe drop off than in the lateral component as can be observed as κ increases with a drop of 29-37% from the maximum generated force to full wheel-spin. This can be seen in Table 3.2. This shows that as wheels approach 100% slip the available transmittable force is reduced. It is not shown here but is also the case for wheels under traction. Therefore to get the best performance from the tyre it needs to be ideally kept in the 12-18% slip region.

Peter Samuel Delves
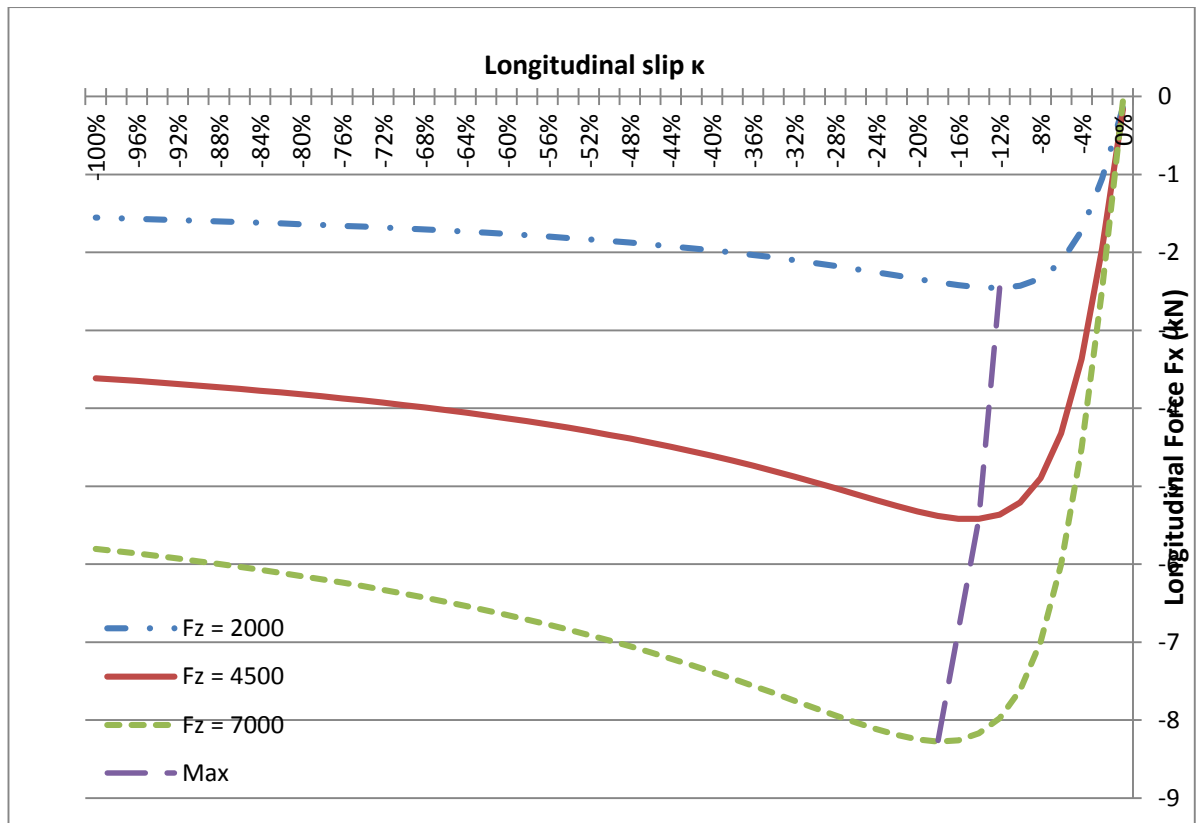
Figure 3.6: Graph showing the behaviour of the pure longitudinal slip 'magic formula' tyre model as negative longitudinal slip is applied at vertical tyre loads of 2000, 4500 and 7000N.

Table 3.2: Table showing peak force transmitted from the longitudinal model and at what % slip. It also shows what the force is at 100% slip and compares the % change between these two.

Fz (N)	Peak force (N)	κ at Peak	Force at κ = 100% (N)	% change from peak force
2000	-2456	12%	-1555	36.7%
4500	-5420	14%	-3613	33.3%
7000	-8275	18%	-5802	29.9%

3.3.4. Combined Slip Model Construction

This model is required for this study, as the crash simulation will induce a spin while tractive forces are applied for control. This results in both lateral and longitudinal slips being produced in the tyre at the same time. The model merges the previous two pure lateral and longitudinal models to create the combined slip model. In doing this the coupling behaviour when a tyre is subjected to both lateral and longitudinal slip simultaneously is introduced.

Again as with the pure slip models, this model was constructed in Simulink. The two equations are as follows:

Peter Samuel Delves

Lateral force (combined)

$$F_y = D_{y\kappa} \cos\left[C_{y\kappa} \arctan\{B_{y\kappa}(\kappa + S_{Hy\kappa})\}\right] + S_{Vy\kappa} \qquad (3.25)$$

Where:

F_y: Lateral Force (Combined model)

κ: Longitudinal slip (0 = No Slip, 1= Full Slip (Wheel Spin))

$B_{y\kappa}$: Stiffness Factor (Determines the slope from the origin)

$C_{y\kappa}$: Lateral Shape Factor (Determines the shape of the curve)

$D_{y\kappa}$: Peak Factor (Determines the maximum lateral force produced. Dependent on coefficient of friction μ)

$S_{Hy\kappa}$: Horizontal shift factor (Offsets the curve horizontally from the origin)

$S_{Vy\kappa}$: Vertical shift factor (Offsets the curve vertically from the origin)

Longitudinal force (combined)

$$F_x = D_{x\alpha} \cos\left[C_{x\alpha} \arctan\{B_{x\alpha}(\alpha + S_{Hx\alpha})\}\right] \qquad (3.26)$$

Where:

F_x: Longitudinal Force (Combined model)

α: Lateral Slip Angle

$B_{x\alpha}$: Stiffness Factor (Determines the slope from the origin)

$C_{x\alpha}$: Lateral Shape Factor (Determines the shape of the curve)

$D_{x\alpha}$: Peak Factor (Determines the maximum lateral force produced. Dependent on coefficient of friction μ)

$S_{Hx\alpha}$: Horizontal shift factor (Offsets the curve horizontally from the origin)

Peter Samuel Delves

3.3.4.1. Combined Slip F_y and F_x Relationship

Figure 3.7 shows the relationship between F_y and F_x and how they share the total available tyre force. The reduction in force produced in one direction when combined slip is present in the tyre is because a tyre only has finite force available which has to be shared between F_y and F_x. For example if torque is applied during cornering effectively demanding more F_x, leading to an increase in κ, F_y will be reduced. But if the tyre is already at a high slip angle α the maximum F_x that can be produced is reduced. Therefore only maximum lateral force is developed at very low value for κ. Alternately if α is increased whist accelerating/braking the force available to accelerate/brake the body F_x will be reduced and thus maximum F_x is only achievable when α = 0°. This behaviour enforces how important it is to use this model for this study as the vehicle will experience both lateral and longitudinal slip in a spin.
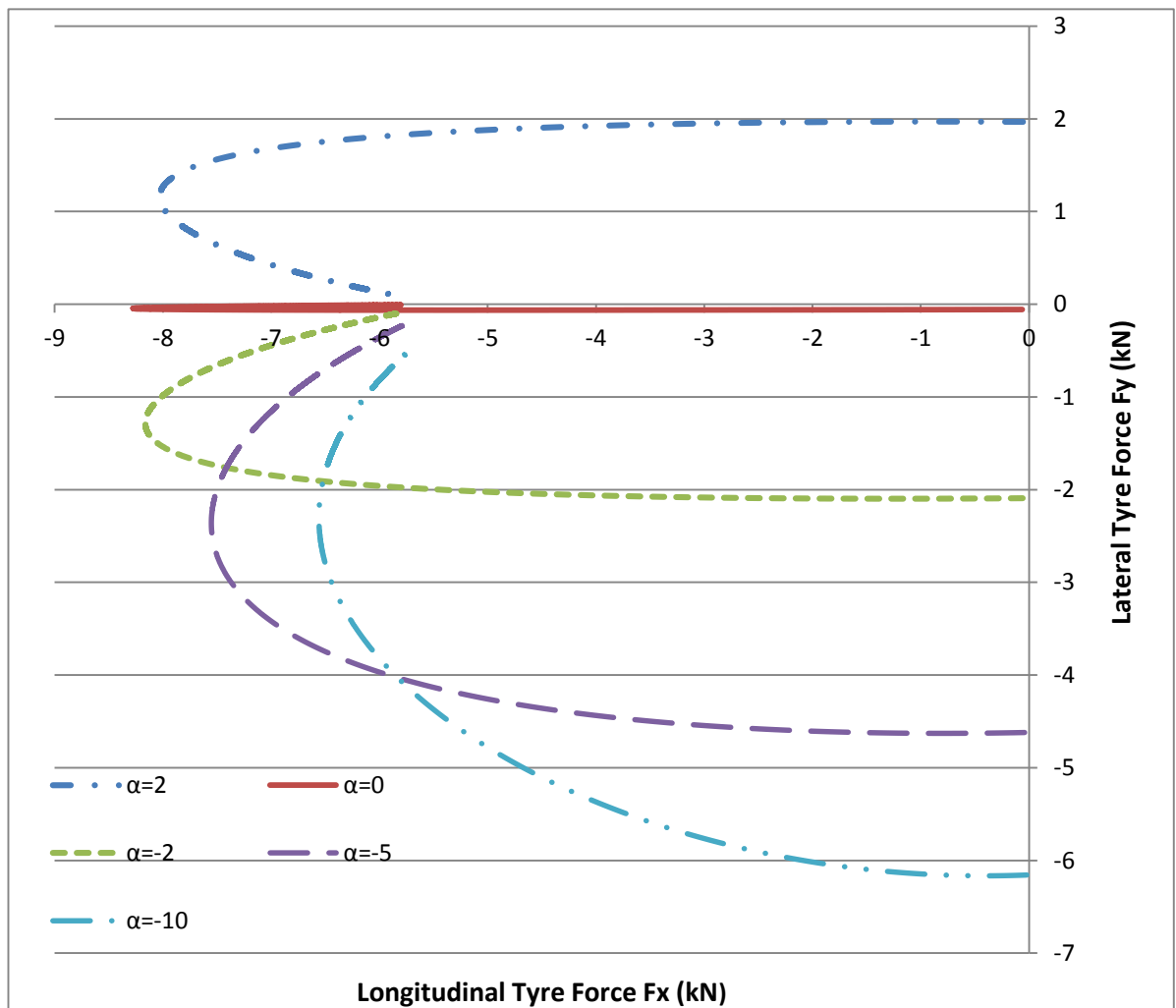
Figure 3.7: Plot showing the relationship between Lateral and Longitudinal tyre force as longitudinal slip is decreased at Lateral slip angles of 2, 0, -2, -5 and -10 degrees

Peter Samuel Delves

3.3.4.2. Combined Slip Model Validation (Lateral Force)

As is seen from the pure lateral slip model α is the main lateral slip component and thus has more influence in the combined lateral model at low levels of longitudinal slip. To generate the combined slip graph in Figure 3.8, κ was swept from 0-100% at five valves of α 2, 0, -2, -5 and 10 degrees with vertical tyre force set at 7000N for comparison with data presented by Pacejka (2002).
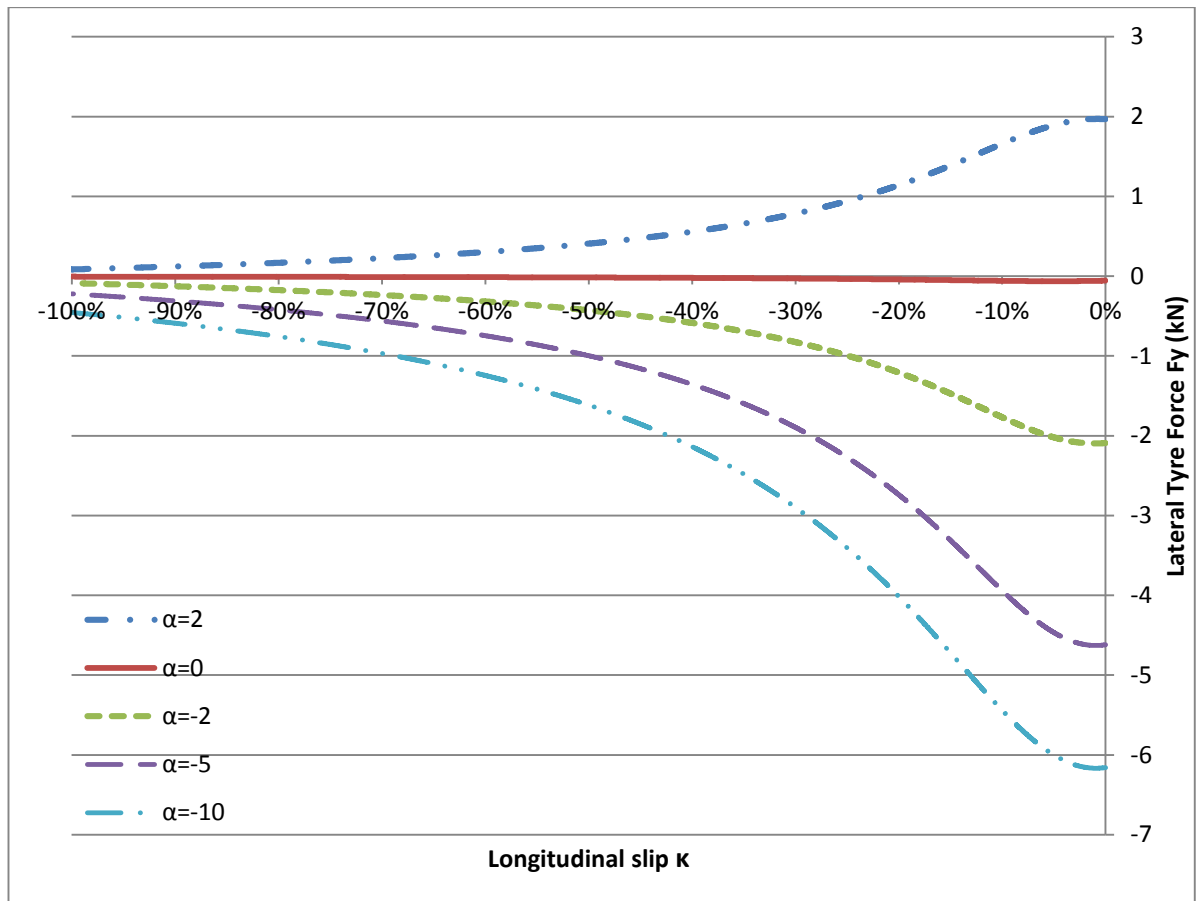
Figure 3.8: Plot showing how Lateral force Fy varies as longitudinal slip is decreased at lateral slip angles of 2, 0, -2, -5 and -10

Table 3.3: Longitudinal slip percentages where maximum lateral force and 90% of maximum force is generated

	α=2	α=0	α=-2	α=-5	α=-10
Fymax (N)	1970	-64	-2097	-4629	-6167
κ at Fymax	0.8%	5.0%	1.0%	0.9%	0.9%
90% Fymax (N)	1773	-57	-1887	-4166	-5550
κ at 90% Fymax	7.8%	10.9%	7.9%	8.1%	9.2%

This cross sectional view shows the effect combined slip has on lateral force generation and correlates with the plot in Pacejka (2002). As explained in the

Peter Samuel Delves

previous section 3.3.4.1 this graph shows the coupling behaviour between α and κ. As a tyre is stiffer in the longitudinal direction κ dominates α. This results in a considerable reduction in lateral force at high κ values. But it is important to highlight that maximum lateral force $F_y max$ is actually generated at κ values between 1-2%, as some longitudinal slip is required to generate lateral force, and that $F_y max$ is still at 90% at κ values of 8-10% as is shown in table 3.3.

3.3.4.3. Combined Slip Model Validation (Longitudinal Force)

Figure 3.9 plots longitudinal force at five valves of α 2, 0, -2, -5 and 10 degrees whist sweeping κ from 0-100% with a vertical tyre load of 7000N. It shows the coupling relationship between κ and α. The longitudinal force component is highly influenced by longitudinal slip $κ$ but when combined with lateral slip the maximum longitudinal force that can be generated is reduced as can be seen in Figure 3.9 and Table 3.4.
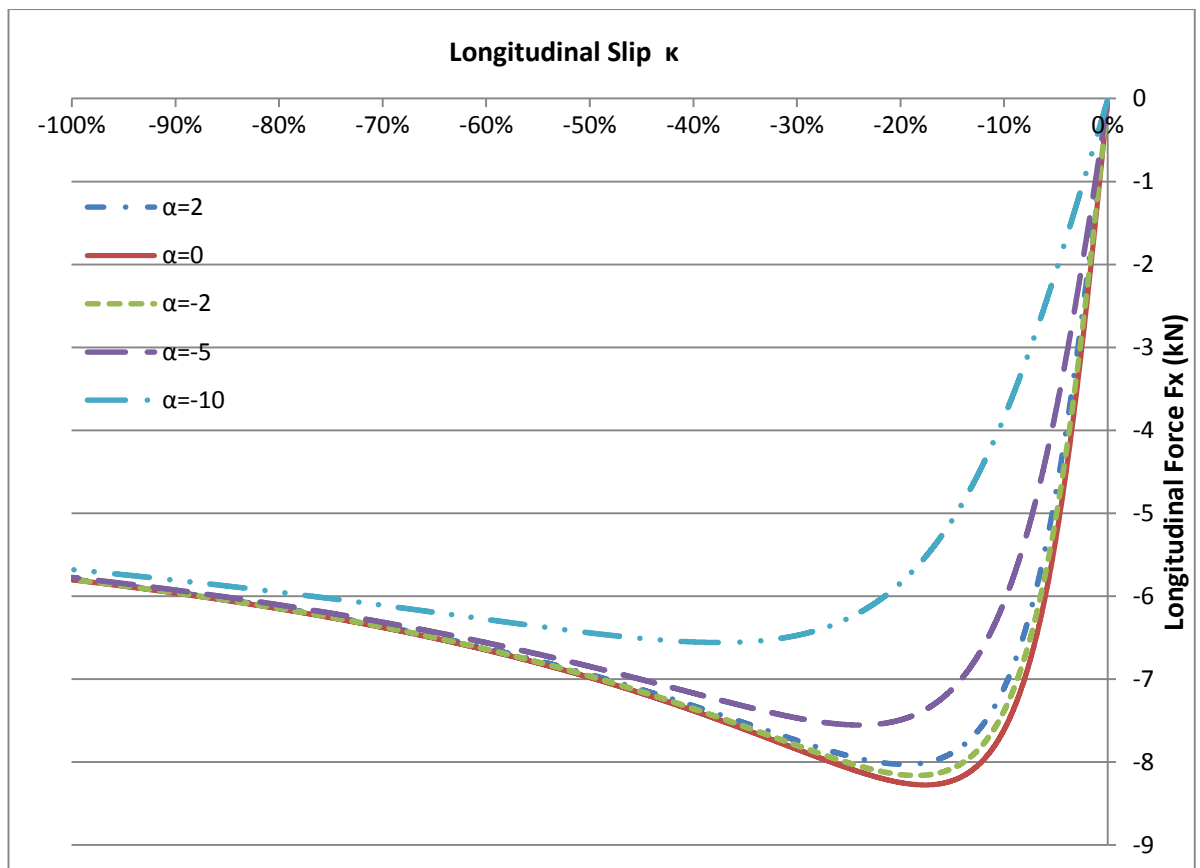
Figure 3.9: Plot showing how longitudinal force changes as longitudinal slip is decreased at lateral slip angles of 2, 0, -2, -5 and -10.

Peter Samuel Delves

Table 3.4: Table showing maximum force transmitted from the tyre at each lateral slip angle and at which longitudinal slip % they occur.

	α=2	α=0	α=-2	α=-5	α=-10
Fxmax (N)	-8028	-8276	-8162	-7553	-6558
κ at Fxmax	19.5%	17.6%	18.4%	23.9%	37.4%

Similarly to the lateral slip plot a peak tyre force $F_x$max of -8276N is generated when the opposed component is held at 0 (α) and is shaped the same as the pure longitudinal slip graph F_x. Than as α is increased $F_x$max reduces as the tyre has to share its available force between F_x and F_y.

The plots highlight why it is important to use this combined slip model to study post-impact dynamics as high values of both α and κ are generated as a vehicle is induced into a spin. This means that total available tyre forces in any one direction (F_x or F_y) are coupled and thus dependent on both κ and α values at any one time. It is especially important as torque control only influences longitudinal slip so when large angles of lateral slip are produced in a spin potential avalible control force is reduced.

3.4. Extended Tyre Slip Calculations

The original 2-DOF base model assumed small slip angles but as large slip angles (approaching 90^0) will be induced during the crash simulation this is no longer a valid assumption. This was implemented using the following equations (Byung-joo Kim and Peng 2012):

$$\alpha_f = atan2((v + a\Psi), u) - \delta_f \qquad (3.27)$$

$$\alpha_r = atan2((v - b\Psi), u) \qquad (3.28)$$

These equations are very similar to the equations assuming small angles but importantly include an atan2 function. This function compares the two inputs to gather information about their sign to assign the correct quadrant of the angle between -180^0 and 180^0.

Initial validation simulations, which induced spins of 180^0 and 360^0, highlighted a computational issue about the switch point in the arctan2 function. The arctan2 function switches sign from -180 to +180 rapidly and when the vehicle was spun

Peter Samuel Delves

through 180^0 the model gets stuck at this point, rapidly oscillating between positive and negative forces, making control of the vehicle impossible.

This is also due to issues with the tyre model. As stated in (Byung-joo Kim and Peng 2012) a tyre model lateral slip force curve should mirror about a line x = y and follows a sine wave form between -180^0 and $+180^0$ but the constructed model was not equipped to do this.

To solve the problem the above tyre slip equations are multiplied by sine. This means that when the vehicle is running backwards (180°) the vehicle slip angle will = zero and therefore tyre force will = zero and solve the discontinuity issue. Resulting in the following equations:

$$\alpha_f = sin((atan2((v + a\Psi), u)) - \delta_f) \qquad (3.29)$$

$$\alpha_r = sin(atan2((v - b\Psi), u)) \qquad (3.30)$$

This resulted in a maximum possible slip angle of 1 radian (approximately 57^0). During the crash phase the vehicle does spin through 60^0+. However, at high lateral slip angles tyre forces have saturated and it is fair to assume that there is little difference in force.

To test this hypothesis further interrogation of the tyre model was carried out to assess the force curve at high slip angles. Figure 3.10 plots the lateral tyre curve from -90^0 to $+90^0$ for the Pacejka tyre model.

The curve shows that the most extreme changes in force are at low slip angles $\pm 10^0$. It is important that the slip angle calculations are accurate at this point as a change of 1^0 in this range can result in the force doubling or halving. Once the slip angles exceed 10^0 the tyre has entered its saturation region and has a small negative gradient resulting in a slight reduction in force. Figure 3.11 enhances the graph at very high slip angles $<55^0$ and table 4.1 shows the forces at 55^0 and 90^0.

Peter Samuel Delves
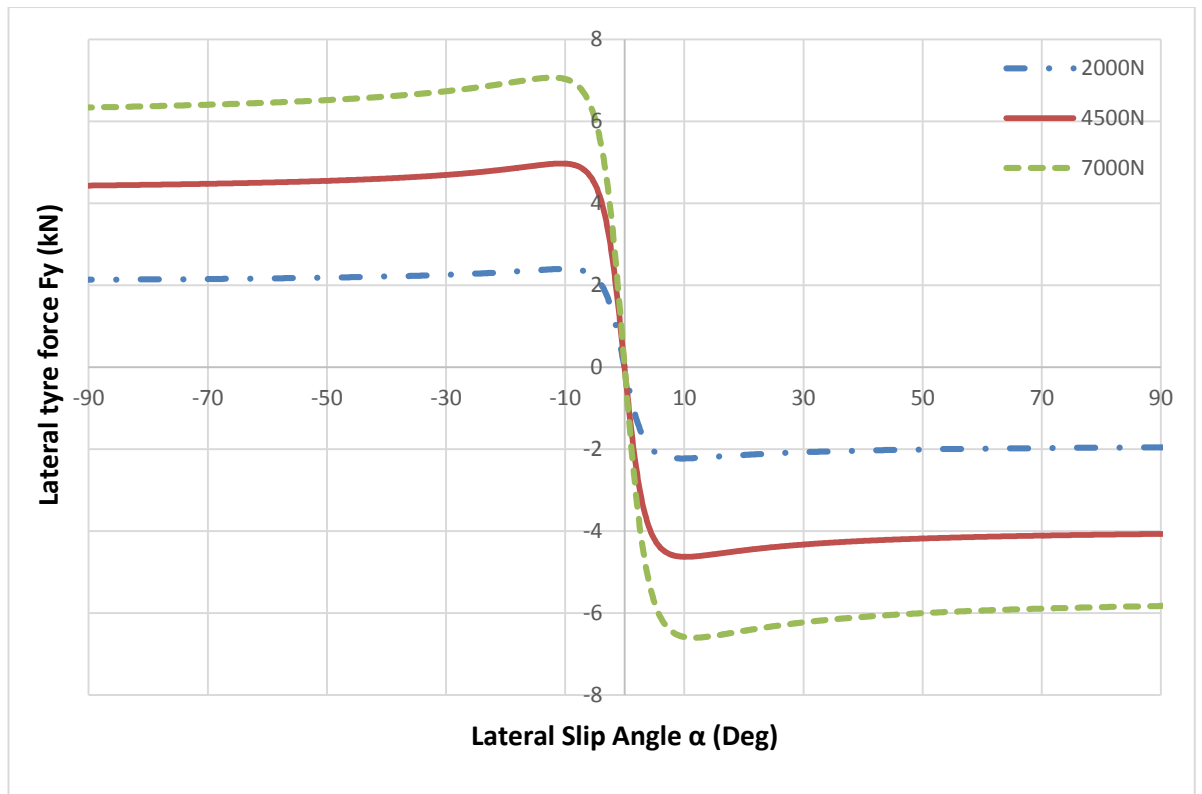
Figure 3.10: -90⁰ to +90⁰ lateral tyre slip curves for vertical loads of 2000, 4500 and 7000N.
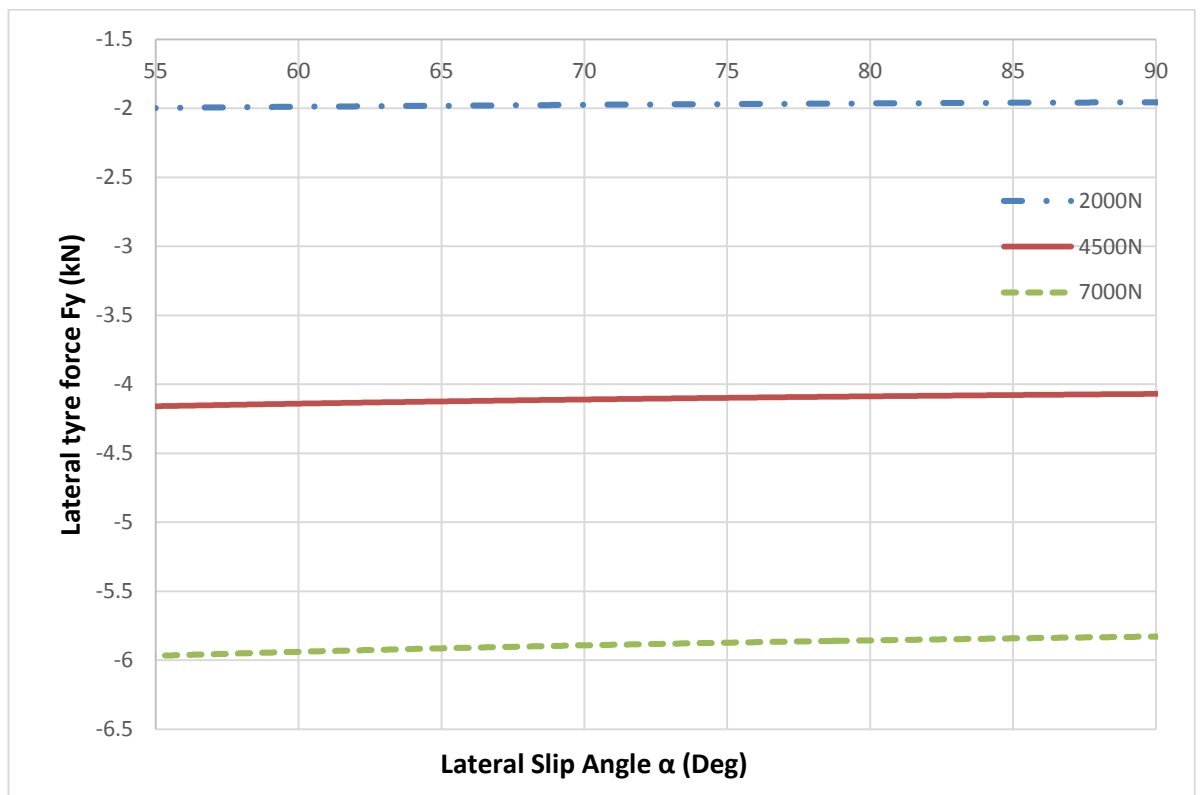
Figure 3.11: Section of slip graph from 55⁰ to 90⁰ to show change in generated force.

Peter Samuel Delves

The first thing to note is the magnitude of force are in the thousands whereas the difference from 55^0 to 90^0 is in the tens. This results in a consistent drop in the region of 1.82-1.98% from 55^0 to 90^0 for the varying vertical loads as is seen in Table 3.5. This is a negligible difference, especially when slip angles are changing as rapidly as they are during a spin, therefore demonstrating that this was a fair assumption.

Table 3.5: Tyre forces generated at 90, 57.3 (1 radian) and 55 to compare % change in transmitted force

	Vertical tyre load (N)		
	2000	4500	7000
Slip angle (^{0})			
90	2133.972	4433.85	6338.815
57.3	2172.303	4518.12	6471.776
55	2176.499	4527.221	6485.868
% Difference	1.80%	1.90%	2.10%

3.4.1. Validation of Extended Slip Angle Calculations

To compare the behaviour of the original equations and the altered equations simulations were run to induce the vehicle into a spin. Assessing the initial crash simulations two sets of force inputs were used, one to cause the vehicle to rotate a full 360^0 and the other result in the vehicle settling facing backwards having rotated around 180^0.

The force inputs were selected from the crash force calculations in the next chapter in section 4.3. The two crash scenarios are both rear impacts with a closing speed of 5m/s. The 360^0 spin incident has an impact angle of 20^0 and the 180^0 incident angle of impact is 10^0

Peter Samuel Delves

Figure 3.12 plots vehicle heading angle over time for Kim's (blue dot-dash line) and modified (red line) tyre slip calculations as the vehicle spins through a full 360^0.
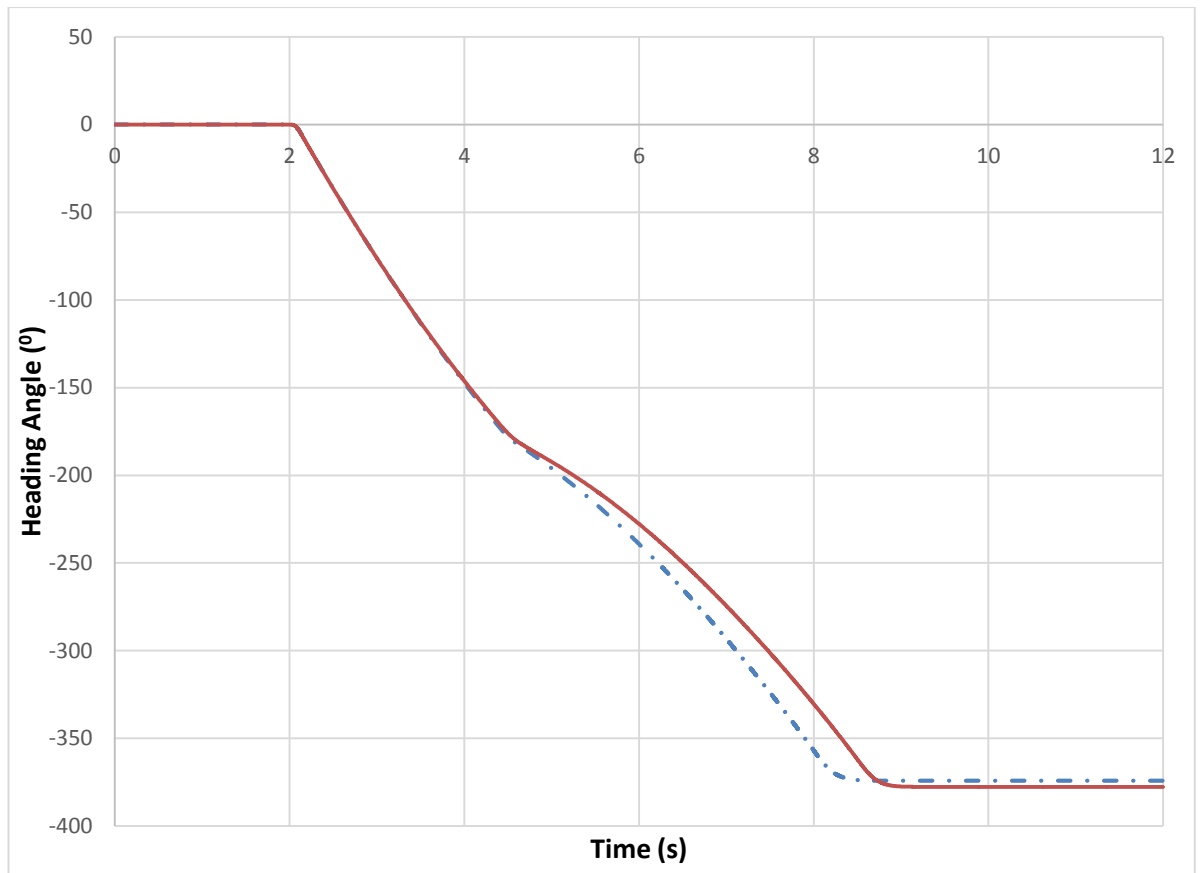
Figure 3.12: Comparison of original and new slip angle calculations showing the difference in heading angle change over time for an impact causing a 360^0+ spin

The crash impulse is input at t=2 s. This simulation results in a final heading angle of 377.4^0 as compared with 373.8^0. The new simulation displays similar behaviour following the same curve but takes 0.5 s longer to settle (9 s as opposed to 8.5 s). This is due to the immediate switch in the arctan2 function in Kim's model from positive to negative force values at 180^0 of slip. The tyre model does not reduce back to 0 between the 175 to -175 transition region as the modified equations do. For comparison Kim's equations result in a switch in the space of 0.001 s whereas the altered equation takes 0.5 s. This is more realistic tyre behaviour as it slips from one direction to the other and load is transferred across the vehicle. The next plot, Figure 3.13, show how the slip angles change over time for this scenario.

Peter Samuel Delves
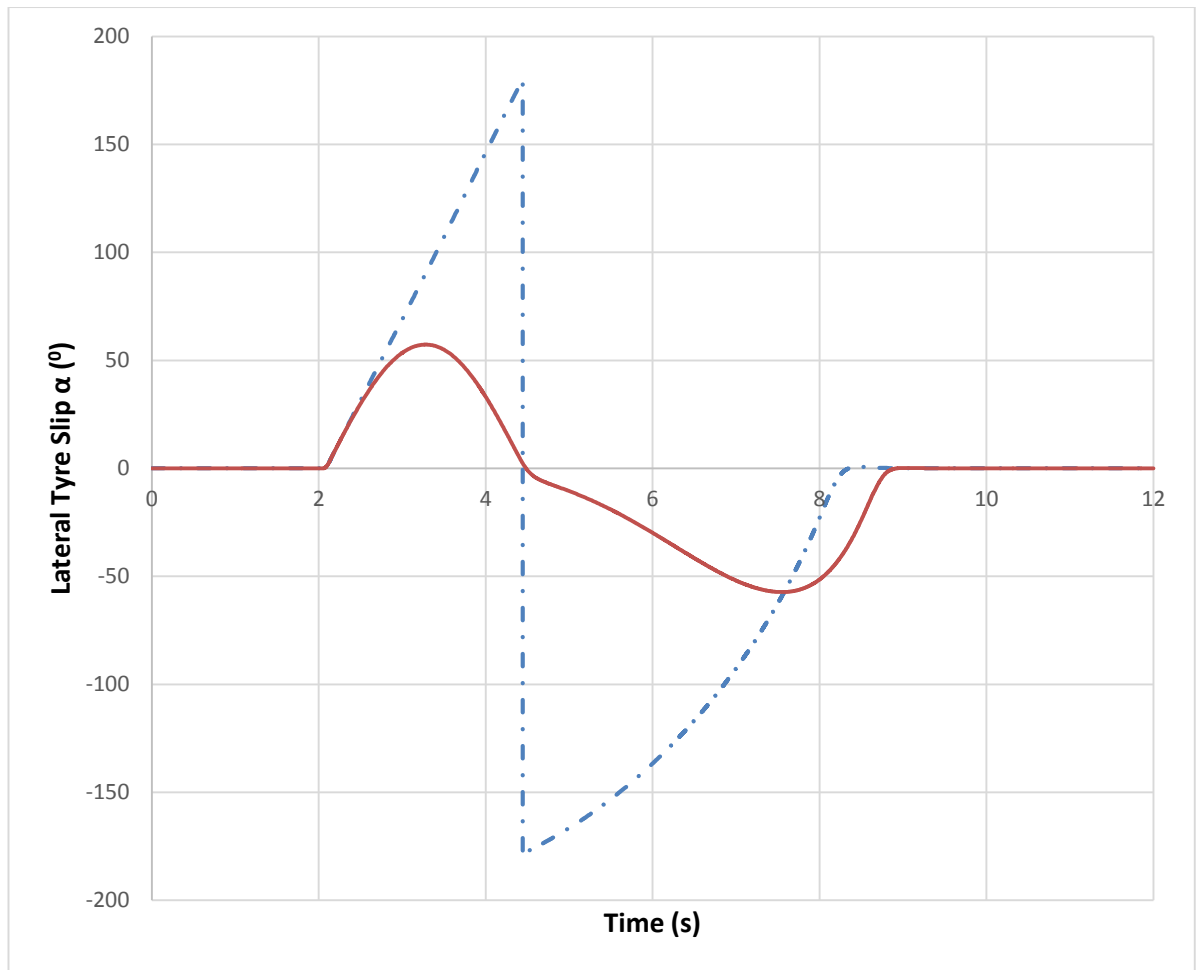
Figure 3.13: Comparison of front tyre slip angles during a 360⁰+ spin using the old and new extended tyre slip calculations

The two models transfer from one direction to the other at the same point. The difference is that Kim's model switching instantaneously from 180^0 to -180^0, whereas the new models switch from its maximum slip angle of 57.3^0 down through 0^0 to -57.3^0 in a more transient nature. Behaviour like this is expected as the tyre 'slips' from one direction to the other as the vehicle spins from being perpendicular to the direction of travel through to parallel and back to perpendicular. This results in a longer time for the model to stop spinning. This is because of the drop in generated force through the transition from positive to negative rather than the instantaneous switch of Kim's.

Figure 3.14 shows the heading angle against time for the two sets of equations for an incident that causes a spin that resulting in a final heading angle close to 180^0.

Peter Samuel Delves
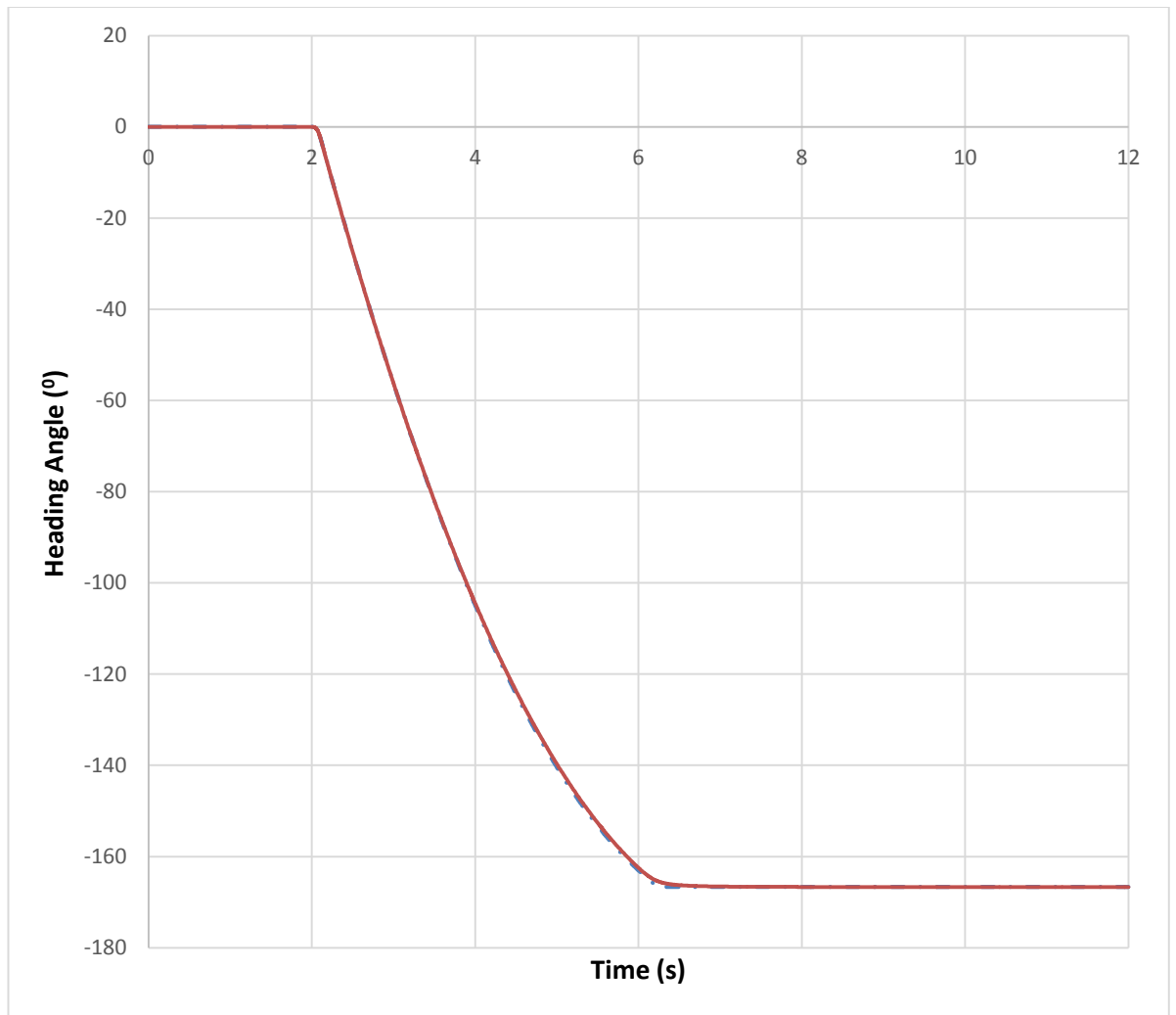
Figure 3.14: Comparison of original and new slip angle calculations showing the difference in heading angle change over time for an impact causing a 180^0 spin

Both simulations result in the vehicle stopping short of 180^0 at 168.6^0 and 168.4^0 for the new and old models respectively. Again the behaviour of both models is very similar, but this time the final settling angles are very close. It still takes longer for the new model to settle because of its transient behaviour about the settling point but the slip angles are not going through as extreme a change as in the 360^0 simulation. The next plot, Figure 3.15, shows the time slip angle relationship for this scenario.

53
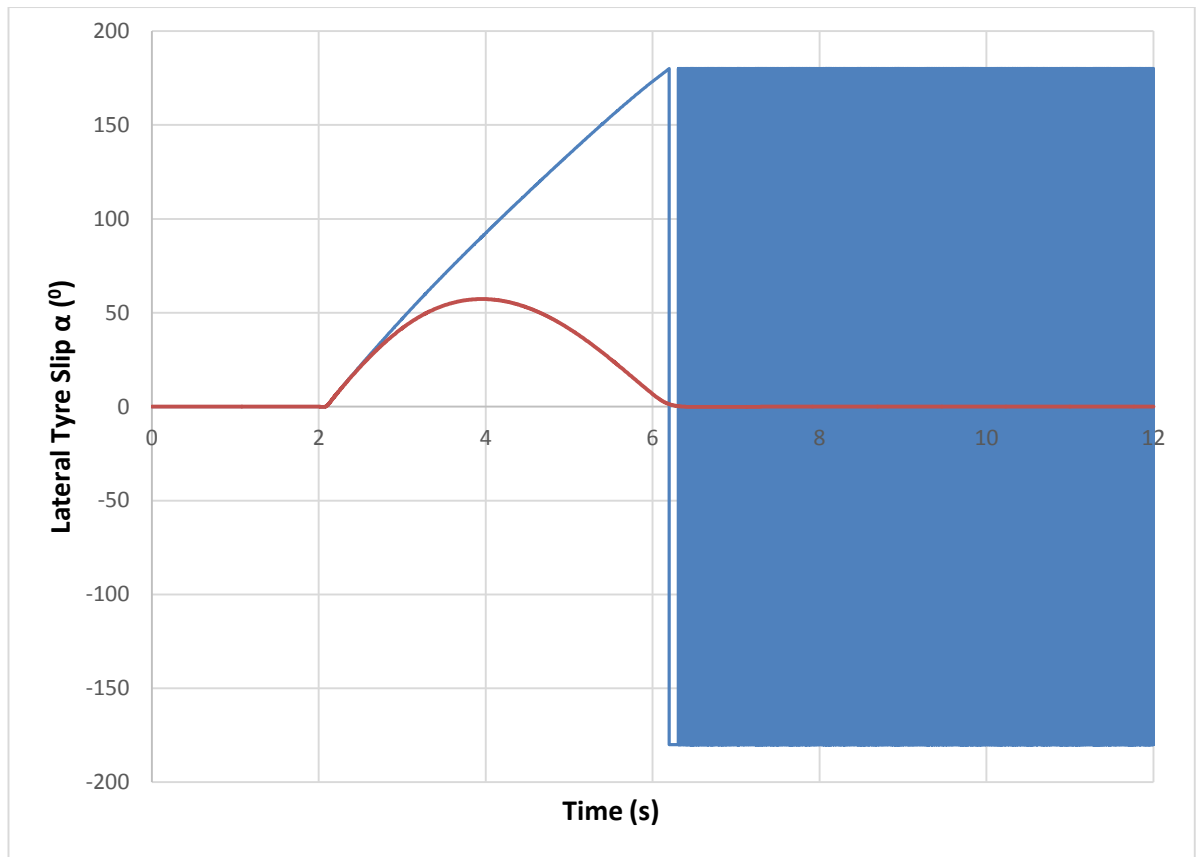
Figure 3.15: Comparison of front tyre slip angles during a 180^0 spin using the old and new extended tyre slip calculations

The new model rises to its maximum value and then curves down to 0^0 where it settles with the vehicle traveling backwards. Whereas the old model gets 'stuck' between 180^0 and -180^0 causing the tyre forces to rapidly oscillate from large positive to large negative force, which balance to give the illusion that the vehicle has settled. This not only causes the vehicle to be marginally stable but overwhelms any control inputs. This is the reason that the alteration to Kim's equations were needed.

This has solved the computational issue by returning to 0^0 when running backwards. This allows control to be applied in either positive or negative directions, as would be the case in a real life situation. It also allows the model to operate over a full 360^0 range.

Peter Samuel Delves

3.5. Model Validation

Three models were validated using two common dynamic steering manoeuvres. These allow comparison to be made between the three models, allowing the relationship between model complexity and model fidelity to be observed. The three models are: Linear 2-DOF bicycle model with cornering stiffness; Non-linear 7-DOF two track model with combined lateral and longitudinal slip Pacejka tyre model; Non-linear 8-DOF two track vehicle model with combined lateral and longitudinal Pacejka tyre model and quis-static weight distribution.

Simulation one is a steady state cornering test. A step steer is applied to the front wheel/s one second to induce a constant cornering radius. Simulation two is a lane change manoeuvre which is generated through a sinusoidal steering input. Simulations where carried out at longitudinal velocities from 10 to 40m/s to cover a representative dynamic range. Both simulations use the vehicle perimeters in appendix 2.

3.5.1. Steady State Cornering Simulation

The first manoeuvre was a step steer. This simulates a vehicle cornering at a constant radius allowing analysis of the models' steady state cornering. It is performed by applying a step input from 0-1° over one second. Figure 3.16 shows the step steer input signal used in Simulink. The input begins at one second to allow the models to initiate and ensure they have settled. Simulation time was set to 6 s to allow any transient behaviour to settle and the vehicle reach steady state.

Each vehicle was kept at a constant forward velocity. The 2-DOF model had a constant value allocated where the two models with longitudinal DOF required a negative feedback PI control loop to maintain a constant velocity. These controllers had a P gain of 100 and I gain of 5 to reduce any initial velocity drop to a minimum and settle the velocity within the model initiation period.

Peter Samuel Delves
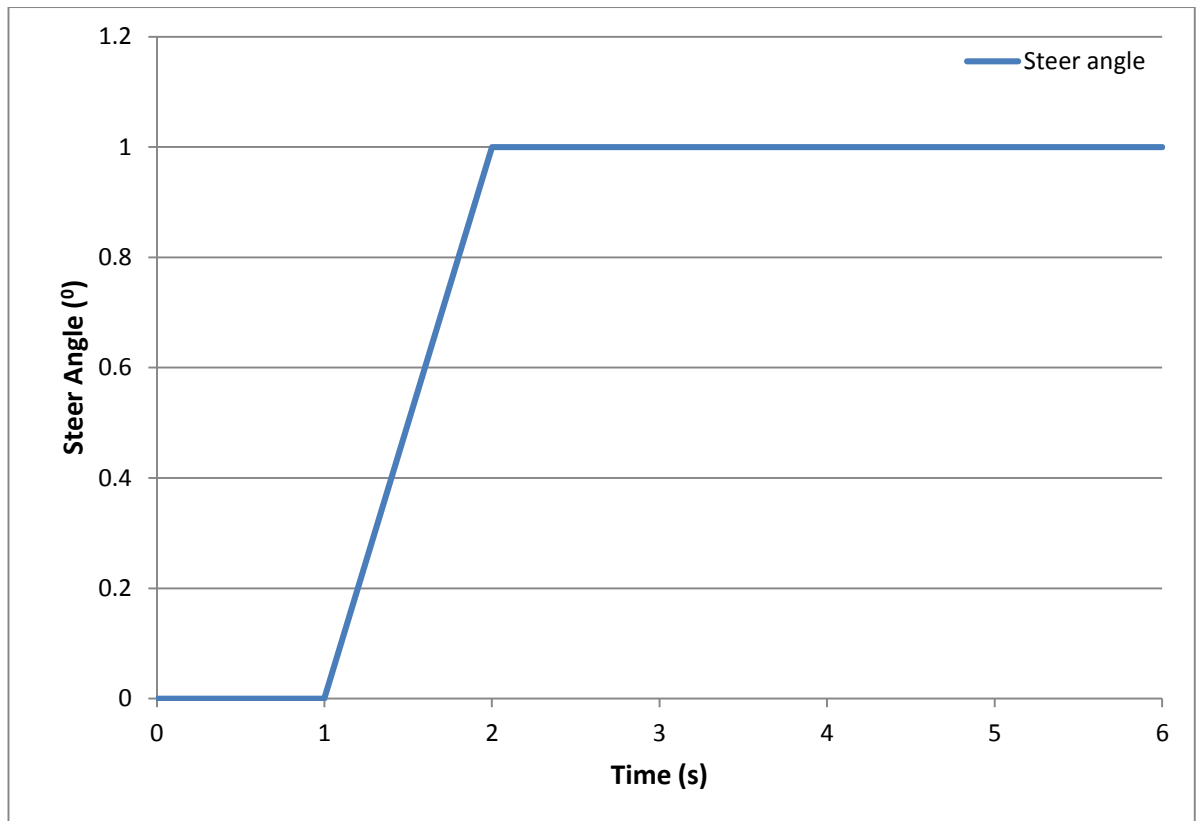
Figure 3.16: Step-steer input used in steady-state cornering validation manoeuvre

Peter Samuel Delves

3.5.1.1. Steady State Cornering Yaw Response Graphs
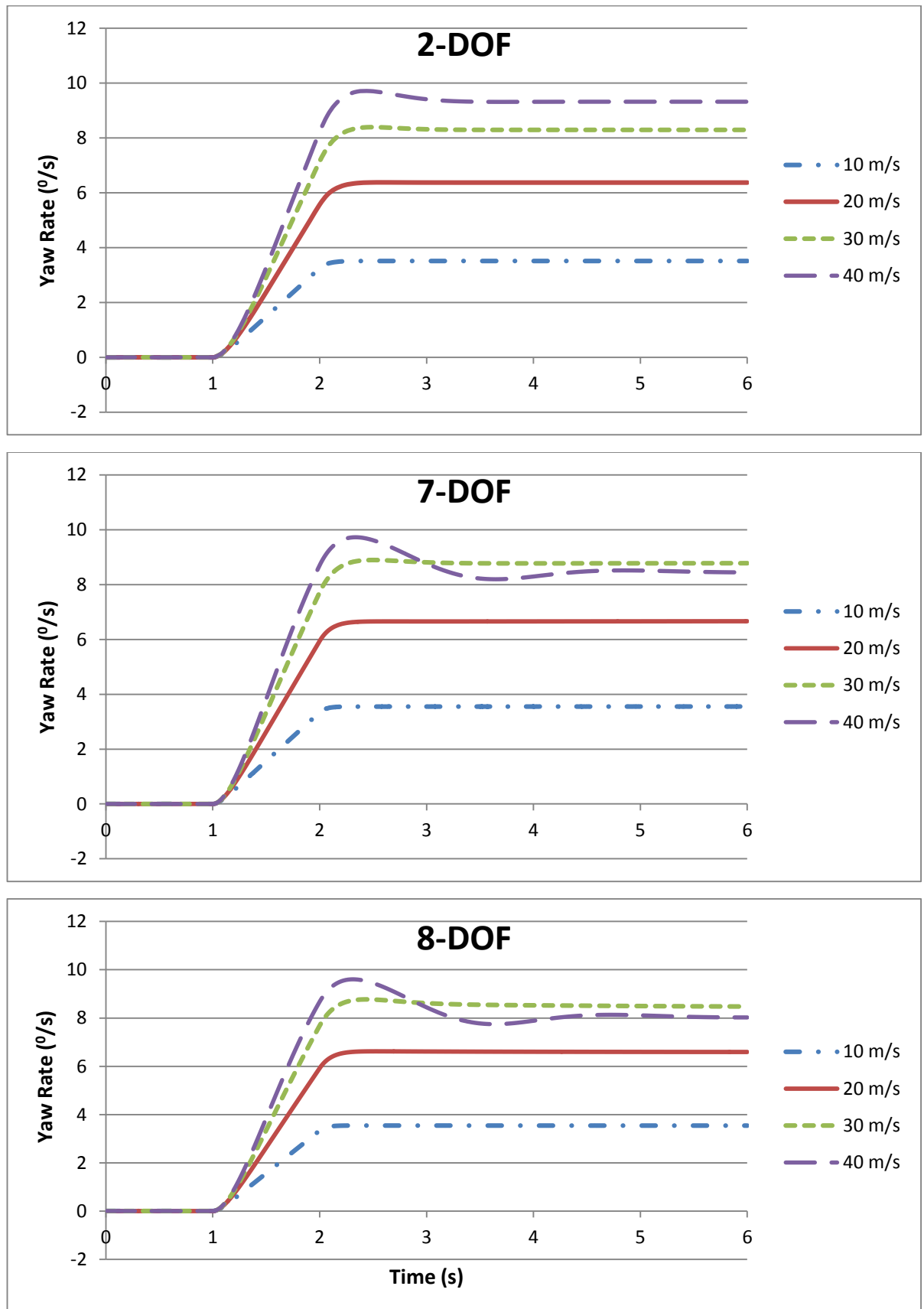
Figure 3.17: Yaw responses of the two, seven and eight DOF models for the steady-state cornering manoeuvre

Peter Samuel Delves

3.5.1.2. Steady State Cornering Lateral Acceleration Graphs
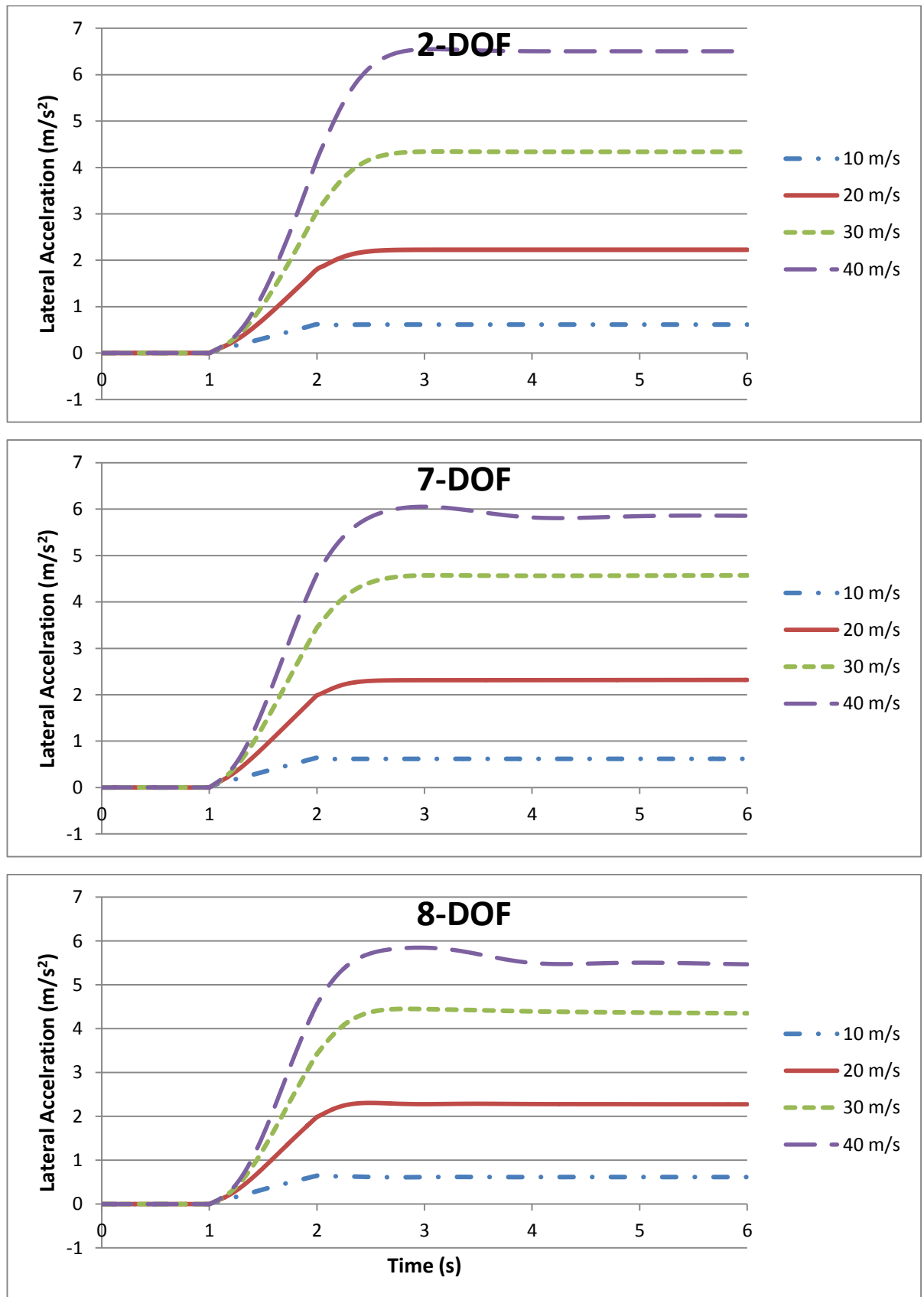
Figure 3.18: Lateral acceleration response of the two, seven and eight DOF models for the steady-state cornering manoeuvre

Peter Samuel Delves

3.5.1.3. Steady State Cornering Lateral Velocity Graphs
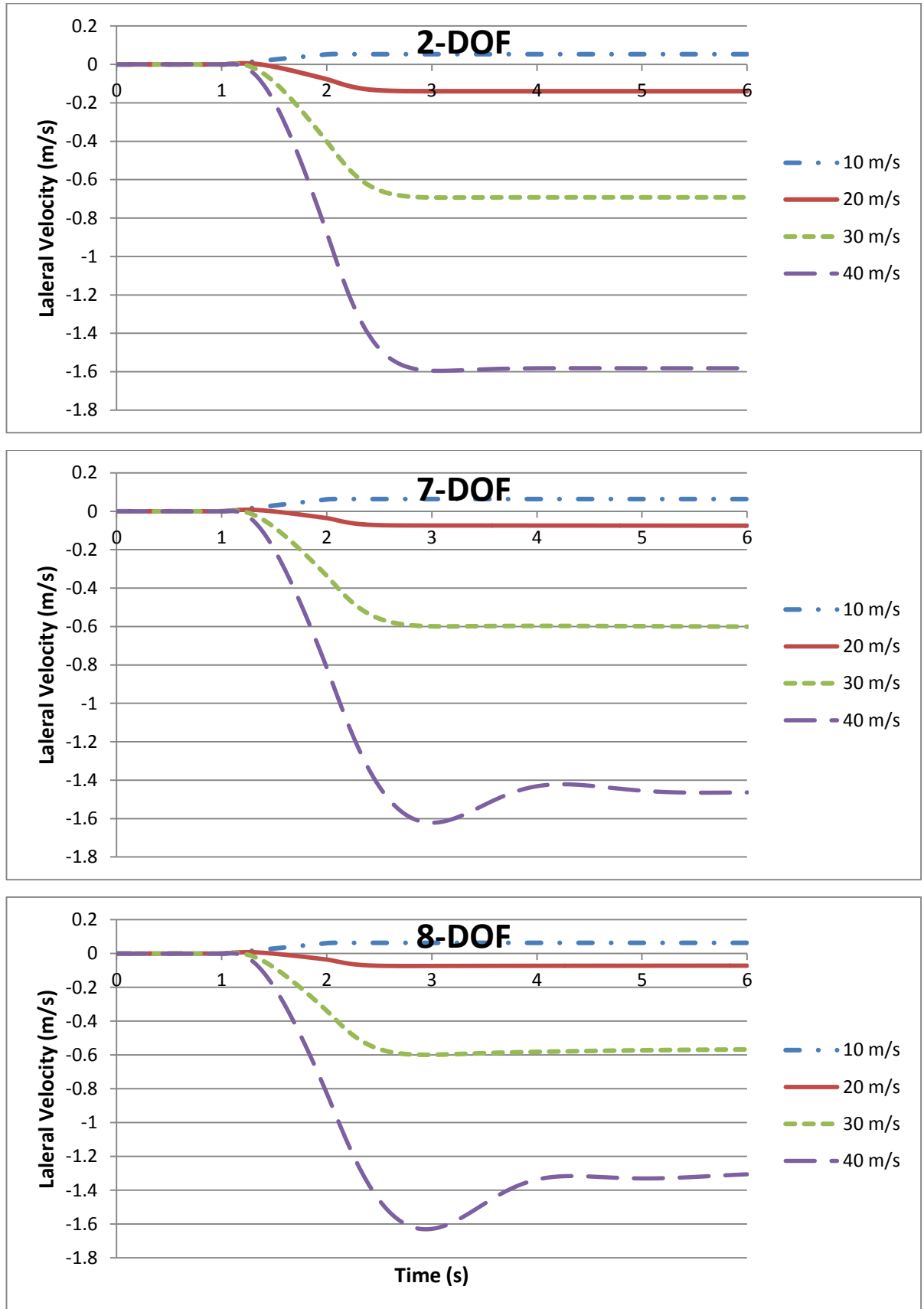
Figure 3.19: Lateral velocity response of the two, seven and eight DOF models for the steady-state cornering manoeuvre

Peter Samuel Delves

Figures 3.17, 3.18 and 3.19 show the yaw rate, lateral acceleration and lateral velocity response of a linear 2-DOF model, 7-DOF model and 8-DOF vehicle models respectively to a step steer manoeuvre. Tables 3.6, 3.7 and 3.8 compare the linear model's yaw, lateral acceleration and lateral velocity responses against that of the two non-linear models at steady state.

Table 3.6: Comparison of the steady state yaw rate response of the linear model against the non-linear models

Steady state Yaw Rate (^{0}/s)				
Test velocity (m/s)	10	20	30	40
Linear model 2-DOF	3.511	6.376	8.293	9.323
Non-linear model 7-DOF	3.554	6.664	8.784	8.446
Non-linear model 8-DOF	3.540	6.593	8.475	8.023
% difference between 2-DOF and 7-DOF models	-1.2%	-4.5%	-5.9%	9.4%
% difference between 2-DOF and 8-DOF models	-0.8%	-3.4%	-2.2%	13.9%

Table 3.7: Comparison of the steady state lateral acceleration response of the linear model against the non-linear models

Steady state Acceleration (m/s^2)				
Test velocity (m/s)	10	20	30	40
Linear model 2-DOF	0.612	2.225	4.340	6.505
Non-linear model 7-DOF	0.620	2.319	4.573	5.856
Non-linear model 8-DOF	0.615	2.276	4.352	5.468
% difference between 2-DOF and 7-DOF models	-1.2%	-4.3%	-5.4%	10.0%
% difference between 2-DOF and 8-DOF models	-0.4%	-2.3%	-0.3%	15.9%

Table 3.8: Comparison of the steady state lateral velocity response of the linear model against the non-linear models

Steady state Velocity (m/s)				
Test velocity (m/s)	10	20	30	40
Linear model 2-DOF	0.053	-0.140	-0.692	-1.582
Non-linear model 7-DOF	0.064	-0.075	-0.601	-1.464
Non-linear model 8-DOF	0.063	-0.072	-0.567	-1.306
% difference between 2-DOF and 7-DOF models	-20.4%	46.4%	13.2%	7.5%
% difference between 2-DOF and 8-DOF models	-20.4%	48.7%	18.1%	17.4%

Peter Samuel Delves

Immediately observable from Figures 3.17-3.19 is that at higher velocities the two non-linear models display oscillatory behaviour, which in turn increases their time to reach steady state then the linear model. Some of the simulations at 40m/s are still showing oscillatory behaviour at the end of the simulation. This is because as the velocity increases from 10 m/s (blue line) through to 40 m/s (purple line) the dynamic intensity of the manoeuvre increases and approaches the saturation point of the tyres.

The lateral acceleration produced by the 2-DOF model is up to 5.4% lower than that of the other two models at the lower velocities of 10-30m/s, but as the velocity increases to 40 m/s the acceleration produced switches to be 10% and 15.9% higher than the 7-DOF and 8-DOF models respectively. This highlights the need for a high fidelity non-linear model when working in high dynamic intensity regions.

The lateral velocity graphs show the largest variation in response between linear to non-linear models. At 40 m/s the 8-DOF and 7-DOF models' final steady state velocities are respectively 17.4% and 7.5% less than 2-DOF model, as seen in table 3.8. Interestingly the largest variations occur at lower velocities in this simulation. This is due in part to the 2-DOF model only having one track so any slide slip effects the vehicle experiences are exaggerated; hence the velocity change of over 60% from 10-20m/s in comparison to the other models. It is also the fact that at these speeds very small values of lateral velocity are produced so a small change can made a large difference.

Yaw rates are similar across all models up to 30 m/s with the greatest difference being between the 7-DOF and 2-DOF models, with the 7-DOF model's yaw rate being 5.9% greater than that of the 2-DOF model. The greatest variation is again seen at 40 m/s where the non-linear models have reached the point of tyre saturation, resulting in yaw rates that are 9.4-13.9% lower than the linear simulation results.

These simulations have shown that a linear model is adequate for simulation up to 30 m/s with a relatively simple manoeuvre as, apart from lateral velocities, results are within 5% of the non-linear models. This does agree with assertion in the literature that a linear model can be used for relatively simple manoeuvres at

Peter Samuel Delves

reasonably high velocity. But as velocities increase above this performance diverges as the non-linear region of the tyre curve is entered. The results of the 8-DOF model correlated with the results of Milehins, Cheng et al. (2010) 8-DOF model.

3.5.2. Lane Change Simulation

The lane change manoeuvre uses a sine wave input to simulate applying a steering angle in one direction then sweeping through to the other direction before returning to zero. It tests how a vehicle behaves when subjected to a change in direction. It also demonstrates how load transfer introduced by the roll DOF affects the vehicles transition from one direction to another.

Figure 3.20 shows the single sine wave input applied to each model's front wheels. The simulation was run for 2 s before any steering is applied so allow the model to initialise. The manoeuvre is performed at four speeds 10, 20, 30 and 40 m/s to test the models behaves in the low (0-0.3g) and high intensity (0.3+g) dynamic regions.
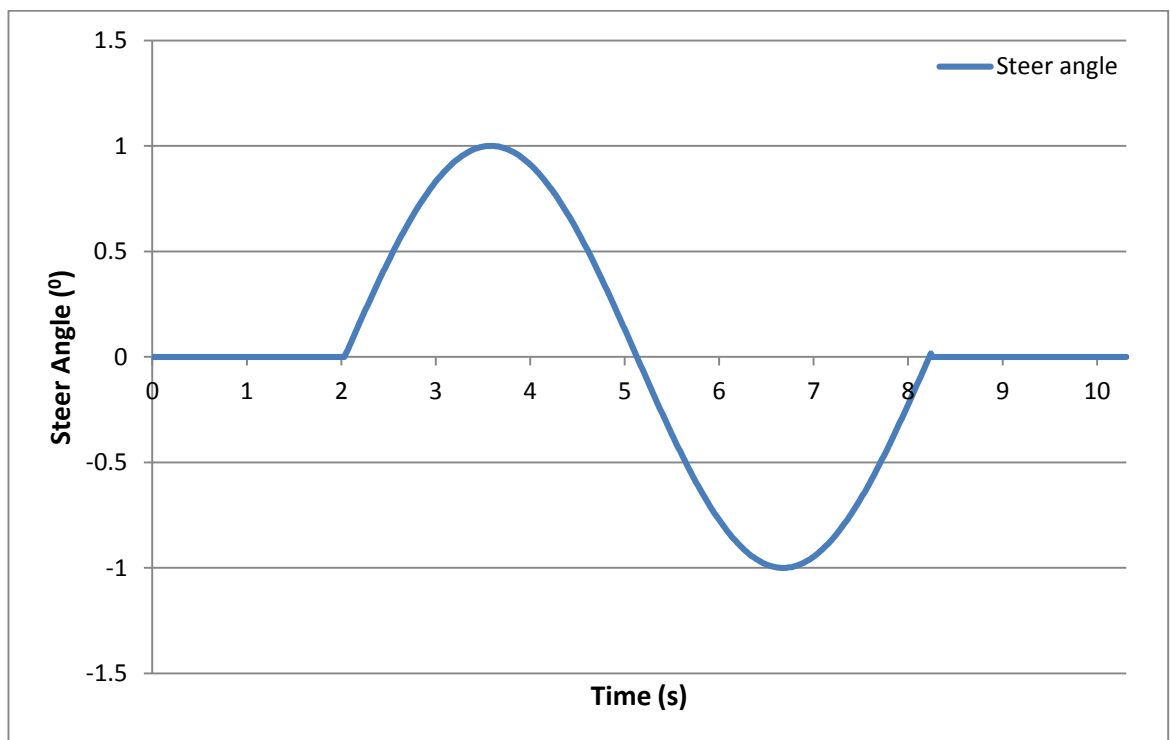
Figure 3.20: Sine steer input to simulate lane change manoeuvre

3.5.2.1. Lane Change Yaw Response
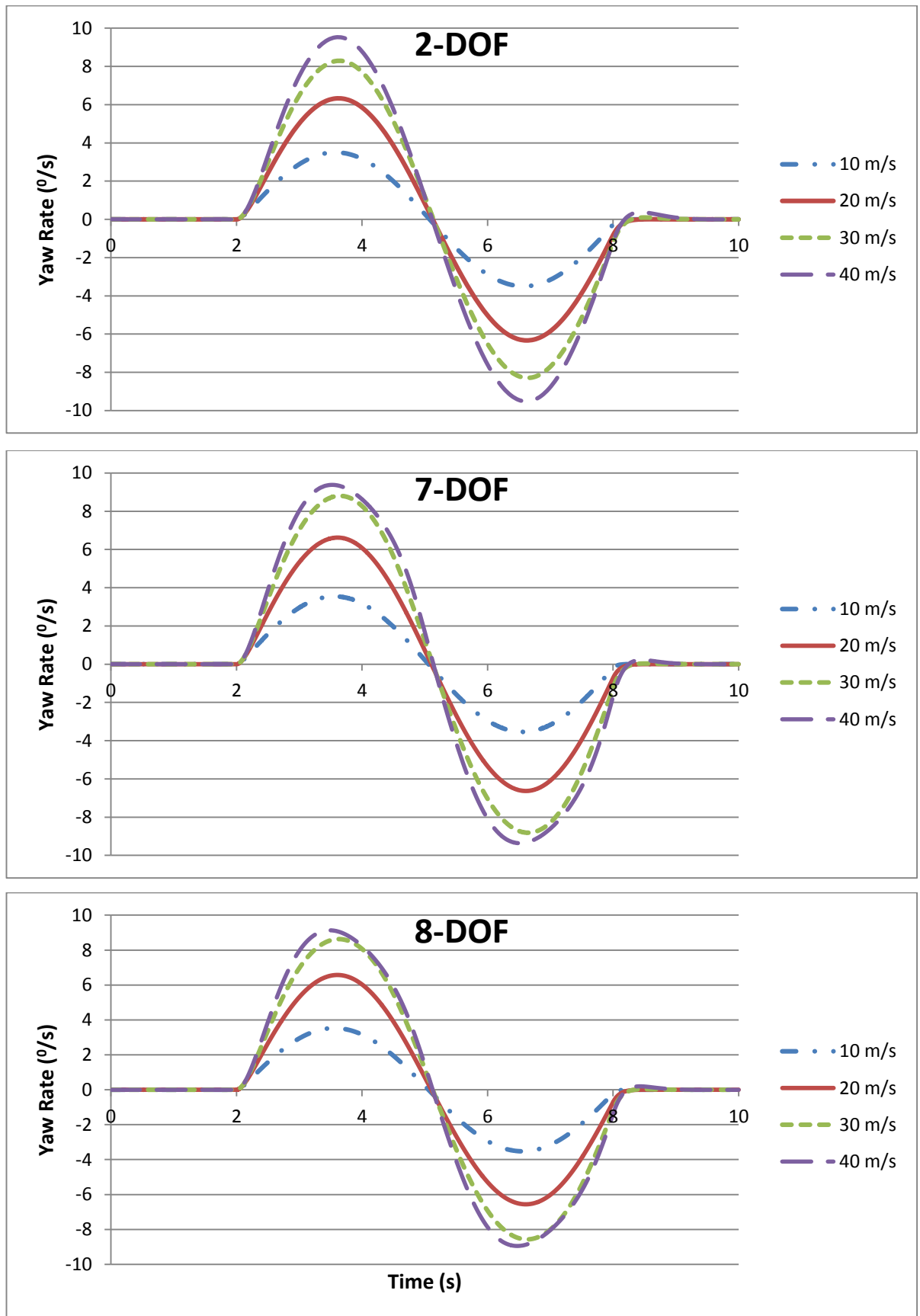
Figure 3.21: Yaw response to a lane change manoeuvre for two, seven and eight DOF model

63

3.5.2.2. Lane Change Lateral Acceleration Response
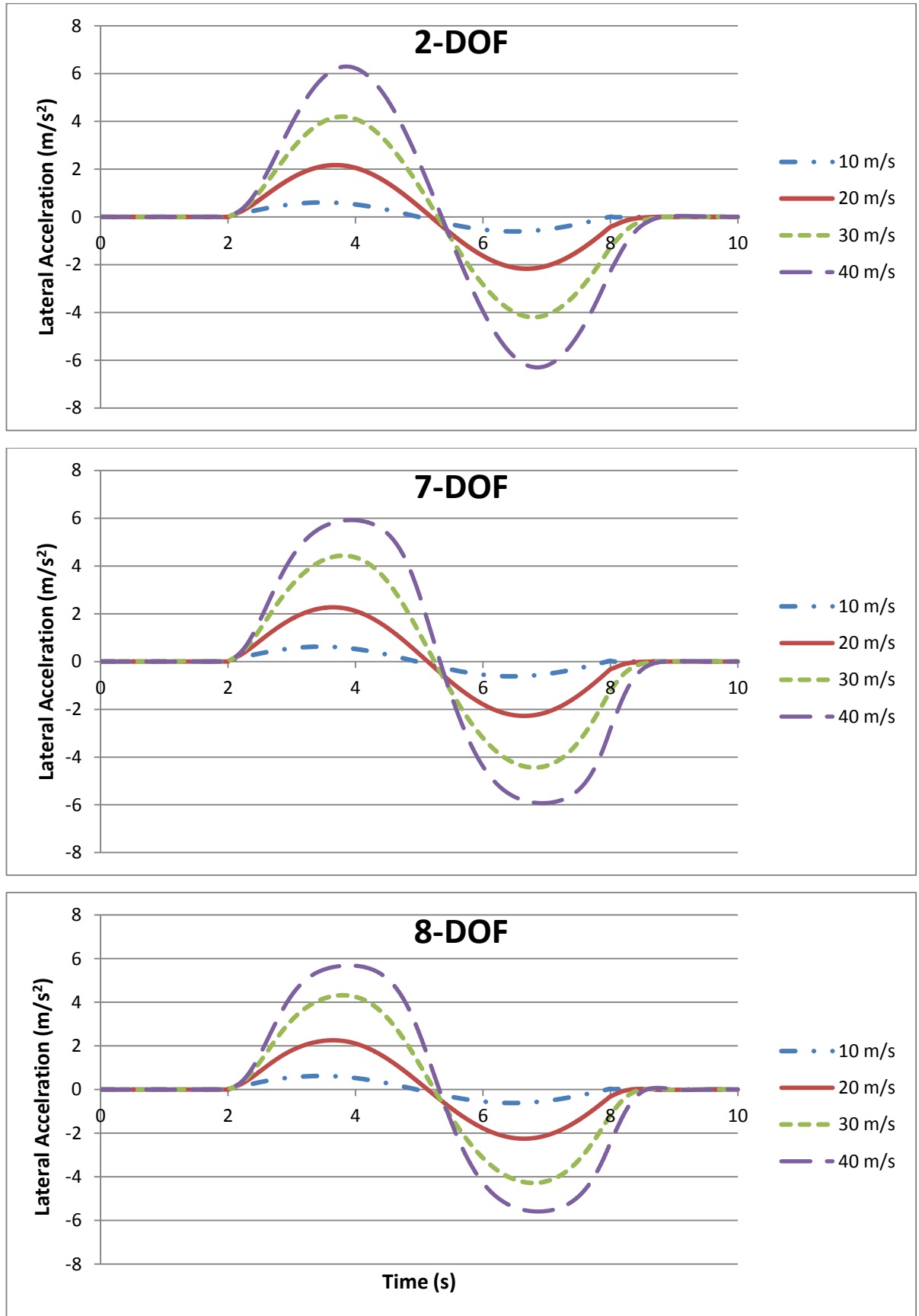
Figure 3.22: Lateral acceleration response to a lane change manoeuvre for two, seven and eight DOF model

64

3.5.2.3. Lane Change Lateral Velocity Response
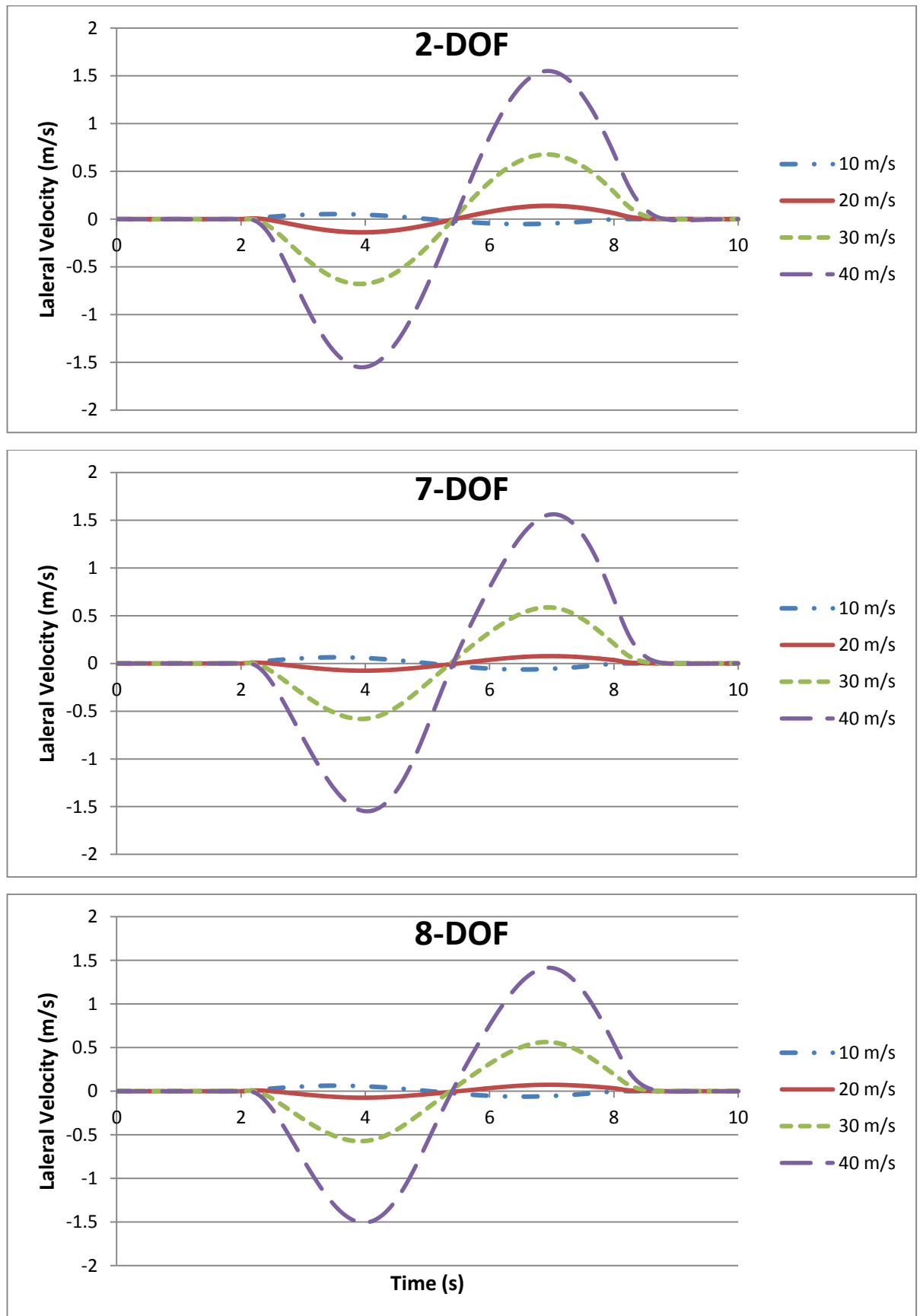
Figure 3.23: Lateral velocity response to a lane change manoeuvre for two, seven and eight DOF model

Peter Samuel Delves

Table 3.9: Comparison of sign steer manoeuvres yaw rate response of the linear model against the non-linear models

Steady state Yaw Rate (^{0}/s)					
Test velocity (m/s)		10	20	30	40
Linear model 2-DOF	Max	3.500	6.328	8.285	9.519
	Min	-3.497	-6.337	-8.297	-9.525
Non-linear model 7-DOF	Max	3.547	6.622	8.806	9.384
	Min	-3.551	-6.630	-8.816	-9.369
Non-linear model 8-DOF	Max	3.533	6.573	8.632	9.137
	Min	-3.532	-6.561	-8.572	-8.943
% difference between 2-DOF and 7-DOF models	Max	-1.3%	-4.6%	-6.3%	1.4%
	Min	-1.5%	-4.6%	-6.3%	1.6%
% difference between 2-DOF and 8-DOF models	Max	-0.9%	-3.9%	-4.2%	4.0%
	Min	-1.0%	-3.5%	-3.3%	6.1%

Table 3.10: Comparison of sign steer manoeuvres lateral acceleration response of the linear model against the non-linear models

Steady state Acceleration (m/s^2)					
Test velocity (m/s)		10	20	30	40
Linear model 2-DOF	Max	0.609	2.168	4.193	6.291
	Min	-0.610	-2.165	-4.187	-6.300
Non-linear model 7-DOF	Max	0.619	2.271	4.428	5.919
	Min	-0.620	-2.277	-4.443	-5.927
Non-linear model 8-DOF	Max	0.619	2.258	4.323	5.688
	Min	-0.620	-2.254	-4.289	-5.593
% difference between 2-DOF and 7-DOF models	Max	-1.6%	-4.8%	-5.6%	5.9%
	Min	-1.7%	-5.2%	-6.1%	5.9%
% difference between 2-DOF and 8-DOF models	Max	-1.6%	-4.2%	-3.1%	9.6%
	Min	-1.7%	-4.1%	-2.4%	11.2%

Table 3.11: Comparisons of sign steer manoeuvres lateral velocity response of the linear model against the non-linear models

Steady state Velocity (m/s)					
Test velocity (m/s)		10	20	30	40
Linear model 2-DOF	Max	0.053	0.140	0.677	1.551
	Min	-0.053	-0.140	-0.678	-1.551
Non-linear model 7-DOF	Max	0.064	0.077	0.588	1.563
	Min	-0.064	-0.076	-0.582	-1.549
Non-linear model 8-DOF	Max	0.064	0.074	0.562	1.416
	Min	-0.064	-0.074	-0.574	-1.507
% difference between 2-DOF and 7-DOF models	Max	-20.3%	45.0%	13.1%	-0.8%
	Min	-20.1%	45.6%	14.1%	0.1%
% difference between 2-DOF and 8-DOF models	Max	-20.3%	47.4%	17.0%	8.7%
	Min	-20.1%	46.8%	15.3%	2.9%

Tables 3.9, 3.10 and 3.11 show the maximum and minimum values for each model and compare the linear model's results with those of the two non-linear models.

Figures 3.21, 3.22 and 3.23 show the responses to a sinusoidal steer manoeuvre of the linear 2-DOF, non-linear 7-DOF, and non-linear 8-DOF vehicle models.

It is important to note that at lower velocities, when a vehicle is in its linear region, the behaviour of all the models is very similar. As previously mentioned this makes the linear model arguably the most sensible choice for low intensity dynamic simulations. But as simulation velocities increase a higher fidelity model is required.

Lateral accelerations' maximum/minimum values are varying by 10-12% in between the 30 and 40m/s results as seen in table 3.10. This difference is a result of an initial higher linear stiffness region in the tyre model meaning the non-linear models actually generate higher velocities. The models then transition into their saturation region, where the force produced is limited, and the linear models' results increase above those of the non-linear models.

The largest variation from model to model is seen in the lateral velocity response. This is due to the non-linear models being two-track models (taking the width of the vehicle into account) with the centre of gravity between the two-tracks in contrast to the 2-DOF 'bicycle' single-track model where the centre of gravity is right between the wheels. This results in large variations especially at low vehicle speeds where the sign is inverted from a two-track to a single-track model. In contrast to the lateral acceleration and yaw rate results the lateral velocities largest percentage difference occurs during the 20 m/s simulation where there is a 45-48% difference.

Yaw rates are the same magnitude difference as the lateral acceleration percentages up to 30m/s. The linear model's yaw rates are 0.9-6.3% lower at low velocities, but again become 1.4-6.1% greater than the non-linear models at higher velocities because the non-linear tyre model reaches its saturation region.

The effects of weight distribution are seen when comparing the results of the seven and 8-DOF models. At 30m/s the 7-DOF model generates 0.1 m/s^2 more peak maximum and peak minimum values increasing to 0.3m/s^2 at 40m/s. The effects of weight transfer can be seen when comparing maximum and minimum values for the 8-DOF model as the values are not equal and opposite as with those of the 7-DOF

Peter Samuel Delves

vehicle. Although a marginal difference of 0.14m/s^2 is observed, it is evident that as peak lateral acceleration increases the effects of weight distribution become more important.

The 8-DOF model's results correlate with the results presented by Milehins, Cheng et al. (2010).

3.6. Vehicle Modelling Discussion

The chapter develops and validates an 8-DOF model for use for the final control simulations. It was developed in 3 phases producing a 2-DOF linear, 7-DOF non-linear and 8-DOF non-linear model.

The three models were compared through two handling manoeuvres to assess the variations in performance between the models at a variety of speeds. Manoeuvre one assessed steady state cornering behaviour of the models, where manoeuvre two tested the behaviour of the vehicle in a lane change manoeuvre. These were selected as they produced steady state and dynamic behaviours respectively.

At low velocities the lateral acceleration values are within 2% of each other but do diverge as velocity increases where differences of 6-16% are seen at 40m/s. Yaw rate responses follow a similar pattern to the accelerations with lower velocity steady state responses correlating closely and diverging as the velocity increases.

The largest variation was observed in the lateral velocity state where at 20 m/s the linear model's values were 46-48.7% higher than the non-linear models. As speed increased to 30m/s and 40m/s the difference reduced to roughly 7.5-18.1%. Although this is an improvement, it demonstrates that across a standard vehicle's dynamic range there are large variations in response between the linear and non-linear models.

On closer observation of the steady state cornering graphs it takes longer for the non-linear models to settle over the linear model. The time that it takes for the non-linear models to settle increases as velocity increases taking up to 3-4 s to reach steady state at 40 m/s.

Peter Samuel Delves

Analysing the graphical response of the lane change manoeuvre the non-linear model's responses lag behind that of the linear models. As with the step steer manoeuvre this becomes more exaggerated as forward velocity is increased. This manoeuvre also reveals how the addition of the roll DOF affects vehicle behaviour, displaying notable differences compared to the 7-DOF model with larger variations observed as lateral acceleration values increase.

These results enforce the assertions in the literature that for studies assessing steady state and low intensity dynamics a less computationally intense 2-DOF model is a valid choice, but as studies start to look at manoeuvres involving high dynamic intensity a non-linear model is required.

As the final control study is analysing control of a vehicle which experiences a large disturbance force inducing large lateral accelerations, the 8-DOF model is the best candidate for this study. To validate this model, results where compared visually against the 8-DOF model presented in Milehins, Cheng et al. (2010). On visual inspection, the responses correlated closely showing similar dynamic behaviour. A Simulink diagram of the full 8-DOF model can be seen in appendix 4.

Peter Samuel Delves

4. Chapter Four: Vehicle Model Crash Simulation

Chapter 4 details the additions made to the 8-DOF model so that the vehicle's trajectory could be analysed in the global co-ordinate system. The global co-ordinate system equations were then tested using the same step steer and lane change manoeuvres used in chapter 3. Vector analysis is carried out to calculate the momentum exchange between the impactor and target vehicles, which in turn are used to calculate crash impulse forces used in the crash simulations. These forces are calculated for two different velocities, 2.5m/s and 5m/s, and three impact angles of 10^0, 20^0 and 30^0 for each velocity. The model was then simulated using two crash scenarios, a rear impact and a side-swipe impact, resulting in 12 simulations in total. Vehicle trajectories, yaw rate vs yaw position and lateral acceleration graphs were plotted to analyses the vehicles behaviour with no control intervention.

Peter Samuel Delves

4.1. Introduction

Crash scenarios considered in this work involve high intensity dynamics with impact forces exceeding 1g, necessitating the use of the 8-DOF model developed in chapter 3. This chapter details the final additions made to the model to allow analysis of the vehicles trajectory during an incident. This involved implementing a set of global co-ordinate equations and crash-force impulse calculations.

The global co-ordinate system was integrated into the model from chapter 3 using the lateral and longitudinal tyre forces and combining them with the heading angle. This set of equations was essential for the final analysis and comparison of post-impact trajectories carried out at the end of this chapter and in chapter 5. These new equations were then tested using the same step-steer and lane change manoeuvres from sections 3.5.1 and 3.5.2 respectively. Their trajectories were plotted to assess if the global co-ordinate system was working correctly. The plots for the steady state steer resulted in constant radius turns and the lane change resulted in a lateral displacement that then stabilised at a constant lateral displacement, as if it had performed a lane change confirming that the global co-ordinate system equations were working correctly.

Crash-force impulse calculations were carried out using momentum theory combined with a coefficient of restitution to estimate the energy loss during the impact. This allowed triangular crash impulses to be calculated for application to the model. These were calculated for 3 impact angles of 10^0, 20^0 and 30^0 at velocities of 2.5m/s and 5 m/s.

These crash impulses were used to simulate a rear impact and side-swipe impact totalling 12 simulation. The results produced a spread of, trajectories, peak yaw rates, lateral accelerations and final heading angles allowing analysis of the model's behaviour over a large range. These results were comparable with results presented by Zhou, Peng et al. (2008).

Peter Samuel Delves

4.2. Model Expansion

4.2.1. Global Co-Ordinate System

To analyse the true trajectory of the vehicle global, co-ordinates need to be calculated. This is formulated around longitudinal (F_{xi}) and lateral (F_{yi}) forces from the vehicle model constructed in section 3.2 and by tracking the vehicle's heading angle ψ. This is expressed as:

$$\dot{U} = \frac{\left(F_{xfr} + F_{xfl} + F_{xrr} + F_{xrl}\right)cos\Psi - \left(F_{yfr} + F_{yfl} + F_{yrr} + F_{yrl}\right)sin\Psi}{m} \quad (4.1)$$

$$\dot{V} = \frac{\left(F_{xfr} + F_{xfl} + F_{xrr} + F_{xrl}\right)sin\Psi - \left(F_{yfr} + F_{yfl} + F_{yrr} + F_{yrl}\right)cos\Psi}{m} \quad (4.2)$$

Where $\dot{U}$ and $\dot{V}$ represent global longitudinal and lateral accelerations respectively.

4.2.2. Global Co-Ordinate Validation (Step Steer)

The same step steer manoeuvre used in the validation simulations in sections 3.5.1 is used and is summarised as follows:

Local longitudinal velocity v_x is set at 20, 30 and 40 m/s and is kept constant using negative feedback PI control. Steering is applied smoothly over one second from 0-1^0. Once the steer angle reaches 1^0 it held constant. The first simulation is run for 6 s in total with a one second model initiation time before any steering is applied. The second simulation extends the simulation time by 80 s.

Peter Samuel Delves
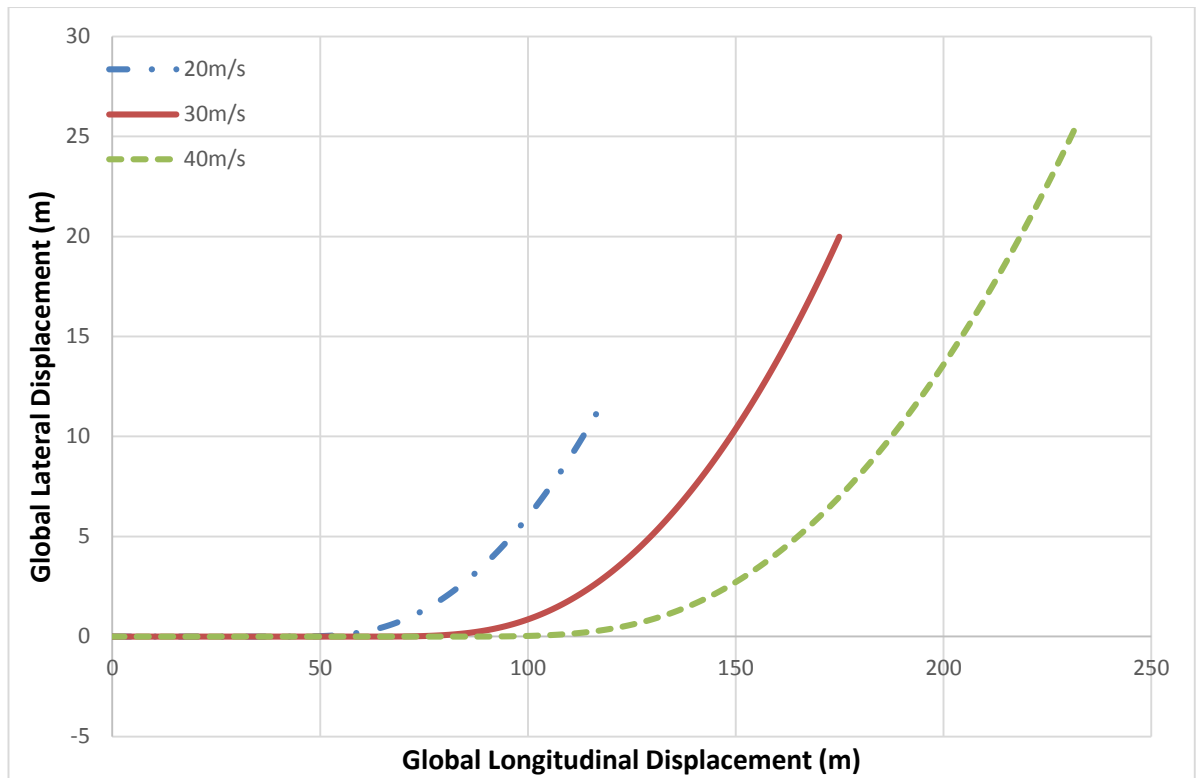
Figure 4.1: Trajectory of simulated vehicles during a steady state cornering manoeuvre performed at 20, 30 and 40 m/s for six seconds.
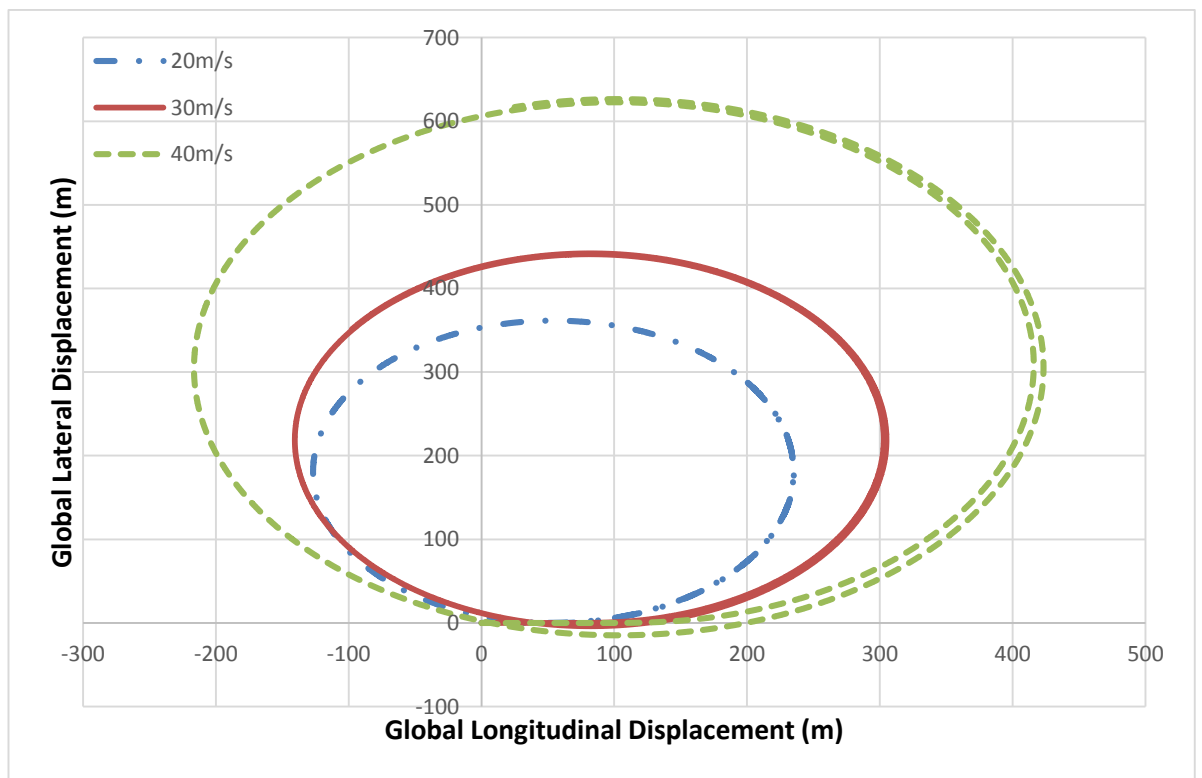
Figure 4.2: Trajectory of simulated vehicle during a steady state cornering manoeuvre performed at 20, 30 and 40 m/s for 80 seconds.

73

Peter Samuel Delves

As steering is applied there is an initial transition period as lateral velocity increases and the vehicle settles into the corner as shown in the velocity plot graphs in section 3.5.1.2. Once the vehicle has settled, it continues to corner at a radius as seen in Figure 4.2

As is to be expected as velocity increases, the diameter of turn increases. At 20 m/s the diameter is approximately 420 m whereas at 40 m/s this diameter increases to around 765 m. The increase in diameter does not have a linear relationship. As at 30 m/s its turning circle is 548 m an increase of 128 m from 20 m/s whereas the increase in diameter from 30 to 40 m/s is 217 m. This is due to the vehicle entering its non-linear region. This behaviour is also explained by the drop in yaw rate between 30 to 40 m/s, shown by the simulation results in 3.5.1.1.

4.2.3. Global Co-Ordinate Validation (Lane Change)

The lane change manoeuvre is the same as in section 3.5.2 where a sine steer is input to the front wheels causing the vehicle to initially yaw and accelerate laterally and then steer in the opposite direction, resulting in the vehicle traveling at its original heading angle having displaced laterally (changing lane). The initial simulation was carried out with the following initial conditions:

Local velocity is set at 30 m/s and kept constant using negative feedback PI control. Steering angle starts at 0^0 increased steadily to 1^0, it is then decreased to -1^0 before returning to 0^0. This is all done in one smooth action following a single sine wave shape. The simulation is run over 10 s with a 2 s model initiation time before any steering is applied.

Peter Samuel Delves

Chapter Four: Vehicle Model Crash Simulation

Results of the lane change manoeuvre are presented in Figure 4.3:
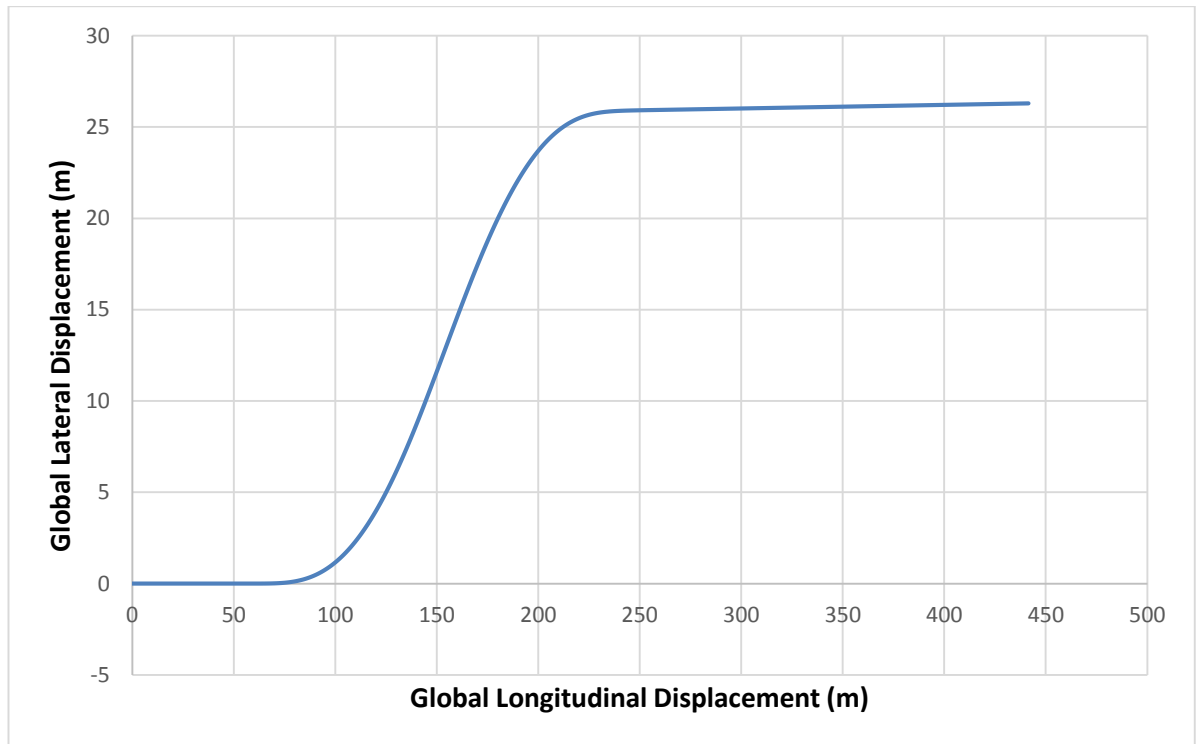
Figure 4.3: Trajectory of simulated vehicle performing a lane change manoeuvre at 30 m/s with a steer angle swept from ±1^0

Figure 4.3 shows the 2 s initiation period where the manoeuvre begins at 60 m longitudinal displacement. The vehicle moves laterally by a total of 26.27 m having travelled around 130 m longitudinally. At motorway speeds these values are to be expected.

The average lane width on UK roads is 3.7 m and the front wheel steer input of 1^0 is large at motorway speed. This demonstrates that when traveling at motorway speeds, small disturbances, in this case the application of steering, cause large displacements. This is also the case when impact force disturbances are applied and is seen later on in the crash model study, section 4.4, later on in this chapter.

The addition of this global co-ordinate system allows the vehicle's trajectory to be analysed.

Peter Samuel Delves

4.3. Crash Force Calculations

To calculate impulse forces vector analysis was carried out to calculate velocity components. This then allowed the momentum exchanged (M) between the impactor and target vehicles.

Two realistic motorway overtaking velocities were selected, which will be known as the disturbance velocity (Vd) for this study. The two Vd values are 2.5 and 5 m/s (5.59 and 11.19 mph respectively). The Disturbance velocities were spilt into longitudinal (Vxd) and lateral (Vyd) components from the Vd vector at three angles of incidence (θ^d) 10^0, 20^0 and 30^0. Results of the component velocity calculations are presented in Table 4.1 below:

Table 4.1: Relative longitudinal and lateral velocity components between bullet and object vehicles

			Angle of incidence (^{0})		
			10	20	30
Vd = 5 m/s	Velocity (m/s)	Vxd	4.924	4.698	4.33
		Vyd	0.868	1.701	2.5
Vd = 2.5 m/s		Vxd	2.462	2.349	2.165
		Vyd	0.4341	0.855	1.25

After the relative pre-impact velocities between the vehicles were calculated the post impact velocities were worked out. As modern vehicles are designed to deform during a collision absorbing some energy means that the collision is not perfectly elastic (some of the crash energy is dissipated). The effects of this energy dissipation are applied using a coefficient of restitution e. Genta (1997) and Zhou, Peng et al. (2008) state that e is commonly in the region of 0.05-0.2 and 0-0.3 respectively. A value of 0.2 was used, as it was assumed that the collision occurred between two identical vehicles (Zhou, Peng et al. 2008). This value of e was then used in the following equations from Genta (1997) to estimate the post-impact velocities of the target vehicle:

$$V_{x2} = V_{x1} + m_2 . V_{xd} \frac{1 + e}{m1 + m2} \qquad (4.3)$$

Peter Samuel Delves

$$V_{y2} = V_{y1} + m_2 . V_{yd} \frac{1+e}{m1+m2} \qquad (4.4)$$

Where V_{x1} and V_{y1} are the pre-impact longitudinal and lateral velocity of the target vehicle = 29 m/s and 0 m/s respectively. V_{x2} and V_{y2} are the post-impact velocities values of which are shown in table 4.3 when Vd = 5 and 2.5 m/s:

Table 4.2: Post-impact velocity components of target vehicle

			Angle of incidence (⁰)
			10	20	30
Vd = 5 m/s	Velocity (m/s)	Vx2	31.9544	31.8188	31.598
		Vy2	0.5208	1.0206	1.5
Vd = 2.5 m/s		Vx2	30.4772	30.4094	30.299
		Vy2	0.26046	0.513	0.75

Once these velocity components were found, the momentum impulse of the impact was calculated using the changes in longitudinal $V_{x2} - V_{x1}$ and lateral $V_{y2} - V_{y1}$ velocities. The study is only interested in the target vehicle so the equations for the momentum impulse for the longitudinal (Moxd) and lateral (Moxd) are,

$$Moxd = m_2(V_{x2} - V_{x1}) \qquad (4.5)$$

$$Moyd = m_2(V_{y2} - V_{y1}) \qquad (4.6)$$

The velocity components from Table 4.2 were then used to calculate the momentum impulses for the six scenarios in Table 4.3.

Table 4.3: Momentum exchange between bullet and target vehicle in longitudinal and lateral directions.

			Angle of incidence (⁰)
\multicolumn{3}{l}{Momentum transfer gained by target vehicle}	10	20	30
Vd = 5 m/s	Momentum (Ns)	Moxd	7238.28	6906.06	6365.1
		Moyd	1275.96	2500.47	3675
Vd = 2.5 m/s		Moxd	3619.14	3453.03	3182.55
		Moyd	638.127	1256.85	1837.5

The model requires a crash force input in Newtons. Therefore, momentum must be divided by an impulse time, which is determined as:

$$\frac{M}{t} = F \qquad (4.7)$$

The impulse time is the time taken to transfer the momentum energy from the bullet to the target (i.e. the time that the two vehicles are in contact). However, a step pulse is not the ideal way to imparting these momentum forces as modern vehicular bodies are designed to crush. A more suitable pulse shape is triangular as in Figure 4.4. The vehicle body deforms up to the peak force then when the crumple zone is fully compressed, the two vehicles start to detach until they are no longer in contact:

$$\frac{M}{t/2} = F \qquad (4.8)$$

For this simulation crash impulse time t is assumed to be 0.15 s (time the two vehicles are in contact) as used in Byung-joo Kim and Peng (2012), Byung-joo Kim and Peng (2014).The final crash impulse forces are presented in Table 4.4.

Table 4.4: Force input needed to impart momentum calculated in table 4.3 with an impact time of 0.15s with a triangular impulse.

Peak force input for momentum impulse (target)			Angle of incidence (^{0})		
			10	20	30
Vd = 5 m/s	Force (N)	Fxd	96510.4	92080.8	84868
		Fyd	17012.8	33339.6	49000
Vd = 2.5 m/s		Fxd	48255.2	46040.4	42434
		Fyd	8508.36	16758	24500

Peter Samuel Delves
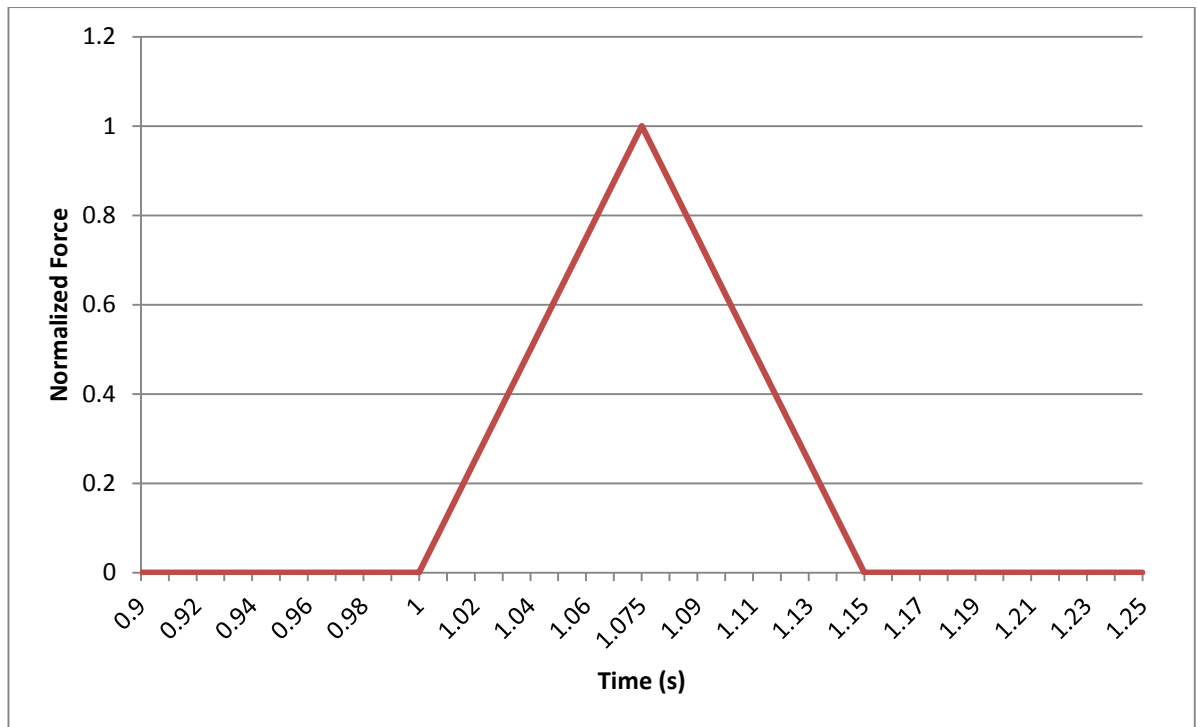
Figure 4.4: Triangular crash impulse applied to vehicle model.

Now that the required impulse force peaks have been calculated the uncontrolled response of the vehicle model was analysed and validated against the work in Byung-joo Kim and Peng (2012), Byung-joo Kim and Peng (2014).

4.4. Crash Model Study

To validate the extended model two crash scenarios have been simulated to test that the model's behaviour is as expected. They are: rear impact and side swipe impacts.

These two scenarios are common in motorway driving incidents. Both scenarios generate yaw moments and lateral acceleration, which induce the vehicle into a spin. This is undesirable as it dramatically increases the chance of a secondary collision with another object, as the vehicle moves across other lanes of traffic, either another vehicle or a static object, increasing the risk of serious injury.

Both impacts are implemented on the model as a triangular impulse signal for 0.15 s as shown in Figure 4.4 (Byung-joo Kim and Peng 2012, Byung-joo Kim and Peng 2014).The magnitude of this impulse represents the momentum exchanged between the two vehicles during the impact as calculated in the previous section 4.3. This signal was then applied to the lateral, longitudinal yaw and roll DOF as follows.

Peter Samuel Delves

$$m(\dot{u} - v\Psi) = F_{xFl} + F_{xFr} + F_{xRl} + F_{xRr} + F_{xd} - F_{areo} \qquad (4.9)$$

$$m(\dot{v} + u\Psi) = F_{yFl} + F_{yFr} + F_{yRl} + F_{yRr} + F_{yd} \qquad (4.10)$$

$$I_{zz}\dot{\Psi} = a(F_{yFl} + F_{yFr}) - b(F_{yRl} + F_{yRr}) + \frac{t}{2}(F_{xFl} + F_{xRl})$$

$$- \frac{t}{2}(F_{xFr} + F_{xRr}) + L_{yd}.F_{yd} + L_{xd}.F_{xd} \qquad (4.11)$$

$$I_{xx}\ddot{\phi} + I_{xz}\dot{\Psi} + m_t(\dot{v} + u\Psi) \qquad (4.12)$$
$$= (m_b g h_r - k_r)\phi - c_r\dot{\phi} + F_{yd}(L_{zd} - h_r)$$

These equations show how the forces calculated using the momentum theorem induce lateral, longitudinal, yaw and roll accelerations in the vehicle model. L_{yd}, L_{xd} and L_{zd} are the impact positions in the lateral, longitudinal and vertical directions. These are used to generate the yaw and roll moments that are input into the vehicle whereas the lateral and longitudinal impact force components are added to the equations 3.16-3.19 in section 3.2.3.

4.4.1. Crash Scenarios

Crash scenario one is referred to as rear impact. The target vehicle is struck on the driver's side rear quarter as shown in figure 4.5 at angels between 10^0 and 30^0. This generates accelerations in both the lateral and longitudinal directions, of travel as well as inducing a spin due to the moment created around the vehicle's centre of gravity.
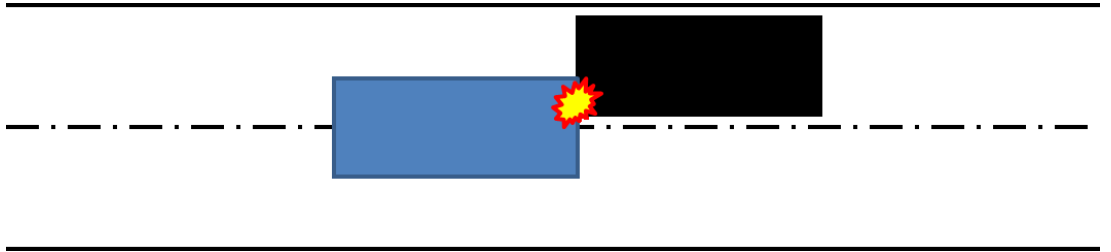
Figure 4.5: Diagram showing crash scenario one where the target vehicle (Black) is struck on the rear quarter by the impactor vehicle (Blue).

The scenario is detailed as follows: The target vehicle is traveling at 29m/s (approximately 65mph) and is struck by an identical impactor vehicle; the 6 sets of crash force values for F_{yd} and F_{xd} calculated in section 4.3 are input at impact

Peter Samuel Delves

positions: $L_{yd} = -b$, $L_{xd} = (0.1 - \frac{t}{2})$ and $L_{zd} = 0.1$. The crash impulse is triangular as shown in Figure 4.4.

The second crash scenario is referred to as side swipe impact. This assumes that the impactor vehicle has turned into the target vehicle striking in on the front quarter at the side of the vehicle as shown in figure 4.6. Like the rear impact this induces lateral and longitudinal forces causing the vehicle to yaw. The total time of the simulation was 12s.
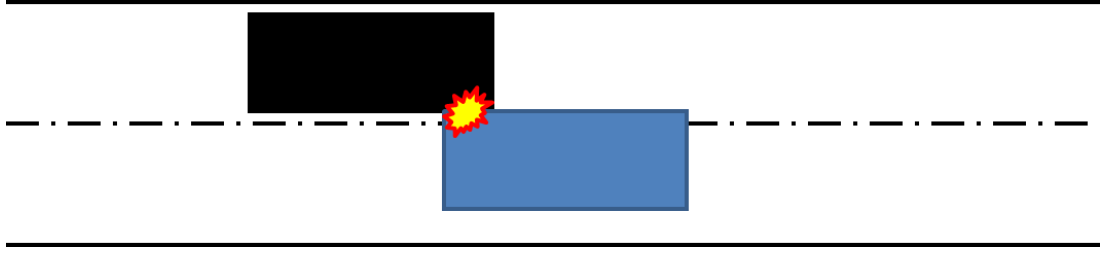
Figure 4.6: Diagram showing crash scenario two where the target vehicle (Black) is struck on the side front quarter by the impactor vehicle (Blue).

The scenario details are the same as the rear impact with the exception that impact positions were changed to: $L_{yd} = a - 0.1$, $L_{xd} = \frac{t}{2}$ and $L_{zd} = 0.1$

To allow comparisons of crash behaviour the vehicle parameters used are the same as those used in Byung-joo Kim and Peng (2012), Byung-joo Kim and Peng (2014) for the 'Baseline big SUV' (m = 2450kg, a = 1.105m and, b = 1.745m). It is traveling on a flat straight road, with zero initial lateral velocity and the yaw rate is zero. The coefficient of friction μ = 0.7. As with the simulations carried out in Byung-joo Kim and Peng (2012), Byung-joo Kim and Peng (2014) the steering angle is locked to 0⁰ for the entirety of the incident.

Peter Samuel Delves

4.4.2. Rear Impact Simulation

Figure 4.7: Lateral acceleration time history for rear impact crashes carried out at a velocity differential of 2.5m/s at three impact angles of 10, 20 and 30 degrees.

Figure 4.8: Lateral acceleration time history for rear impact crashes carried out at a velocity differential of 5m/s at three impact angles of 10, 20 and 30 degrees.

Peter Samuel Delves

Chapter Four: Vehicle Model Crash Simulation

Table 4.5: Maximum lateral acceleration of the six rear crash simulations.

Maximum lateral Acceleration (g)					
5 m/s 10^0	5 m/s 20^0	5 m/s 30^0	2.5 m/s 10^0	2.5 m/s 20^0	2.5 m/s 30^0
0.46	1.06	1.65	0.22	0.51	0.78

Figures 4.7 and 4.8 show the lateral acceleration time history of the target vehicle for the rear impact crash scenarios. As the impact occurs lateral accelerations between 0.22 - 1.65g are induced and the vehicles start to move laterally out of their original lanes. These initial peaks in acceleration during the impact quickly decelerate as the tyre forces start to oppose the spin settling at 0.6g during the sliding phase. This continues until either the vehicle reaches its final heading angle when lateral slip angles reduce to 0^0 or, the vehicle has enough momentum to continue spinning past 180^0. When the vehicle passes this point lateral deceleration switches sign as the slip angles of the tyre change direction. After some transient behaviour, the deceleration settles back to around 0.6g until the spin loses enough momentum for the tyres to exit their saturation point and the vehicle stops spinning.
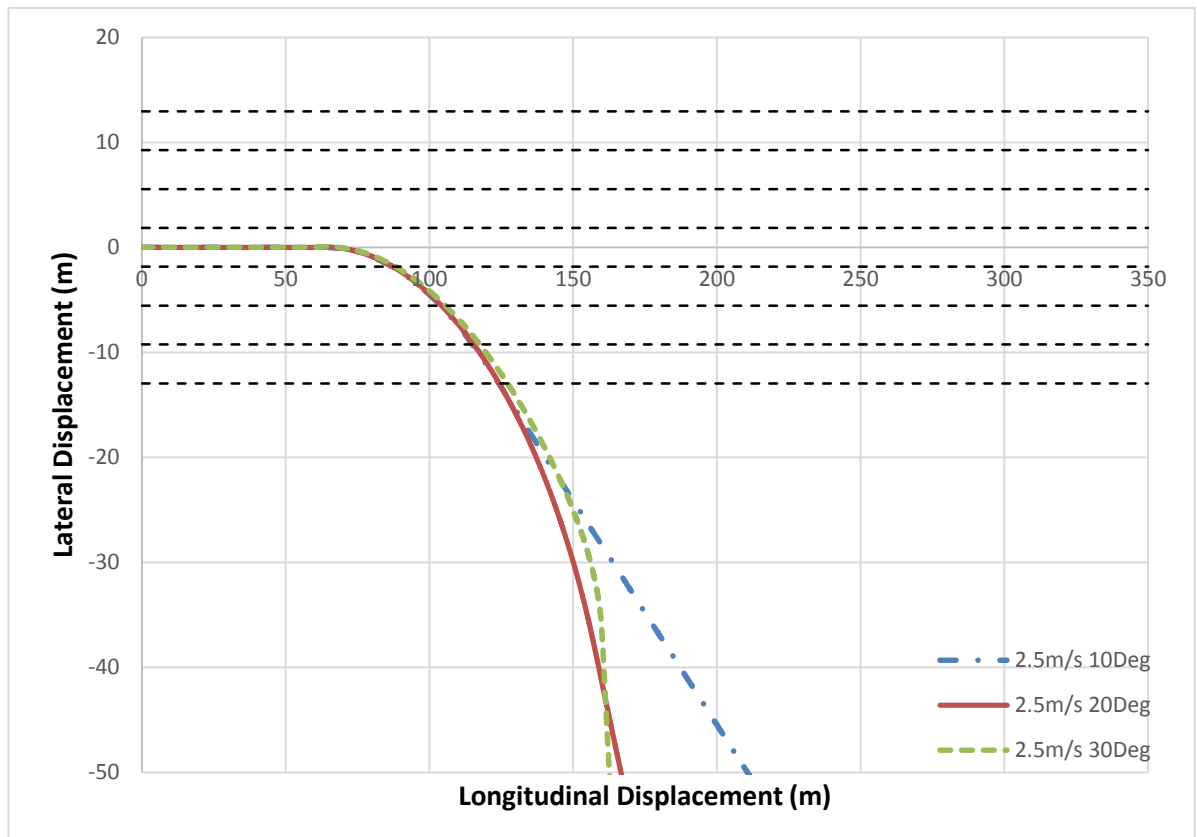
Figure 4.9: Trajectory of the three rear-crash simulation vehicles at a speed differential of 2.5m/s

Peter Samuel Delves
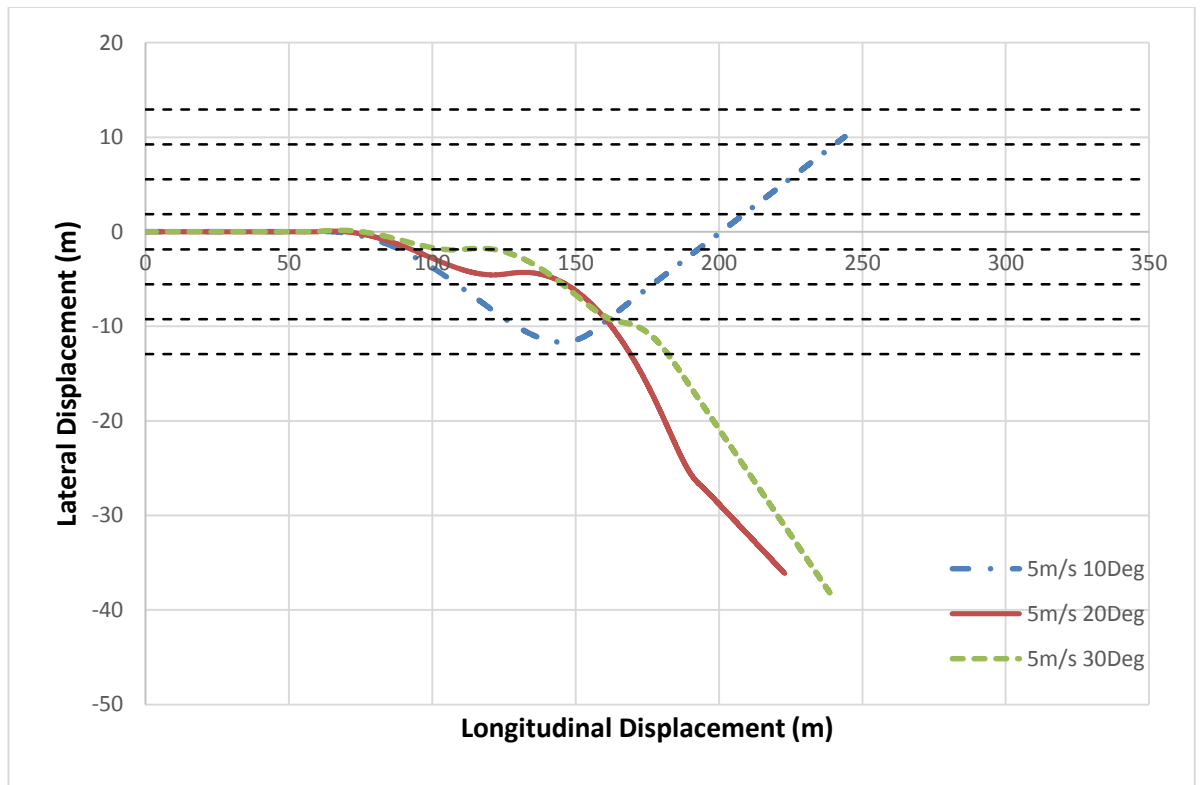
Figure 4.10: Trajectory of the three rear-crash simulation vehicles at a speed differential of 5m/s

Table 4.6: Maximum lateral displacement of each of the six rear crash simulations

Maximum lateral displacement (m)					
5 m/s 10^0	5 m/s 20^0	5 m/s 30^0	2.5 m/s 10^0	2.5 m/s 20^0	2.5 m/s 30^0
-11.68	-36.14	-38.79	-96.82	-127.97	-67.16

Figures 4.9 and 4.10 show the trajectory of the vehicle throughout the incident. The horizontal dotted lines denote lane boundaries with a lane width of 3.7m. The middle of the vehicle's initial lane starts at 0 on the vertical axis. All of these vehicles have a large chance of a second impact as they stray across lanes at an angle exposing their side to other collisions.

The lower velocity 2.5m/s impacts result in arguably the worst trajectories then the higher velocity impacts. They cause the vehicles to skid sideways across lanes exposing their sides to secondary collisions and result in final heading angles which continue to take them across lanes. The lack of spinning also causes higher final velocities as speed is not reduced by prolonged lateral tyre slip and thus the vehicles travel further.

Peter Samuel Delves

The higher velocity 5m/s simulations all result in the vehicles spinning and initially do not travel as far off their original line as the lower velocity impacts. The impacts at 20^0 and 30^0 have enough yaw energy to continue spinning through a full 360^0. The point at which they are close to 180^0 can be seen where the blue and red curves straighten up around the 100m and 125m respectively. As the 10^0 impact does not quite reach 180^0 the vehicle ends up travelling back across it original lane. In addition, as the spin speed is lower the vehicle lateral displacement is larger in the initial phase of the crash.

This highlights the requirement for post-impact crash control as it shows how any vehicle-to-vehicle accident on a motorway results in trajectories that carry a vehicle across multiple lanes. This greatly increases the likelihood of a secondary impact with other vehicles or inanimate objects occurring.

Figure 4.11: Plot showing the relationship between yaw rate and heading angle for the three simulated rear end impact vehicles at a speed differential of 2.5m/s.

Peter Samuel Delves
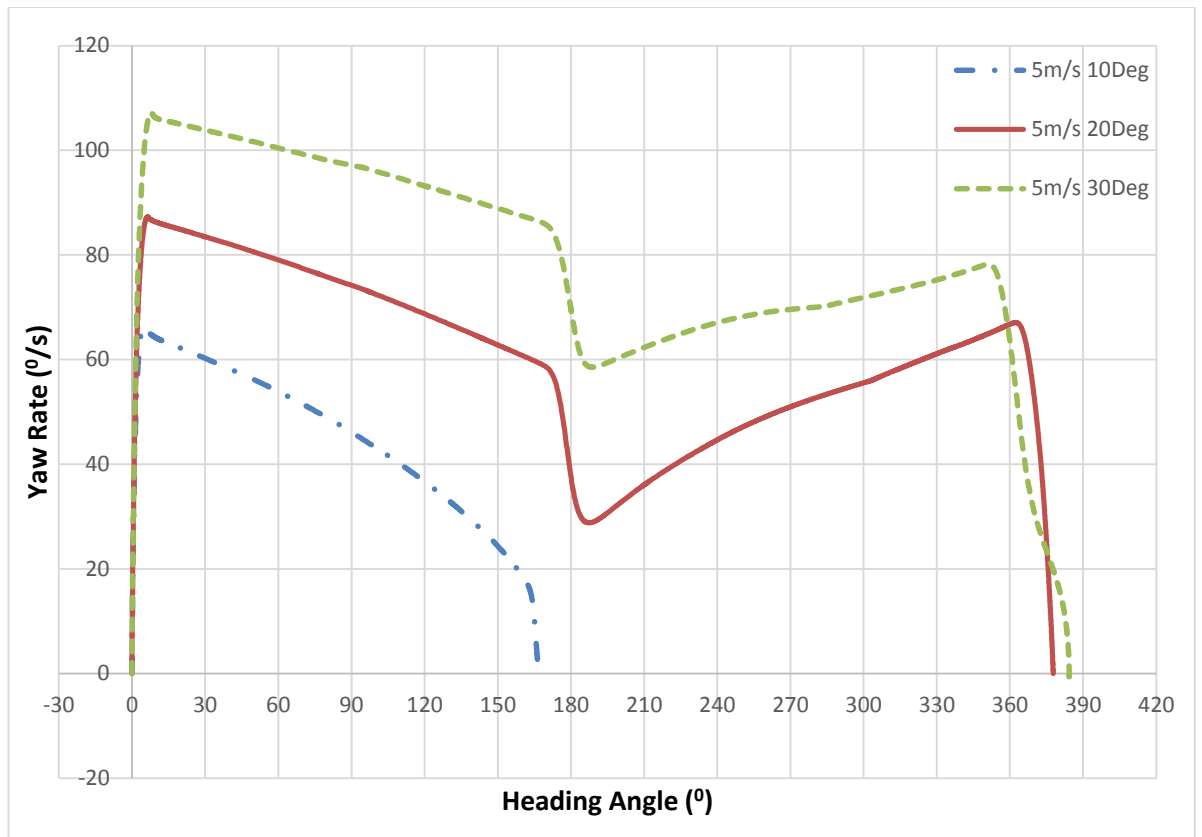
Figure 4.12: Plot showing the relationship between yaw rate and heading angle for the three simulated rear end impact vehicles at a speed differential of 5m/s.

Table 4.7: Peak yaw rates developed by the crash impulse for the six rear impact simulations.

Peak yaw rate (^{0}/s)					
5m/s 10^0	5m/s 20^0	5m/s 30^0	2.5m/s 10^0	2.5m/s 20^0	2.5m/s 30^0
66.29	87.28	107.12	31.52	41.08	50.02

Table 4.8: Final heading angles of the six rear impact scenarios.

Final heading angle					
5m/s 10^0	5m/s 20^0	5m/s 30^0	2.5m/s 10^0	2.5m/s 20^0	2.5m/s 30^0
166.89	377.76	384.13	23.12	51.76	79.23

In Figures 4.9 and 4.10 the trajectory of the vehicles were analysed and did give some insight into the spin behaviour, but it is important to analyse the vehicles yaw behaviour in more depth. Figures 4.11 and 4.12 shows the yaw rate of the vehicle during the incident in relation to the heading angle of the vehicle. Unsurprisingly there is a large peak in yaw rate as the impact occurs. Once this initial region of intense dynamic change passes, the tyres start to work against the spin.

Peter Samuel Delves

The most interesting regions of the graph to observe are where the vehicle approaches heading angles parallel to the original direction of travel (e.g. 180^0, 360^0). At these points there is a sharp decrease in the yaw rate of the vehicle as the longitudinal components of the tyres reaches their optimal region where they can best influence the vehicle's yawing moment, followed by a steep increase as the vehicle continues to spin out of this region. The vehicle then finally comes to a rest close to one of these regions when the spin has lost sufficient energy that the lateral tyre forces are no longer saturated.

The final heading angles settle where the vehicle is travelling longitudinally with no lateral slip. This is because a vehicle's longitudinal tyre stiffness is higher than its lateral stiffness. It thus tends to settle in the direction of the greatest stiffness in a state of rolling (as this requires less energy) rather than sliding laterally.

Even though the vehicle has a tendency to settle traveling forwards the initial impact does actually send the vehicle off its original trajectory. It shows that even a few degrees of rotation past or short of the 180^0 and 360^0 points still causes large lateral displacements and increases the chance of a secondary impact.

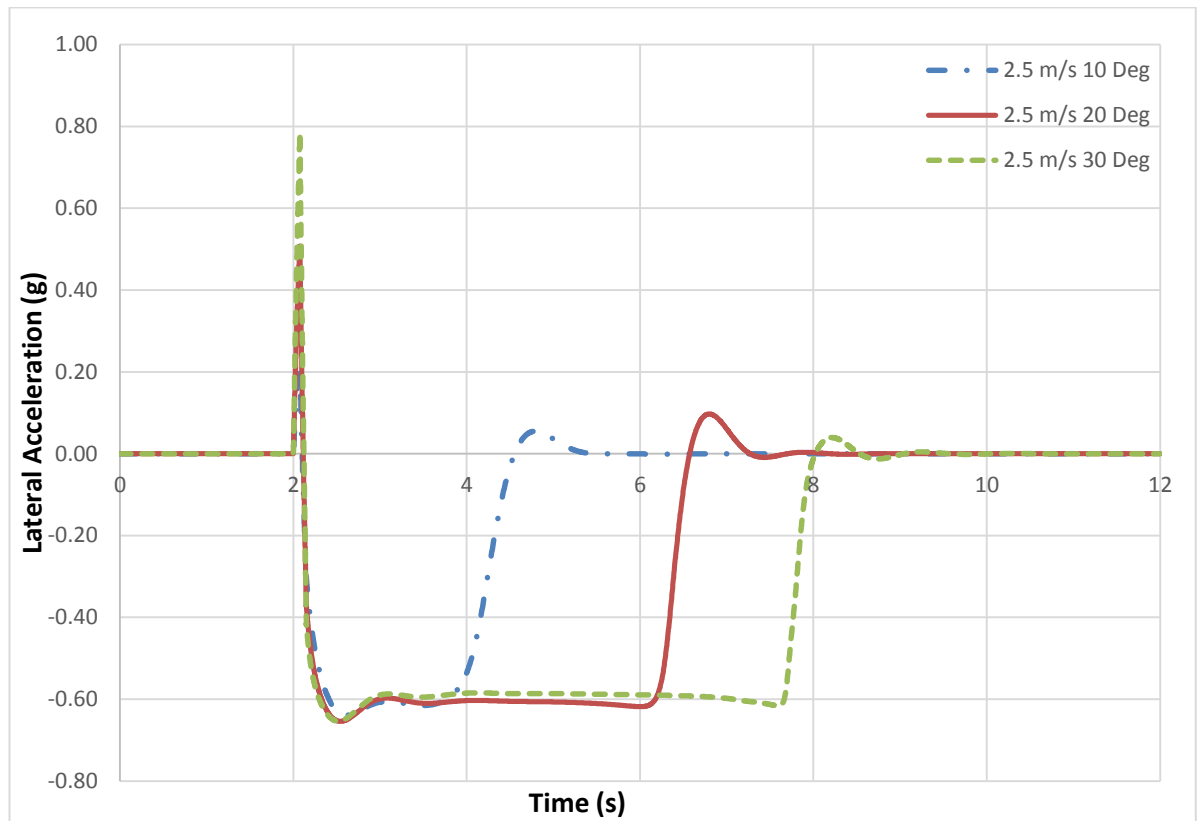### 4.4.3. Side Swipe Impact Simulation
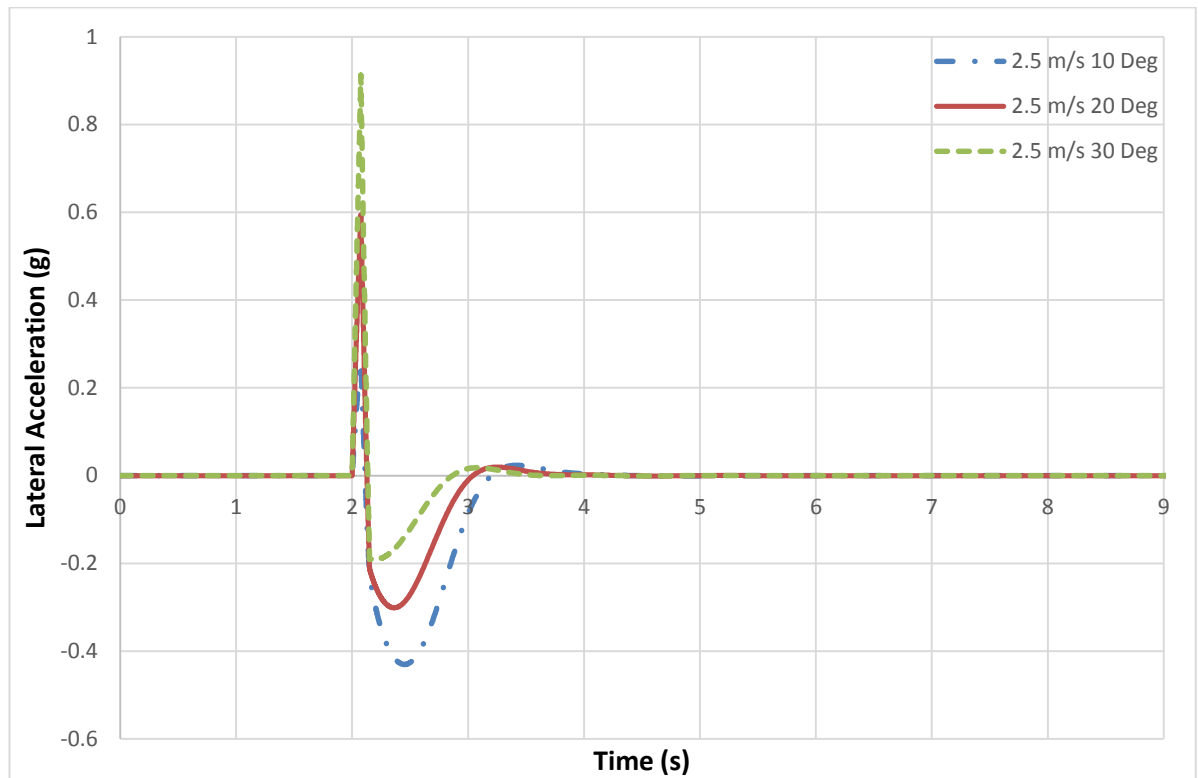
Figure 4.13: Lateral acceleration time history for side impact crashes carried out at a velocity differential of 2.5m/s at three impact angles of 10, 20 and 30 degrees.
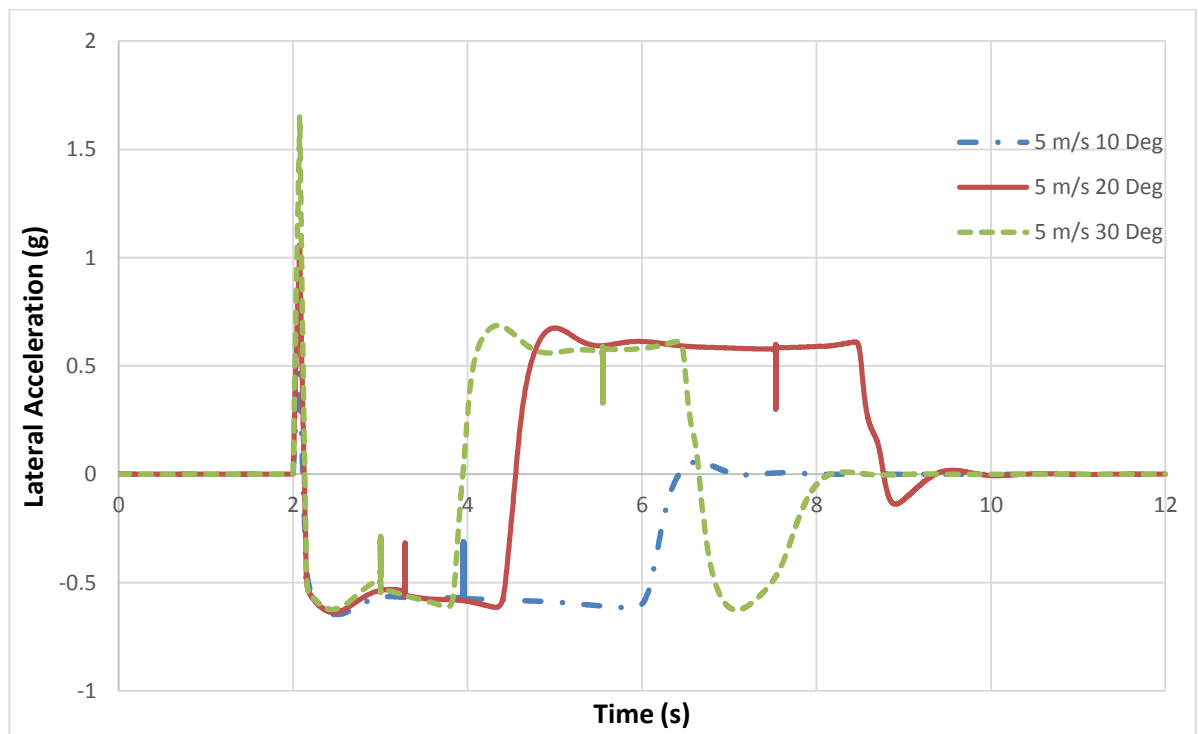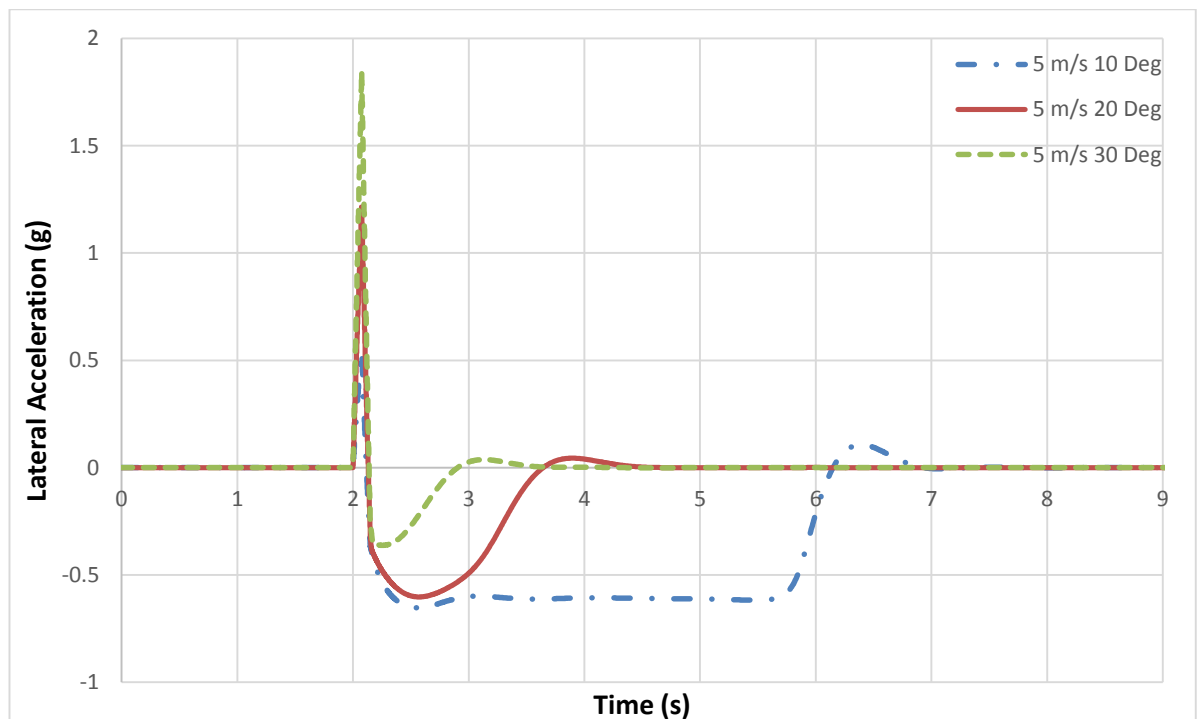

Figure 4.14: Lateral acceleration time history for side impact crashes carried out at a velocity differential of 5m/s at three impact angles of 10, 20 and 30 degrees.

Peter Samuel Delves

Table 4.9: Maximum lateral acceleration of the six side swipe impact simulations.

Maximum lateral Acceleration (g)					
5 m/s 10^0	5 m/s 20^0	5 m/s 30^0	2.5 m/s 10^0	2.5 m/s 20^0	2.5 m/s 30^0
0.54	1.21	1.85	0.26	0.59	0.91

Figures 4.13 and 4.14 show the lateral acceleration time history of the target vehicle for the side swipe impact crash scenarios. Initial lateral acceleration is higher than that of the rear impact with values ranging from 0.55-1.85g. This is because the impact occurs closer to the centre of gravity so more of the energy is transferred into lateral acceleration rather than a yaw moment. As with the rear impact once the initial impact phase has finished, acceleration switches to deceleration as the tyres oppose the induced lateral acceleration, but none of the vehicles are induced into a full spin, instead they only skid. This is to be expected as lower yaw rates are developed since the impact occurs closer to the centre of gravity, leading onto Figures 4.15 and 4.16, which plot yaw rate against heading angle.
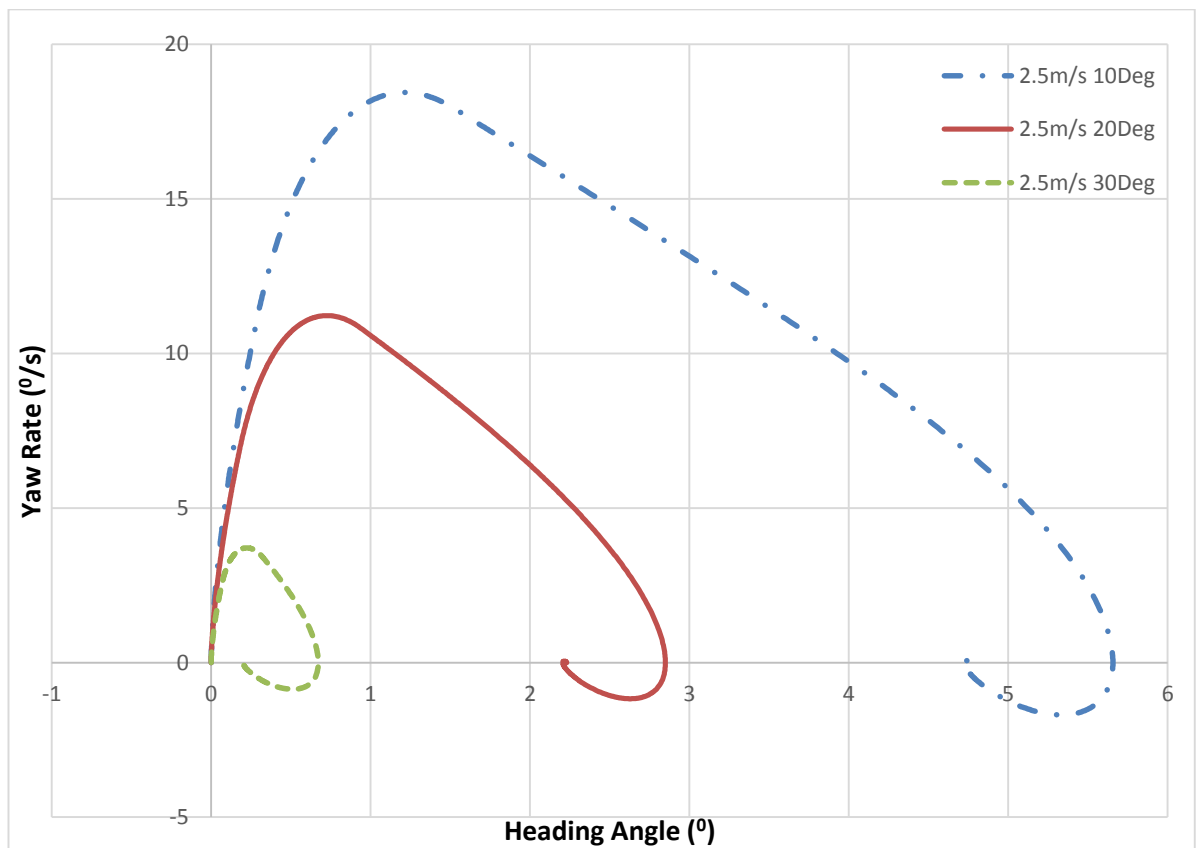
Figure 4.15: Plot showing the relationship between yaw rate and heading angle for the three simulated side-swipe impact vehicles at a speed differential of 2.5m/s.

Peter Samuel Delves
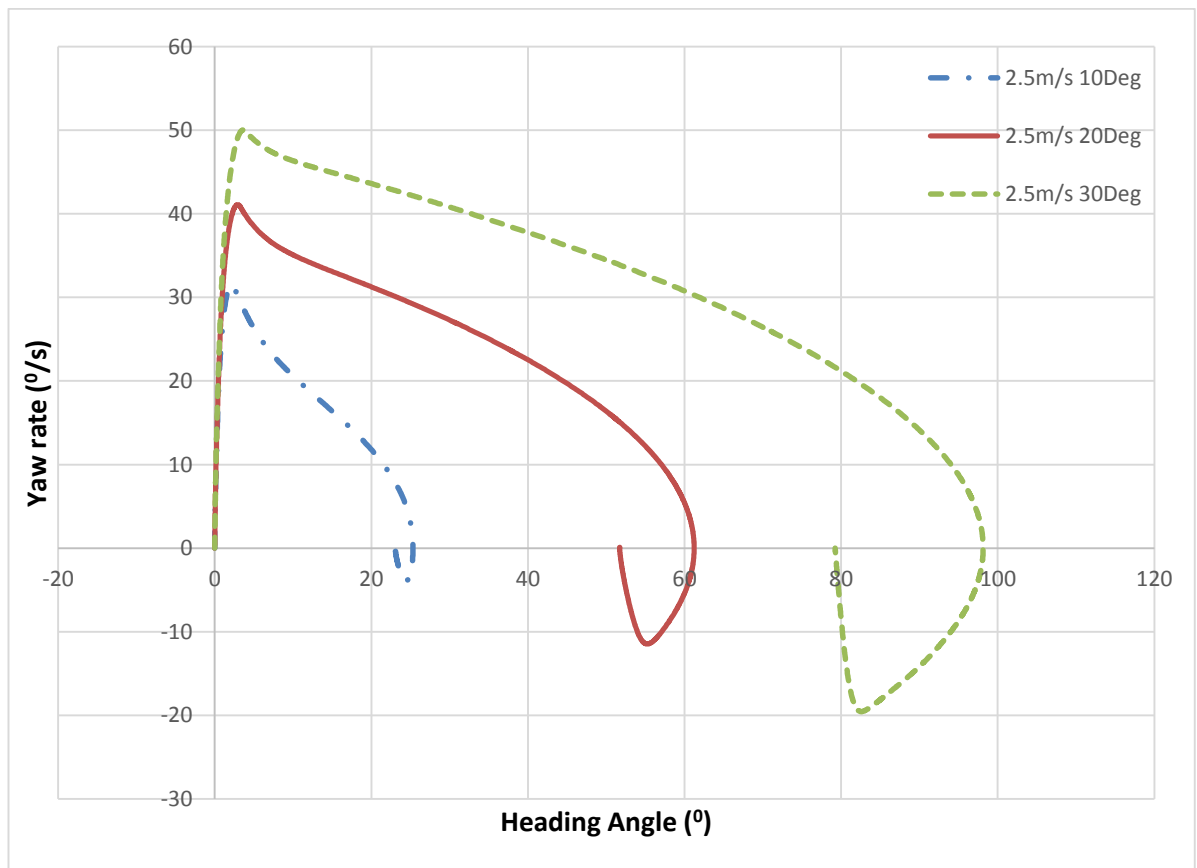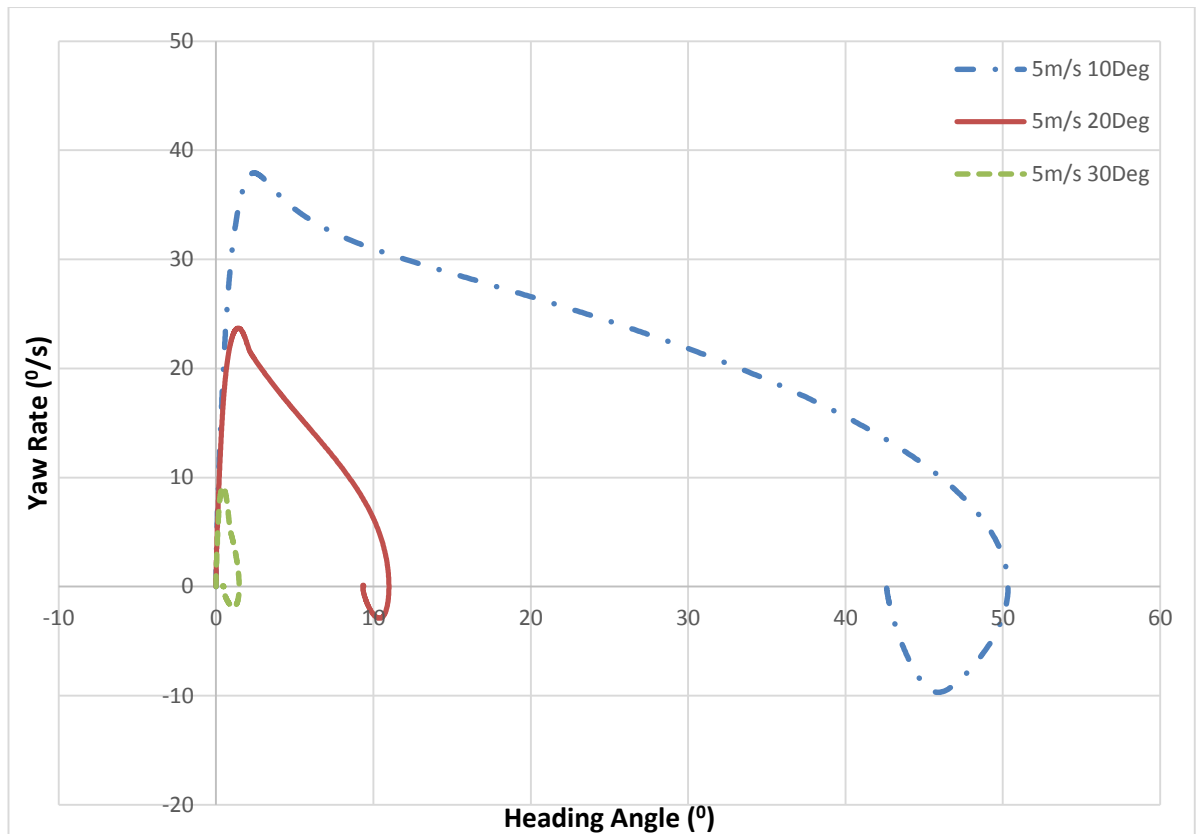
Figure 4.16: Plot showing the relationship between yaw rate and heading angle for the three simulated side-swipe impact vehicles at a speed differential of 5m/s.

Table 4.10: Peak yaw rates, maximum heading angles and final heading angles for all six side swipe impacts

Peak yaw rate (^{0}/s)					
5m/s 10^0	5m/s 20^0	5m/s 30^0	2.5m/s 10^0	2.5m/s 20^0	2.5m/s 30^0
37.93	23.70	9.11	18.44	11.23	3.71
Maximum heading angle (^{0})					
5m/s 10^0	5m/s 20^0	5m/s 30^0	2.5m/s 10^0	2.5m/s 20^0	2.5m/s 30^0
50.33	10.99	1.47	5.66	2.85	0.67
Final heading angle (^{0})					
5m/s 10^0	5m/s 20^0	5m/s 30^0	2.5m/s 10^0	2.5m/s 20^0	2.5m/s 30^0
42.72	9.39	0.48	4.76	2.23	0.22

The impact point for this second collision is closer to the vehicle's centre of gravity and therefore the vehicle spin response has changed. This has resulted in a reduction of peak yaw rates for all of the vehicles. As the lateral moment of the impact has been reduced the lateral impact force components effect is reduced and thus low yaw rates are reduced. Therefore all of the vehicles rotate no further than 50.33^0 and result in large lateral displacements as seen in Figures 4. 17 and 4.18 below that are similar to the 2.5m/s velocity differential impact rear results seen in Figure 4.9.

Peter Samuel Delves
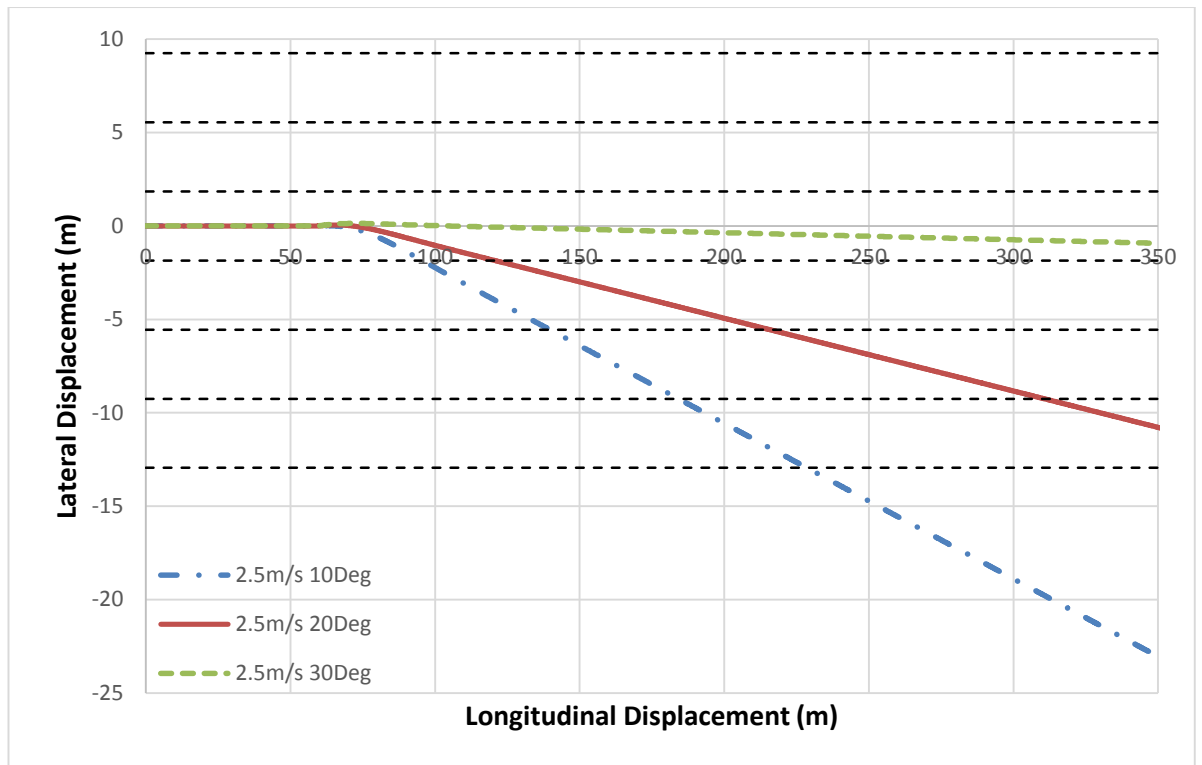
Figure 4.17: Trajectory of the three side-swipe impact simulation vehicles at a speed differential of 2.5m/s.
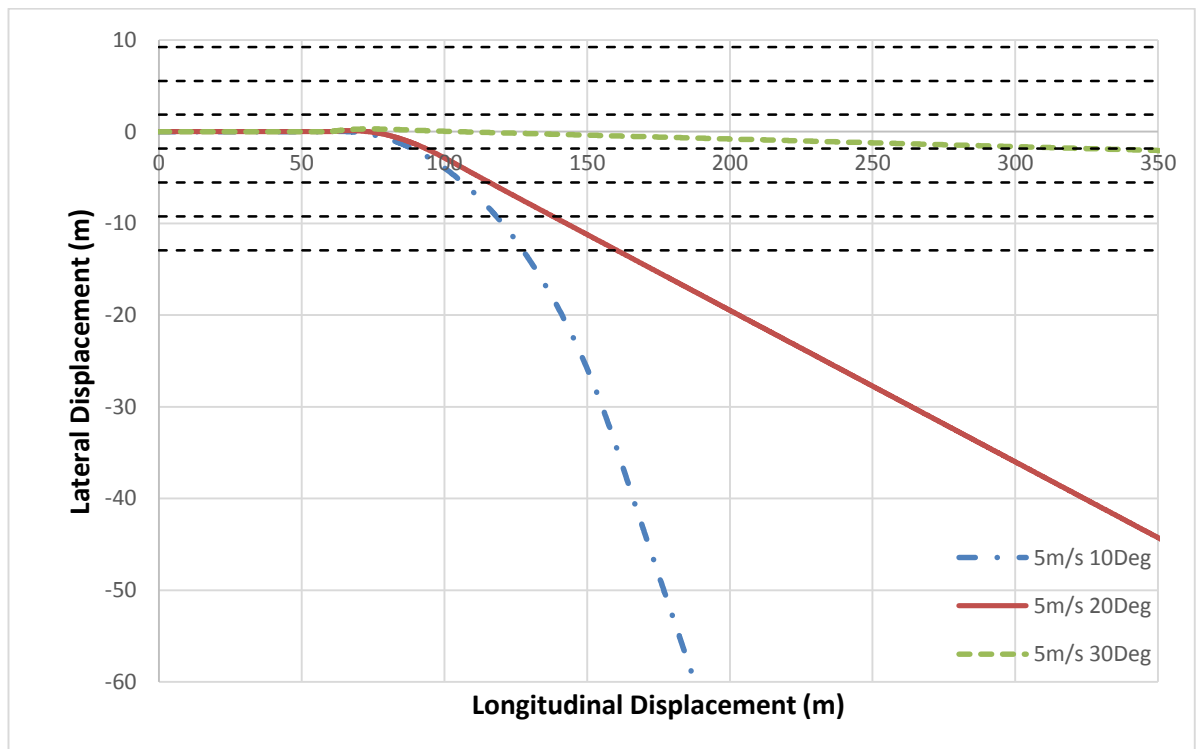
Figure 4.18: Trajectory of the three side-swipe impact simulation vehicles at a speed differential of 5m/s.

Peter Samuel Delves

Table 4.11: Maximum lateral displacements for the six side swipe impacts.

Maximum Lateral Displacement (m)					
5 m/s 10^0	5 m/s 20^0	5 m/s 30^0	2.5 m/s 10^0	2.5 m/s 20^0	2.5 m/s 30^0
-133.61	-45.47	-2.15	-23.09	-10.83	-0.93

Figures 4.17 and 4.18 show the trajectory of the target vehicle after the side swipe impact. The resulting yaw rates are lower than those of the rear impact and thus result in lower heading angles. The lowest speed impact stays close to the original lane and will require little intervention to correct. However at higher speed the final heading angles begin to cause the vehicle to stray across lanes as the vehicle is put into a skid rather than a spin. This results in a dramatic increase in the chance of a secondary collision and more severe injury.

To validate results, comparison with Zhou, Peng et al. (2008) was carried out. The work uses a 4-DOF model which does not include the wheel rotation DOF and also uses different simulation software so some variation is to be expected. However from their contour plots of rear impacts, there is an observable correlation. Their study shows peak yaw rates of over 100^0/s at a velocity difference of 4.5m/s and collision angle of 30^0 compared with results from this study which produces a peak yaw rate of 107^0 at a velocity difference of 5m/s at a 30^0 angle of impact. Later work from Byung-joo Kim and Peng (2012) also shows the phenomena where yaw rate drops steeply around 180^0 heading angle, as is seen in these results.

4.5. Crash Modelling Discussion

Global-coordinate transformation equations were integrated into the model to allow detailed analysis of the vehicle trajectory in the global reference frame. The transformation equations were checked by running the same step steer and lane change manoeuvres used to validate the vehicle model in chapter 3 section 3.5.

Crash forces were then calculated based on momentum theory. Speed differentials of 5 and 2.5m/s were selected and 3 angles of incidence: 10^0, 20^0 and 30^0. These vectors were then used to calculate the velocity components in both lateral and longitudinal directions. A coefficient of restitution $e = 0.2$, which represents the energy dissipated during the incident, was used to calculate the post-impact vehicle

Peter Samuel Delves

velocities, which in turn allowed calculation of the momentum exchanged in the impact. Triangular shaped force impulses were then calculated so that the momentums could be applied to the vehicle model. The study is only interested in the behaviour and control of the target vehicle so values were only calculated for this vehicle.

Finally, the completed model was tested for two crash scenarios to check that the vehicle was behaving as expected and results correlated with Zhou, Peng et al. (2008). The two scenarios selected were a rear end and a side swipe impact. They were selected as they represent two common scenarios that can occur on a motorway. The results of the simulation showed the rear impact generating larger yaw rates due to larger moments being generated and on visual inspection results correlated closely with Zhou, Peng et al. (2008). The most interesting part of the simulation to note was the phenomena present when the vehicle approached heading angles perpendicular to the original undisturbed heading angles, which is also seen in Byung-joo Kim and Peng (2012). At this point there is a large drop in yaw rate as the longitudinal stiffness component of the tyre is able to influence the vehicle's dynamics and the final heading angles once a spin has been induced settle at angles close to perpendicular to the original heading angle.

Now that the vehicle model is equipped to simulate vehicle crashes, torque vectoring control can be applied to the model to ascertain its effectiveness during an incident. A Simulink diagram of the full 8-DOF model can be seen in appendix 4.

Peter Samuel Delves

5. Chapter Five: Drive Torque Vectoring for Post-Impact Vehicle Control

The construction of the post-impact Proportional Integral Derivative (PID) switching control strategy is detailed in this chapter. Simulation of the controller is then carried out using the same crash scenarios as those in chapter 4. The controlled simulation results were then compared against the chapter 4 simulations to assess its effectiveness. A six-phase switching controller was developed using a set of 'Settling' and 'Holding' controllers to control heading angle to achieve re-alignment of the vehicle's front or rear crash structures with the road carriageway. All 12 of the simulations managed to re-align the front or rear crash structures of the vehicle with the main carriageway and reduced lateral displacements compared with chapter 4 simulation results. These simulation results demonstrated that drive torque vectoring is a viable candidate for post-impact control.

94

5.1. Introduction

The work in this chapter investigated the effect electric motor torque vectoring had on post-impact dynamics of a vehicle. The controller used for this study was a PID switching controller with six-phases, which were able to stabilise all 12 vehicle crashes presented in chapter section 4.4. As discussed in previous chapters during multiple impact incidents the chance of sustaining serious injury increases dramatically. Therefore it was desirable for the controller to reduce the chance of this occurring. This was performed by controlling the vehicle's heading angle. The objective was to control the vehicle so as to achieve heading angles parallel to the initial heading, irrespective of how many times the vehicle spins, so as to re-align the vehicle's main crash structures with the road carriageway so that if a secondary collision were to occur, the chance of serious injury would be reduced. It also discusses the advantages that electric drivetrains have over traditional ICV because of the layout flexibility they have. This flexibility allows implementation of four-wheel drive which increases available control torque over a two-wheel vehicle. The available control torque at each wheel is set +/- 400 Nm. It was discovered that torque needed to be boosted as a function of the vehicles weight distribution on the front axles up to the 400 Nm threshold to improve stability of the vehicle during control.

PID switching control was used as the control objective required alteration based on the initial yaw rate produced in the impact. To achieve this a sequence of 'settling' and 'holding' PID controllers were combined to produce a switching control. The settling controllers were active around the settling objective angles of 0^0, 180^0 and 360^0. These had high proportional gain because the vehicles need to reduce the spin rate as fast as possible about these points to potentially stabilise the vehicle. In between these settling areas were holding controllers. These were activated when the vehicle was deemed to have too much spin energy to be controlled back to the original target angle. These controllers switch the control objective to the next target angle and hold the yaw rate so that the vehicle can reach the next point where the next settling controller is switched in about the target angle.

Peter Samuel Delves

This switching controller was implemented on the vehicle crash model developed through chapters 3 and 4. The same crash scenarios and crash impulses in section 4.4 were used so that direct comparison could be drawn between the controlled and uncontrolled vehicles. It was found that the switching control system was able to stabilise all vehicles in each scenario at one of the desired target angles. The controller was able to reduce settling times for some but not all of the simulations. However in all cases deviation of the final heading from parallel to the initial heading was reduced and thus with it lateral displacement. This demonstrated the great potential that such a control system has in reducing serious injury and death still seen on the roads today.

5.2. Vehicle Powertrain Considerations

As discussed in the literature review section 2.4 electric powertrains allow application of the three standard powertrain layouts: Front wheel drive only, rear wheel drive only and four wheel drive. The available drive torque to each wheel was set at +/- 400 Nm. This figure is based on the use of a YASA (2015) motor. This results in a maximum torque differential of 800 Nm from side to side. This means that the four-wheel drive vehicles should perform better as double total net torque is available to that of the front and rear wheel drive only vehicles. For this reason it is evident that the four-wheel drive system offers the greatest potential for control and is why it is used for this study.

To aid stability in control a torque bias was applied between the front and rear axles boosting desired torque to the front wheels as a proportion of the vehicle's weight distribution. As more weight is at the front of this vehicle, more torque was applied to the front wheels. Limits were applied after this calculation to make sure the maximum torque output did not exceed the torque limits of +/-400 Nm.

5.3. PID Differential Control

5.3.1. Control State Considerations

Negative feedback PID control was used for this study as it allowed fast implementation and flexibility in tuning. It was set up in the form of a differential controller which split torque equally between left and right sides of the vehicle but

Peter Samuel Delves

in opposite directions so that yaw moments can be produced to counteract the spin induced by the impact. The study assumed that full local state feedback was available.

Three states were considered for control: Global lateral velocity, global lateral position and heading angle. Global state control was not pursued as direct control of these states was not possible and required control of multiple local states. Whereas controlling heading angle resulted in a practical method of reducing global lateral velocity to zero stopping any further lateral displacement. It also allowed re-alignment of the vehicle's crash structures with the road carriageway and gave direct control of spin rate.

To perform the carriageway re-alignment the following considerations were made: if the yaw rate of the induced spin is large it is more desirable to allow the vehicle to continue rotating and attempt to settle the vehicle facing backwards (180^0). If the yaw rate is sufficiently large that it continues passed 180^0 it is safer and requires least control actuation to switch the control objective to 360^0 then to attempt to reverse yaw rate to return to 180^0. Once the vehicle's heading angle is stabilised the vehicle is in optimum alignment for hard controlled braking.

5.3.2. Switching Control for Heading Angle Control

Switching control was used as one single PID controller was not sufficient to perform the desired control action across the full range of accidents presented, which required multiple switching thresholds and control gains to stabilise all vehicles. The controller was implemented on the 8-DOF model presented in chapter 3. The model is set up as a single negative feedback loop referencing heading angle and uses the four wheel torque as control inputs.

Control was performed over a possible maximum of six-phases depending on the severity of the initial impact. The phases consist of a set of 'settling' and 'holding' controllers. The settling controllers are aggressive, reducing yaw rates quickly in an attempt to settle the vehicle at the desired heading angle. The holding controllers are lower gain and activate once various heading angle thresholds are crossed to

sustain yaw rate so that the vehicle could reach the next settling point whereupon the next settling controller was activated.

The two crash scenarios, crash impulse length and the vehicle parameters in section 4.4.1 are used so that direct comparison between controlled and uncontrolled response could be carried out. These crash impulses were applied to the model after 2s to allow the model to initiate. A control delay of 0.25 s was applied to emulate sensor lag, and included the identification and verification time a real world system would need to reduce the chance of unnecessary triggering of the system (Byung-joo Kim and Peng 2012, Byung-joo Kim and Peng 2014).

Once the 0.25 s delay had passed, the phase one settling PID controller was activated with the objective of reducing the vehicle's heading angle to 0^0. This controller arrested initial yaw rates when compared with the uncontrolled response. It performed well on the crash force impulses that produced initial peak yaw rate under 50 °/s. This meant it was able to reduce the heading angle to 0^0 for all six of the side swipe impacts and the three lower speed impacts for the rear crash scenario, reducing all of their lateral displacements relative to the uncontrolled vehicles.

For all the 5m/s rear impacts the initial controller was not able to settle the vehicle without causing it to stray back across multiple lanes and expose its side for a greater amount of time. This resulted in the need to implement the second phase of the switching controller.

Phase two was activated once the vehicle had reached threshold heading angle of 60^0 or 90^0 depending on initial peak yaw rate. When the vehicle reached these thresholds it was switched to the holding controller with the objective of stabilising the vehicle traveling backwards (a heading angle of 180^0). This 'holding' controller required the gain to be reduced considerably so that the vehicle holds enough of its original yaw rate so that it can reach the new control objective. It was found that if gains were high enough that they increased yaw rate the vehicle would overshoot its target point. This resulted in the vehicle's yaw rates being held steady and then slowly reduced as it approached its target angle of 180^0.

Peter Samuel Delves

As the vehicle approached the 180^0 set point the phase two controller was not able to settle the vehicle at the 180^0 objective. This is because it did not have fast enough torque response due to the lower control gains. This resulted in the need for a settling controller similar to phase one to be implemented as a third phase.

Phase three consisted of another settling controller to give the vehicle the response required to settle at the desired point. This also took advantage of the phenomena observed in Figure 4.10 in section 4.4.2 where the tyres regain traction about points close to their rolling plane. Phase three was activated at a heading threshold of 173^0. This heading threshold was found through simulating the controller at values from 170^0 to 179^0 at 1^0 increments. This is because the vehicle needed enough time to arrest the spin and not overshoot, but also not switch too early, which would result in applying large controlling torques causing the vehicle to once again overshoot. This resulted in two of the three final vehicle settling again reducing the lateral displacement dramatically.

As the final vehicle still had a high yaw rate at the 180^0 settling threshold another two further holding controllers and a final settling controller were required. These are known as phases four, five, and six respectively, with the final heading angle target set at 360^0.

Phase four consisted of a holding controller with target angle of 180^0. This stopped the large rise in yaw rates seen in the uncontrolled scenario once a vehicle has passed its line of longitudinal trajectory holding it steady. This controller was activated at a threshold of 190^0. This controller continues to act on the vehicle until the vehicle passes 300^0 where a similar holding controller is activated but changes the target heading angle to 360^0. This sustains the steady yaw rate until the vehicle is within 7^0 of the desired heading angle as used for the settling controller in phase three. Once this threshold is reached the final phase six settling controller is activated with the object of stabilising the vehicle at 360^0 from the original heading angle.

For the purposes of this research it is assumed that there is no lag in the electric motors' torque application. Reasonably large differential terms are used in the control gains to reflect this. This could lead to damage to the motors themselves but

Peter Samuel Delves

as the vehicle has just undergone a collision and control is being performed to mitigate the effects of the collision and reduce the chance of injury, the condition of the electric motors after the incident is not of concern.

Control types, target heading angle, activation thresholds and deactivation thresholds for each of the six phases are summarised in the table below:

Table 5.1: Detailed overview of the target heading angles, activation thresholds and de-activation thresholds for the six phases of the PID switching control.

Control Phase	Control type	Target heading angle (^{0})	Activation threshold (^{0})	De-activation threshold (^{0})
One	Settling	0	After crash detection validation of 0.25 s	45,60 or 90 dependent on initial yaw rate
Two	Holding	180	45,60 or 90 dependent on initial yaw rate	173
Three	Settling	180	173	190
Four	Holding	180	190	300
Five	Holding	360	300	353
Six	Settling	360	353	367

5.3.3. PID Switching Controller Tuning

The PID controllers were tuned phase-by-phase using a heuristic method until all 12 crashes had been stabilised at a desirable heading angle parallel with the carriageway. This method was used as the vehicle model was able to run all crash scenario one or two simulations concurrently in a couple of seconds. The final heading angles, trajectories and yaw rates were analysed using the bank of scopes seen in figure 5.1 below after each simulation to ascertain if the controller had achieved its objective for all vehicles with P, I and D terms altered as required.

The tuning began using the side-swipe scenario values as they resulted in smaller final heading angles than the rear impact value. Phase one was tuned first in the following manner. Proportional gain was increased to achieve the desired heading for as many of the simulations as possible until overshoot was seen. Integral and differential terms were then altered to reduce overshoot and steady-state settling error. Once it had been judged that the maximum amount of vehicles had settled within this phase without reversing the yaw rate excessively the next phase was tuned.
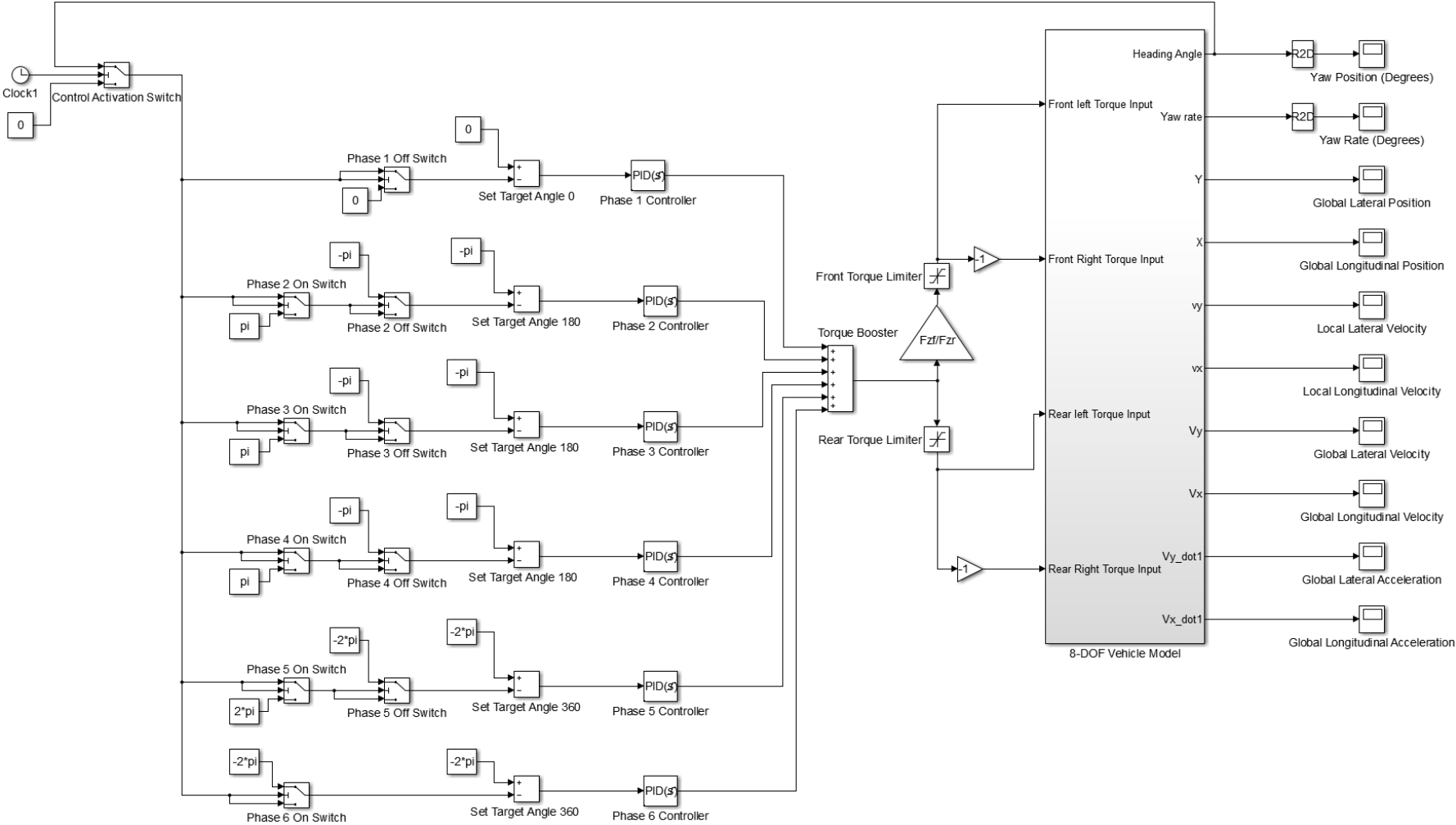
Figure 5.1: Diagram of the six phase switching PID controller

Peter Samuel Delves

The final heading angles of the remaining vehicles were then analysed so that the phase one-to-two switching threshold could be determined. These switching thresholds were also established experimentally alongside the tuning of the phase two and three controllers. As mentioned in section 5.3.2 the phase two holding controller was tuned so that the yaw rate at the threshold switching point was sustained, allowing the vehicle to reach the next target angle. This resulted in a considerable drop in the proportional gain so that yaw rate was held relatively steady. As the vehicle approached the next heading angle the phase three controller was activated which replicated the phase one controller gains striving to settle as many of the vehicles at the next target angle as possible. This process was then replicated for the phase four, five and six controllers until the final vehicle settled at 360^0.

5.4. Post Impact Control Results

To assess performance of the control system all simulations carried out used the same perimeters, crash impulses and crash scenarios as those in section 4.4. This allowed direct comparison to be carried out between the benchmark vehicle with no-control and the vehicle with the control system. A full list of vehicle data is presented in appendix 3.

5.4.1. Rear Impact Control Results
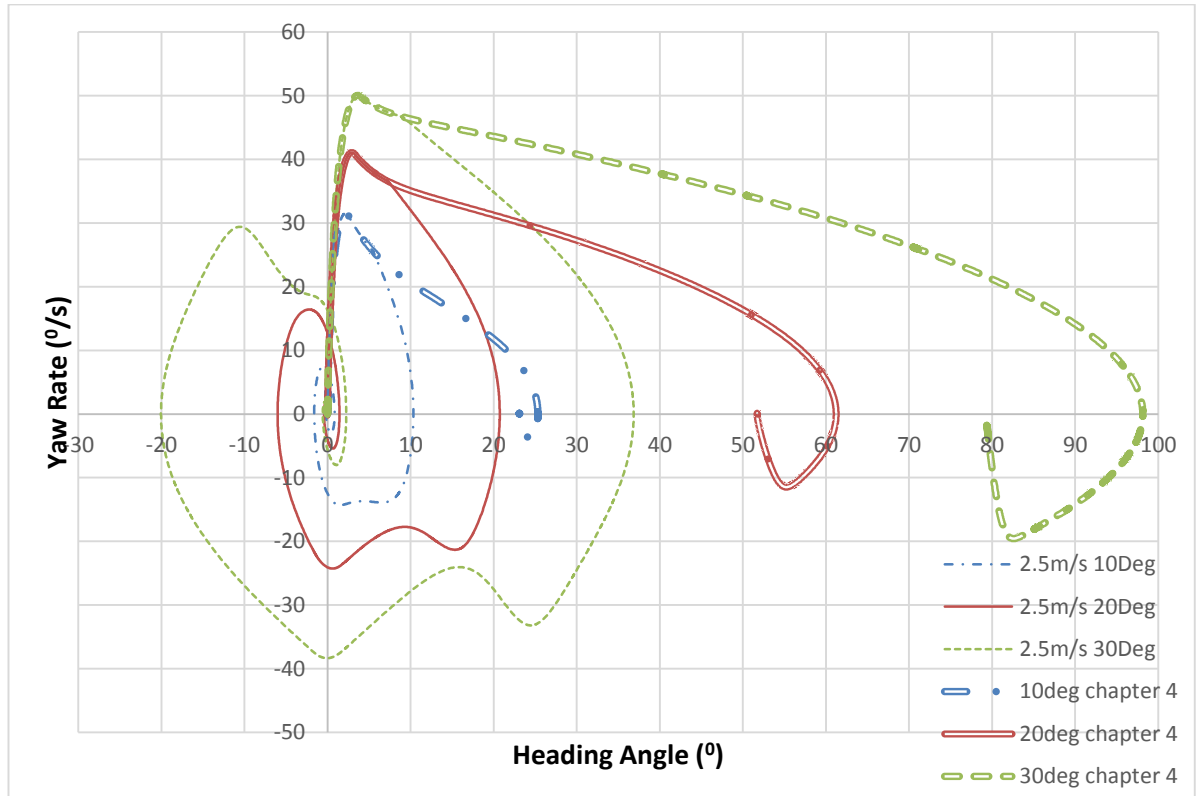
Figure 5.2: Plot comparing the yaw rate vs heading angle behaviour of the controlled (single lines) to uncontrolled (double lines) for the rear impact scenario vehicles at a speed differential of 2.5m/s.
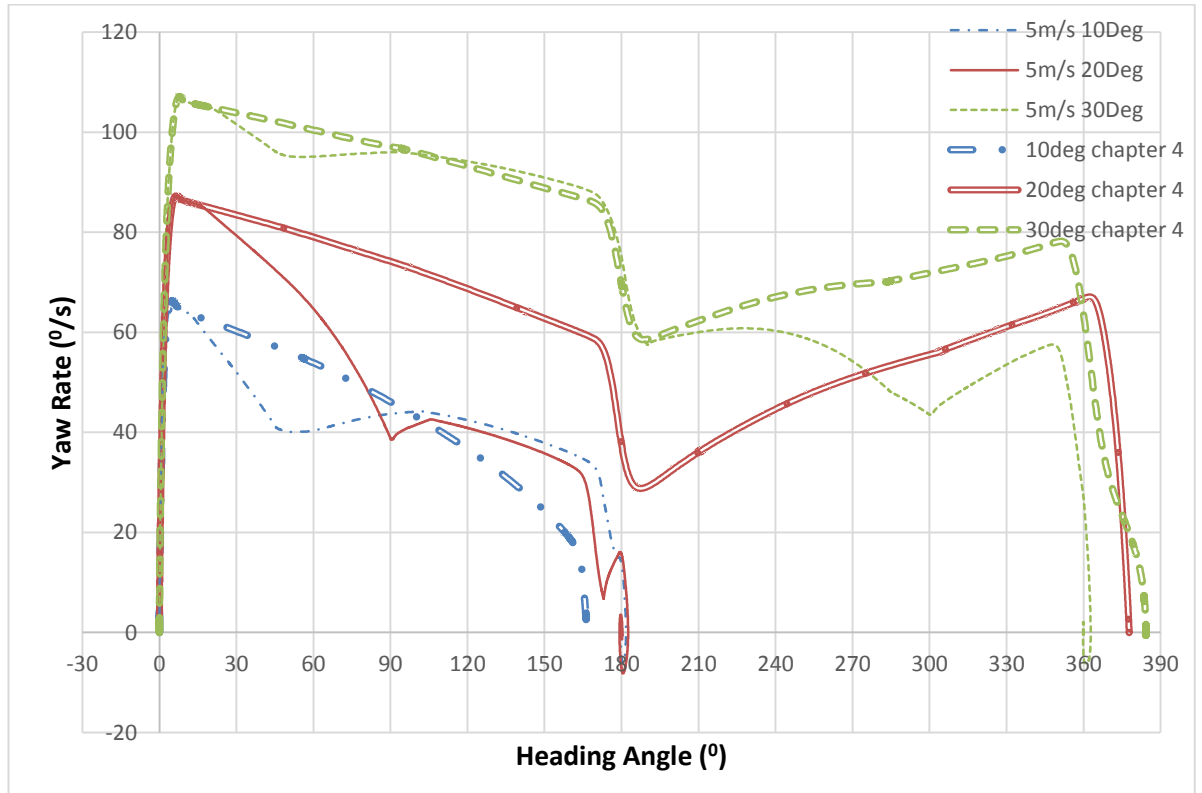
Figure 5.3: Plot comparing the yaw rate vs heading angle behaviour of the controlled (single lines) to uncontrolled (double lines) for the rear impact scenario at a speed differential of 5m/s.

Peter Samuel Delves

Table 5.2: Comparison of the maximum heading angles and final heading angles of the controlled and uncontrolled vehicles for all rear impacts.

Maximum heading angle (^{0}) comparison						
Closing velocity	2.5m/s			5 m/s		
Impact angle (^{0})	10	20	30	10	20	30
Controlled	10.33	20.73	36.86	181.76	182.57	362.76
Uncontrolled	25.32	61.23	98.14	166.89	377.76	384.35
Final heading angle (^{0}) comparison						
Closing velocity	2.5m/s			5 m/s		
Impact angle (^{0})	10	20	30	10	20	30
Controlled	0.00	0.00	0.00	180.04	180.02	360.00
Uncontrolled	23.12	51.76	79.23	166.89	377.76	384.13

Figures 5.2 and 5.3 show the controlled yaw position (heading angle) against yaw rate. As the control system is not activated until 0.25 s after the impact, initial yaw rates are the same as those of the uncontrolled vehicles. The most improved results are those of the 5m/s 20° vehicle which has not only settled parallel to the original heading trajectory, but has reduced the total change in heading angle by 197^0 so that only one side of the vehicle is exposed during the crash reducing the chance of a serious side impact occurring and thus serious injury.

As can be seen all vehicles achieve their control objective and settle at heading angles parallel to the original trajectory of travel. This in turn means that the vehicle is either travelling forward or backwards aligning its main front and rear crash structures for any secondary impacts. This also allows the vehicle to be brought to a controlled stop along this final settled trajectory, as is seen in Figures 5.4 and 5.5 below.

All the vehicles in Figure 5.2 settled at 0^0 to the original heading trajectory rather than the uncontrolled simulations which all resulted in large lateral displacements with settling angles between 20-80^0. This again reduces the exposure of the side of the vehicle and thus the chance of serious injury occurring.

Peter Samuel Delves

Table 5.3: Comparison of the time taken for each controlled and uncontrolled vehicle to settle at their final heading angle and their lateral displacement at this settling time for all rear impacts.

Heading angle settling time (s) comparison						
Closing velocity	2.5m/s			5 m/s		
Impact angle (^{0})	10	20	30	10	20	30
Controlled	4.59	6.07	7.87	6.96	7.14	7.91
Uncontrolled	4.55	6.53	7.80	6.28	8.84	7.49
Lateral displacement at settle time (m) comparison						
Closing velocity	2.5m/s			5 m/s		
Impact angle (^{0})	10	20	30	10	20	30
Controlled	-3.999	-9.8668	-18.126	-13.176	-1.8278	-11.144
Uncontrolled	-15.3613	-41.0767	-36.694	-10.015	-27.1796	-11.8585

Table 5.3 shows the time taken for each vehicles' heading angle to settle. This is taken as the vehicle stabilising within 2% of its final heading angle or within 1^0 of its final heading for the vehicles with large rotations. The second part of the table shows the lateral displacement of the vehicle at this settling time.

There is a mix of reduced and increased settling times when comparing the controlled responses against the uncontrolled responses. The cost of increase in settling time is justified by the final heading angle control given and subsequent reductions in lateral displacement. This is because if settling time is increased but lateral displacement is decreased the increased time to settle is acceptable. It is also important to note that all of the lateral displacements of the uncontrolled vehicles continue to change as they have all settled at angles to their original heading whereas all of the controlled vehicles' lateral displacements change very little once they have stabilised.

All but the 5 m/s 10^0 simulation reduce lateral displacement at the settling time but has settled at an angle of 377.76^0 to its original heading, exposing the side of the vehicle. This results in it travelling back towards its original lane and hence reducing the displacement. In Table 5.4 the final displacement at the end of the 12 s simulation is 11.53 m. After this analysis this value does not appear to be an improvement on the final displacement of -13.18 m the controlled vehicle has achieved.

Peter Samuel Delves
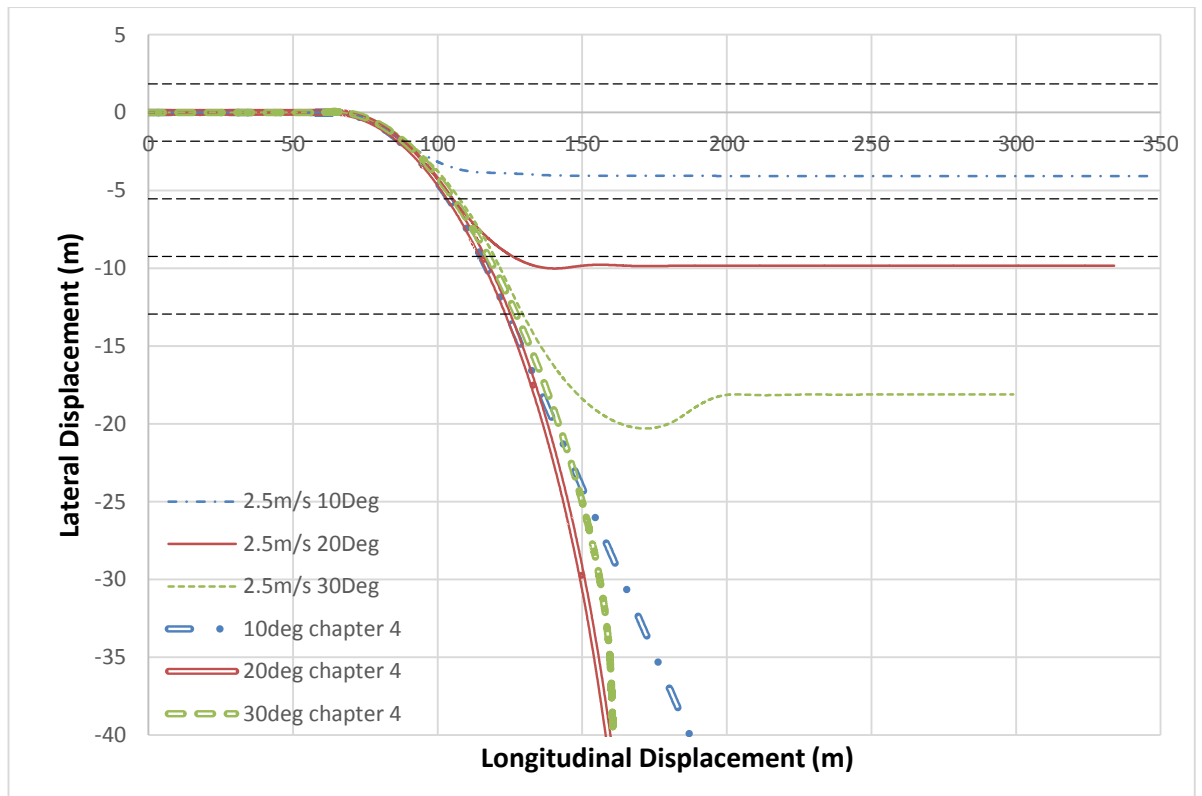
Figure 5.4: Comparison of the controlled (single lines) and uncontrolled (double lines) post-impact trajectories for the rear impact scenario with a speed differential of 2.5m/s.
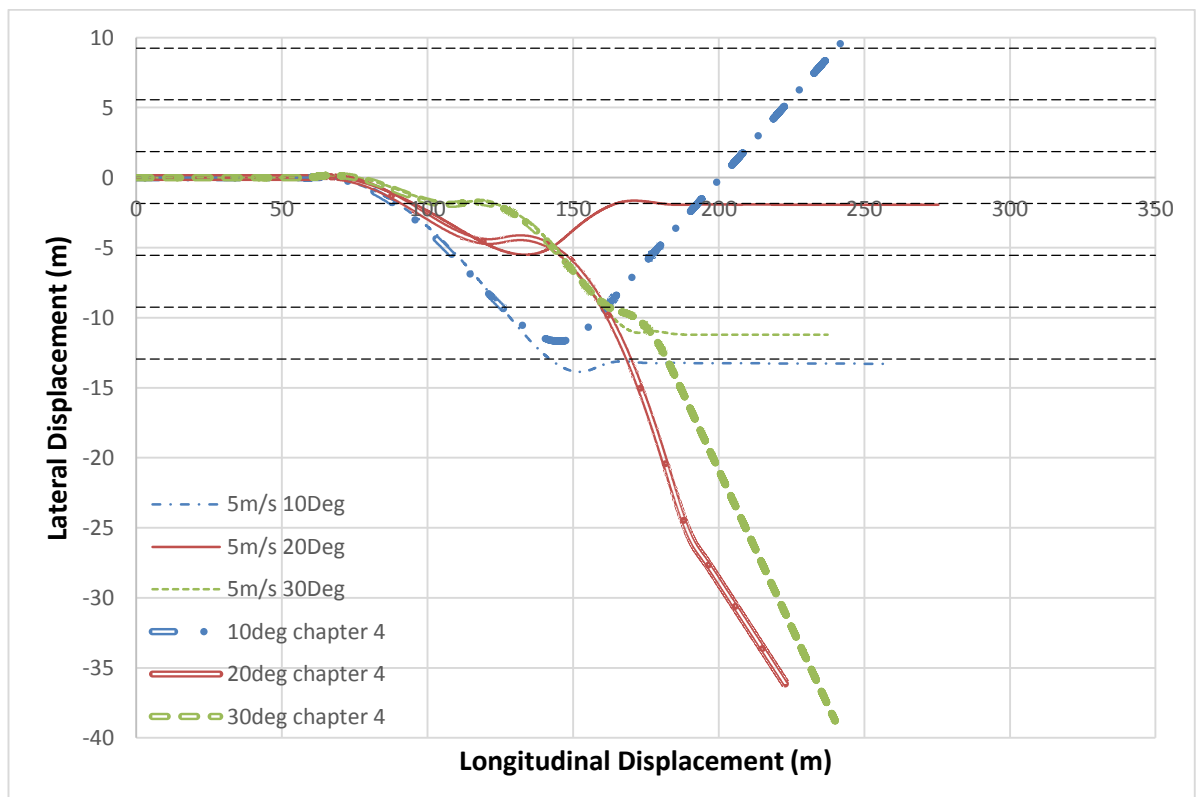
Figure 5.5: Comparison of the controlled (single lines) and uncontrolled (double lines) post-impact trajectories for the rear impact scenario with a speed differential of 5m/s.

Peter Samuel Delves

Table 5.4: Comparison of maximum displacements and final displacements of the controlled and uncontrolled vehicles for the rear impact scenario at 2.5m/s and 5m/s.

Maximum displacement (m) comparison						
Closing velocity	2.5m/s			5 m/s		
Impact angle (^{0})	10	20	30	10	20	30
Controlled	-4.07	-10.02	-20.30	-13.86	-5.50	-11.21
Uncontrolled	-96.82	-127.97	-67.16	-11.68	-36.14	-38.79
Final displacement (m) comparison						
Closing velocity	2.5m/s			5 m/s		
Impact angle (^{0})	10	20	30	10	20	30
Controlled	-4.07	-9.85	-18.12	-13.29	-1.95	-11.21
Uncontrolled	-96.82	-127.98	-67.16	11.53	-36.14	-38.79

All of the controlled vehicles lateral displacements are reduced compared to the uncontrolled vehicle. It has also stabilized all vehicles at trajectories parallel to their original ones. Maximum displacement for all but one of the uncontrolled vehicles is the same as their final displacement. This is because the heading trajectory of these vehicles has settled heading away from the original carriageway position resulting in them continuing to increase. The only vehicle different to this is the 5 m/s 10^0 impact where it can be seen that the sign has changed as the vehicle final heading angle is less than 180^0 at 166.89^0 resulting in it drifting back across its original lane.

Most of the controlled results maximum displacement is larger than the final displacement. This is because the control system is regaining control and producing a counteracting yaw moment and takes some time to settling at the desired heading angle. This is observed in Figures 5.2 and 5.3 as the yaw position and rate circle the objective point until it settles. This could be seen as undesirable but as the system needs to arrest the spin quickly some overshoot is tolerable.

Peter Samuel Delves
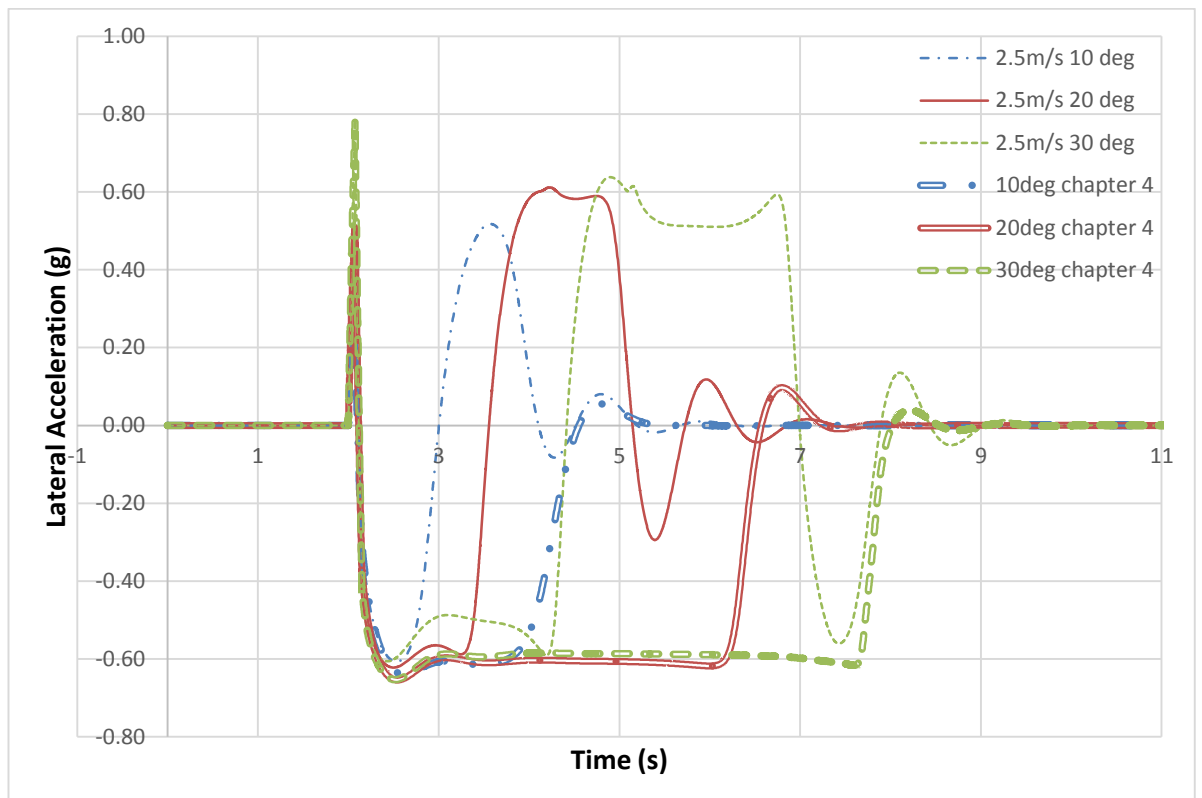
Figure 5.6: Comparison of the lateral acceleration time history of the controlled (single lines) and uncontrolled (double lines) for the rear impact scenario with a speed differential of 2.5m/s.
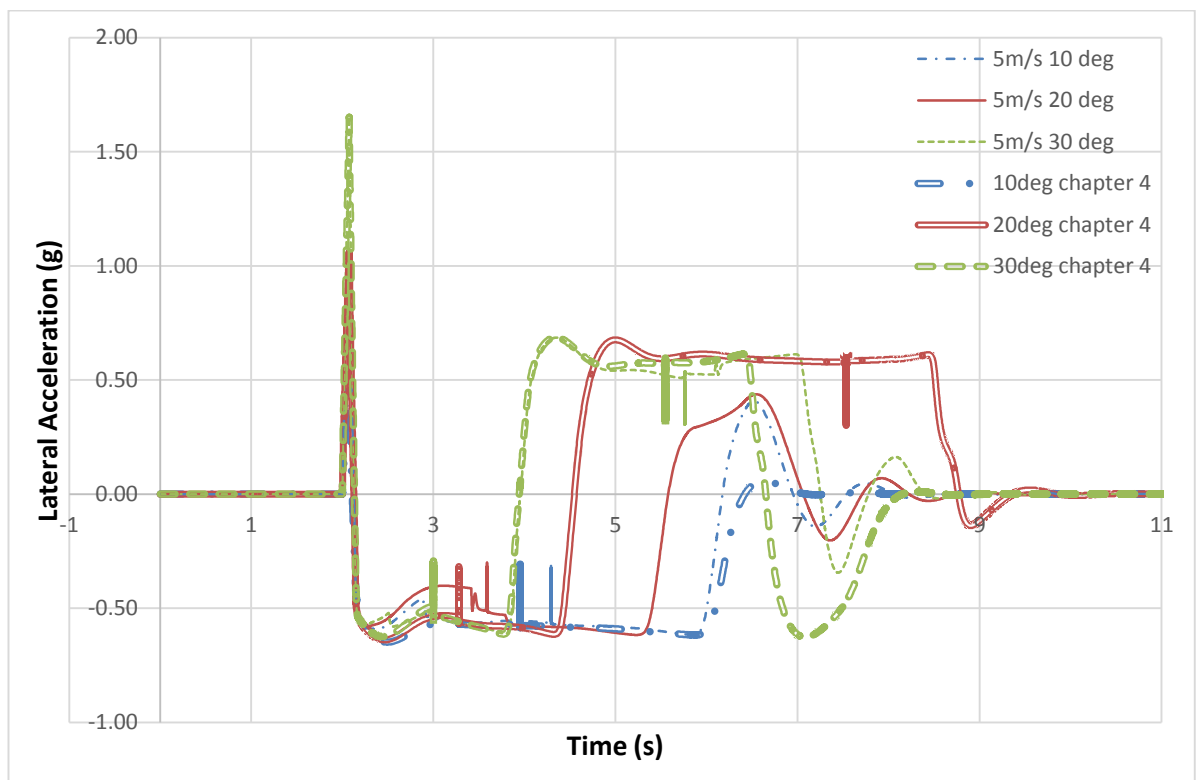
**Figure 5.7: Comparison of the lateral acceleration time history of the controlled (single line) and uncontrolled (double line) for the rear impact scenario with speed a differential of 5m/s.**

Peter Samuel Delves

Table 5.5: Maximum lateral acceleration generate by both controlled and uncontrolled vehicle sets for the rear impact scenario.

Maximum lateral acceleration (g)					
5m/s 10^0	5m/s 20^0	5m/s 30^0	2.5m/s 10^0	2.5m/s 20^0	2.5m/s 30^0
0.46	1.06	1.65	0.52	0.61	0.78

Figures 5.6 and 5.7 show the lateral acceleration time history in g for the rear impact scenario. Maximum lateral g is not reduced in this scenario as the control system has a 0.25 s validation and triggering delay. The interesting comparison is to be drawn is in the lateral g time history. The control system generates a counteracting acceleration of 0.6g around 3.5-4.2 s by the control system works to restore the vehicles to their original heading angle. Comparing this to the uncontrolled results where original acceleration of -0.6 g are sustained until the vehicle reaches its settling position resulting in the larger heading angles and displacements seen.

The 5 m/s incidents original responses are similar to those of the settling controller as it attempts to keep the vehicles spinning until they get close to the desired heading angle of 180^0. There is a small difference as the controlled 20^0 impact vehicle reduces to around -0.35 g between in the 3 to 4 s region to reduce the yaw rate but then increases again to make sure it reaches the 180^0 target. The 10^0 and 20^0 scenarios continue as -0.6 g until the settling controller is triggered where a contracting acceleration is induced as with the 2.5 m/s scenarios so that the vehicles will settle at their target angle.

The 5 m/s 30^0 uncontrolled and controlled responses are similar up to 6.5s where the uncontrolled vehicle's acceleration switches direction for the second time as it spins past 360^0 with it finally settling at around 7.5s at 377^0. The controlled vehicle has had some of the energy taken out of the spin so takes longer to reach 360^0 where at 7 s the control system switches from the second holding controller to its final settling controller. As control gains are high at this point some oscillation is seen but the target angle is reached and is considered settled at 7.9 s.

Peter Samuel Delves

5.4.2. Side Swipe Impact Control Results
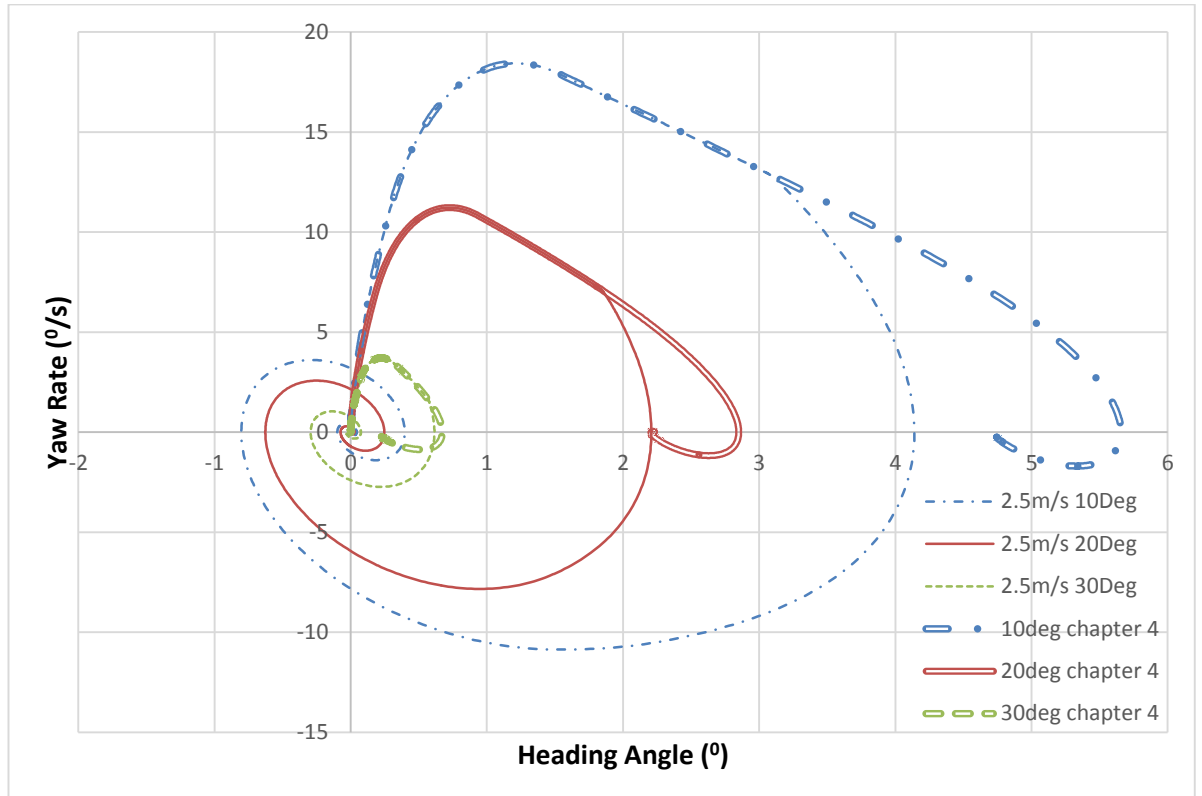
Figure 5.8: Plot comparing the yaw rate vs heading angle behaviour of the controlled (single lines) to uncontrolled (double lines) for the side swipe impact scenario at a speed differential of 2.5m/s.
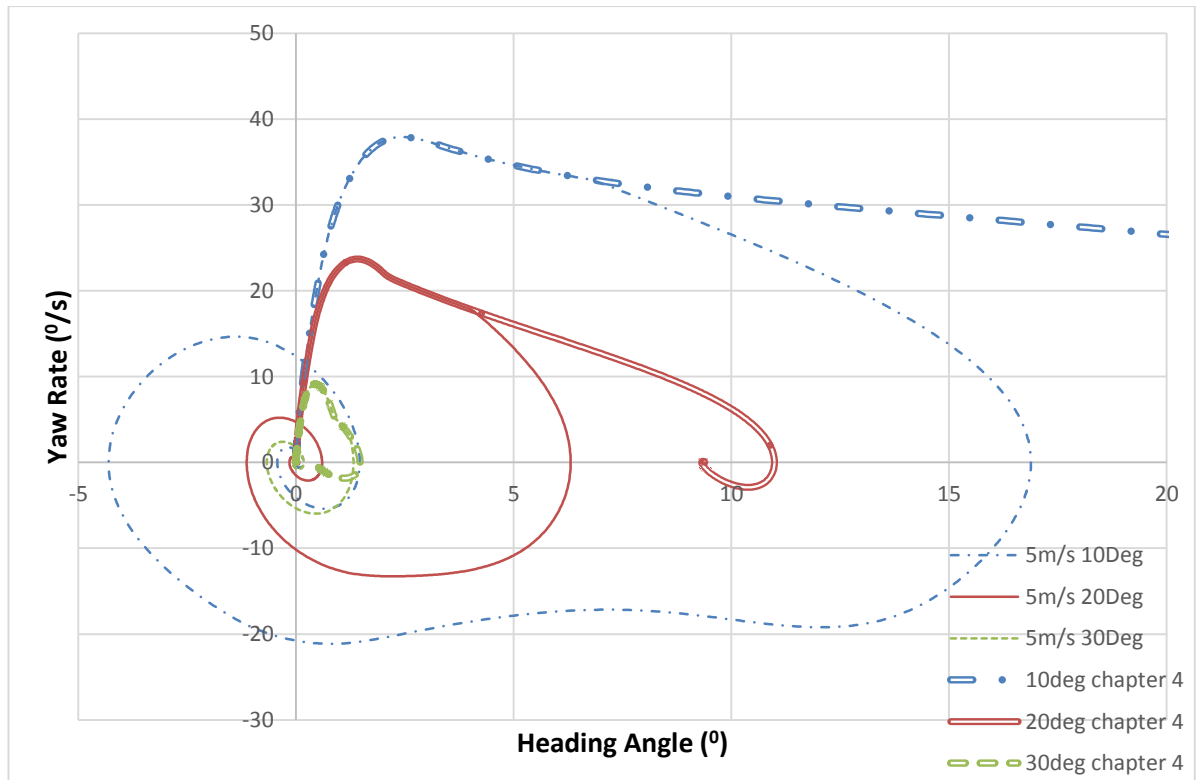
Figure 5.9: Plot comparing the yaw rate vs heading angle behaviour of the controlled (single lines) to uncontrolled (double lines) for the side swipe impact scenario at a speed differential of 5m/s.

110

Peter Samuel Delves

Table 5.6: Comparison of the maximum heading angles and final heading angles of the controlled and uncontrolled vehicles for all side swipe impacts.

Max heading angle (^{0}) comparison						
Closing velocity	2.5m/s			5 m/s		
Impact angle (^{0})	10	20	30	10	20	30
Controlled	4.14	2.21	0.61	16.88	6.31	1.32
Uncontrolled	5.66	2.85	0.67	50.33	10.99	1.47
Final angle (^{0}) comparison						
Closing velocity	2.5m/s			5 m/s		
Impact angle (^{0})	10	20	30	10	20	30
Controlled	0.00	0.00	0.00	0.00	0.00	0.00
Uncontrolled	4.76	2.23	0.22	42.72	9.39	0.48

Figures 5.8 and 5.9 show the yaw rate and heading angle of the controlled vehicles. These graphs are similar to the rear impact 2.5 m/s control graphs as they all bring the vehicles back to 0^0 heading angle. Maximum yaw rates are the same as the uncontrolled vehicles because of the validation and actuation lag of the control system so the comparison is not shown.

As with the 2.5 m/s rear impact vehicles they all reduce the yaw rate quickly resulting in less angular displacement and reverse the yaw rate as the control system attempts to bring the vehicles back to their original heading angle. There is some overshoot on heading angle as the first high gain settling controller tries to bring the vehicles back to 0^0 as quickly as possible and then circle the objective point before settling. Maximum overshoot is in the region of 25% of the maximum displacement but as this is 4^0 it does not expose the other side of the vehicle to unnecessarily large angles as to increase the chance of a side impact.

From Table 5.6 maximum heading angles are all reduced. This demonstrates that the control system is effective across the whole range of impact scenarios and induced yaw rates. The advantage of these reductions is that exposure of the side of the vehicle is reduced, which in turn means that the chance of a secondary side impact is also reduced.

Peter Samuel Delves

All of the controlled vehicles settle at their original heading angle. Therefore they not only reach their control objective but in turn reduced the lateral displacement of all the vehicles.

Table 5.7: Comparison of the time taken for each controlled and uncontrolled vehicles to settle at their final heading angle and their lateral displacement at this settling time for all side swipe impacts.

Heading angle settling time (s) comparison						
Closing velocity	2.5m/s			5 m/s		
Impact angle (^{0})	10	20	30	10	20	30
Controlled	4.35	4.23	4.21	5.69	4.56	4.22
Uncontrolled	3.37	3.26	3.96	6.16	3.76	4.03
Lateral displacement at settle time (m) comparison						
Closing velocity	2.5m/s			5 m/s		
Impact angle (^{0})	10	20	30	10	20	30
Controlled	-0.968	-0.2166	0.196	-7.793	-1.503	0.456
Uncontrolled	-2.1147	-0.8597	-0.05	-37.943	-4.885	-0.128

The controlled vehicles were considered stable when they were within 2% of their final settling point or within 1^0. The uncontrolled vehicles were considered stable when they were within 2% of their final value. These maximum and final angles are presented in Table 5.6.

Lateral displacement has been reduced in all but two of the simulations. The two that seem to have increased the lateral displacement have done so by 0.2 m and 0.58 m, which is less than half a lane width, meaning that the vehicle will not exit its original lane. All of the other systems have reduced displacement with three of them stopping the vehicle from exiting its original lane entirely. The 5 m/s 10^0 vehicle has the largest lateral displacement but has reduced it by 30m compared with the uncontrolled results. This results in the vehicle only travelling the equivalent of two lanes.
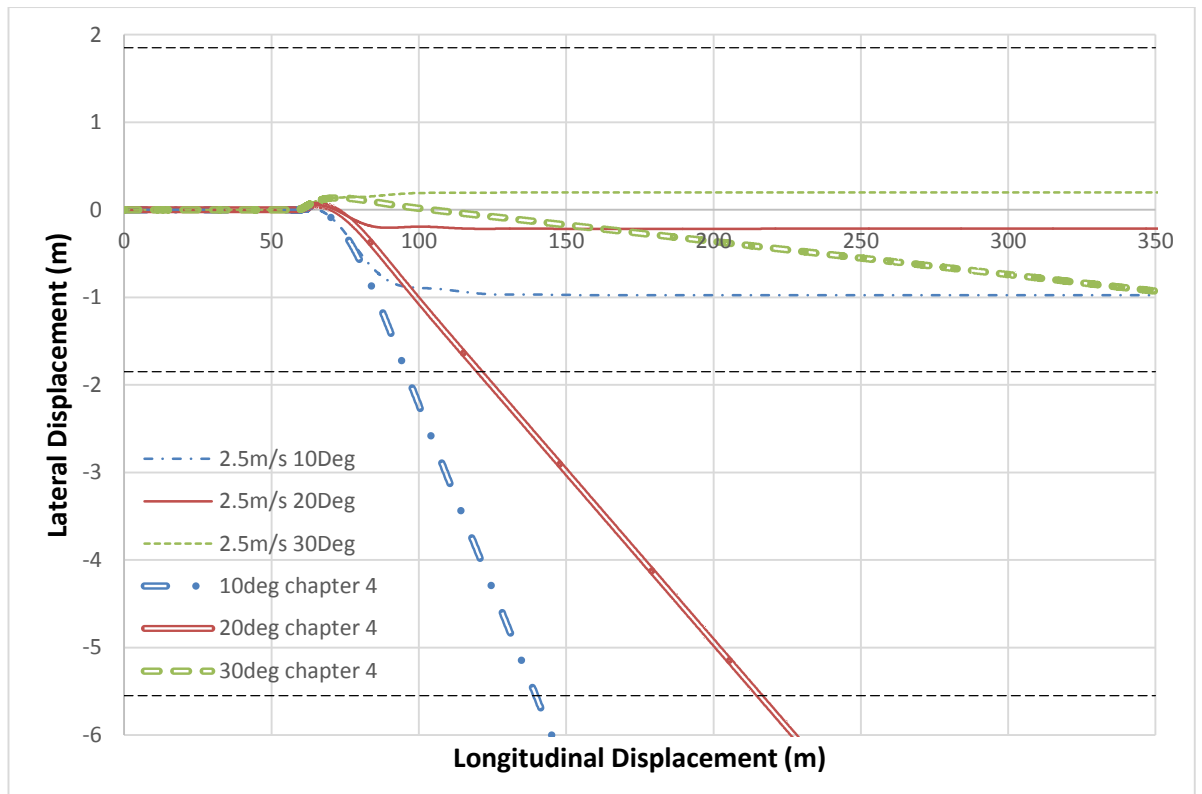
Figure 5.10: Comparison of the controlled (single lines) and uncontrolled (double lines) post-impact trajectories for the side swipe impact scenario with a speed differential of 2.5m/s.
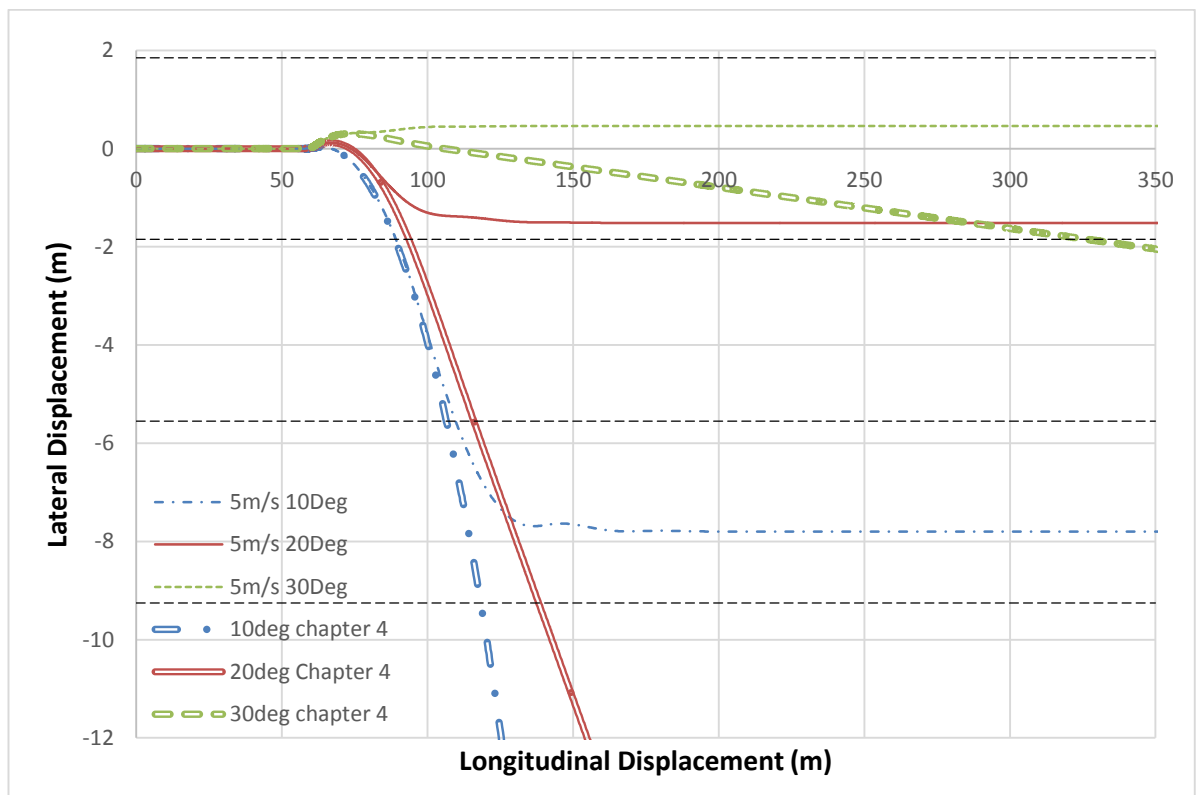
Figure 5.11: Comparison of the controlled (single lines) and uncontrolled (double lines) post-impact trajectories for the side swipe impact scenario with a speed differential of 5m/s.

Peter Samuel Delves

Table 5.8: Comparison of maximum displacements and final displacements of the controlled and uncontrolled vehicles for the side swipe impact scenario at 2.5m/s and 5m/s.

Maximum displacement (m) comparison						
Closing velocity	2.5m/s			5 m/s		
Impact angle (^{0})	10	20	30	10	20	30
Controlled	-0.97	-0.22	0.20	-7.80	-1.52	0.46
Uncontrolled	-23.09	-10.83	-0.93	-133.61	-45.47	-2.15
Final displacement (m) comparison						
Closing velocity	2.5m/s			5 m/s		
Impact angle (^{0})	10	20	30	10	20	30
Controlled	-0.97	-0.22	0.20	-7.80	-1.52	0.46
Uncontrolled	-23.09	-10.83	-0.93	-133.61	-45.47	-2.15

Figures 5.10 and 5.11 show the vehicle trajectories for the six side impact simulations with the control system activated. Immediately observable is that all the vehicle trajectories end up parallel to the original lane. This has aligned the vehicle with the road carriageway so that the front crash structure is ready for any potential secondary impact.

Table 5.8 shows the maximum vehicle displacement and the final displacement at the end of the simulation. All the values are the same for the final and maximum displacement as all of the controlled vehicles are now parallel to the original lane and thus no longer have lateral global velocity whereas the uncontrolled vehicles have all settled at heading angles away from the original so are constantly travelling laterally.

As with the rear impact results there is an argument that if the uncontrolled vehicles have stabilised before the controlled vehicles the driver would be able to steer the vehicle back to a parallel heading. This is true but the driver will potentially be in shock reducing reaction times so the results presented in Table 5.8 will continue to increase for some time, whereas once the controller has stabilised the vehicle it will be at a safe heading.

Peter Samuel Delves
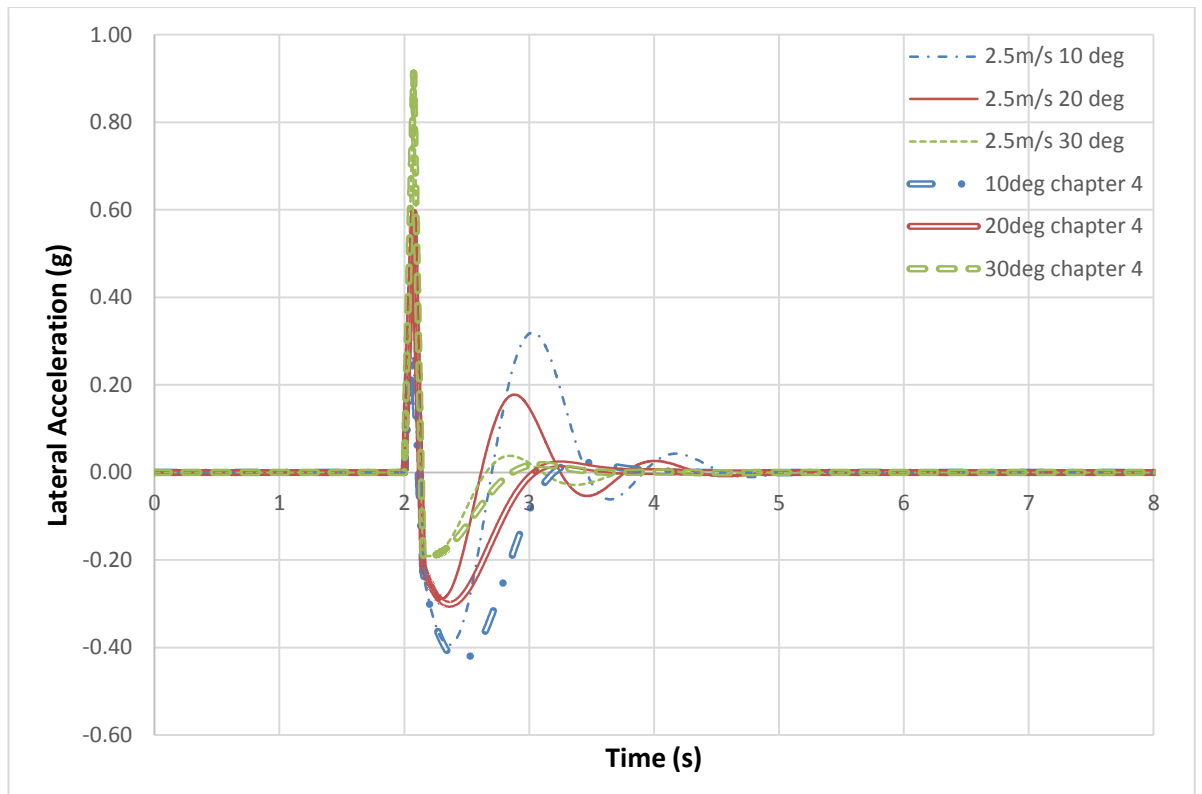
Figure 5.12: Comparison of the lateral acceleration time history of the controlled (single line) and uncontrolled (double line) for the side swipe impact scenario with a speed differential of 2.5m/s.
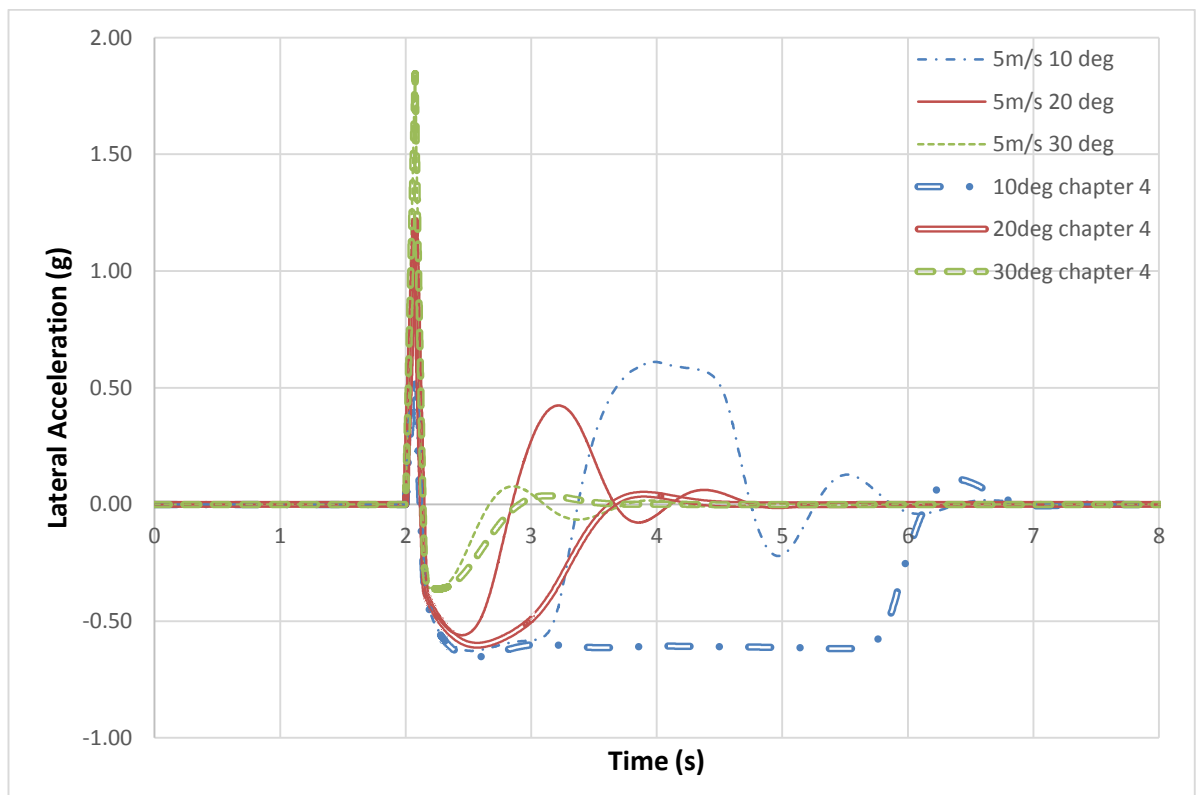
Figure 5.13: Comparison of the lateral acceleration time history of the controlled (single line) and uncontrolled (double line) for the side swipe impact scenario with a speed differential of 5m/s.

Peter Samuel Delves

Table 5.9: Maximum lateral acceleration generate by both controlled and uncontrolled vehicle sets for the side swipe impact scenario.

Maximum Lateral Acceleration					
5m/s 10^0	5m/s 20^0	5m/s 30^0	2.5m/s 10^0	2.5m/s 20^0	2.5m/s 30^0
0.61	1.21	1.85	0.32	0.59	0.91

Figures 5.12 and 5.13 plot the lateral acceleration time history in g for the side-swipe impact scenario. Maximum lateral acceleration is the same as that in the uncontrolled vehicle. This is again due to the control actuation delay of 0.25 s. The second peak is similar to that of the uncontrolled vehicle but this is where the interaction of the control system is seen. Compared to the uncontrolled results there is a marked difference as large opposite accelerations are developed by the control system to counteract the original disturbance. The control intervention did increases some of settling times but as discussed in the heading angle section this increase is acceptable as the vehicles are stabilised at safe heading angles.

5.5. Post-Impact Control Study Discussion

The control system results presented in this chapter show the potential that drive torque vectoring control has for post-impact control and shows it is a viable option for use in reducing serious injury occurring in secondary impacts.

The control system demonstrated that torque vectoring is a viable option for post-impact control as it was able to stabilise all 12 of the post-impact crashes presented in the previous section at one of the desired heading angles. This was achieved by developing a six-phase switching PID controller made up of a set of high gain settling controllers and lower gain holding controllers with the control objective to stabilise the vehicle at heading angles parallel to the initial heading angle. The stabilising controllers were activated when the vehicle was close to these heading angles, 0^0, 180^0 or 360^0 to original heading. The settling controllers had aggressive high gains which attempted to reduce yaw rate rapidly to settle the vehicle at the desired heading angle as soon as possible. Once the vehicle reach certain threshold angles where the system was going to settle outside these angles the holding controller was activated. These holding controllers attempted to hold yaw rates until the next settling threshold was crossed at which point the next settling controller was

Peter Samuel Delves

activated. This system actually brought a twofold improvement compared to the benchmark results as it not only re-aligned the vehicles' main crash structures with the carriageway but also reduced the maximum lateral displacement dramatically. The majority of the simulation settling times were increased by the control systems' intervention but the increased cost in settling time is justified by the safer final heading and the reduction in the lateral displacements achieved in comparison to the uncontrolled vehicles.

The advantages of using heading angle as the control state is that when the vehicle is at 0^0, 180^0 or 360^0 to the original heading the vehicle is parallel to its original lane and is thus no longer exposing its side to other potential impacts. This will also allow for a controlled deceleration of the vehicle either by an automated system or by the driver. In reality once the uncontrolled vehicles have stabilised they can be steered to align themselves with the carriageway but this would require a shocked driver to react. Also the lateral displacement of the uncontrolled vehicles is already greater than that of the controlled vehicles. Therefore even if the driver was able to respond promptly, the trajectory would not be an improvement on the controlled response.

Peter Samuel Delves

6. Chapter Six: Conclusion and Further Work

6.1. Conclusion

A large amount of research has been and continues to be conducted in the area of dynamic vehicle control and pre-crash avoidance and mitigation. Work has been centred around dynamic vehicle control systems that aid the driver in day-to-day driving. These systems increase a vehicle's stability region. Systems take the form of ABS, TCS and ESC, which reduce the risk of incidents occurring without being intrusive and can be found on the majority of consumer vehicles. Research into more autonomous systems that step in when a crash is imminent continue to be developed. This pre-crash control work is centred on systems such as automatic emergency braking, collision warning or collision avoidance. These systems activate when they sense a collision is imminent, aiming to reduce the severity of the collision by reducing speed or avoiding the collision altogether. Work concerning control of the vehicle in the post-impact phase of an accident is still in its infancy, with schemes using the braking and or steering systems achieving reasonable levels of success. However, the use of drive torque vectoring, which appears to be an ideal candidate, has received little attention.

To investigate drive torque vectoring as an option for post-impact control, a vehicle model was developed with longitudinal, lateral, yaw, roll and 4 wheel rotation DOF to produce an 8-DOF model. This model transmitted forces through a non-linear Pacejka tyre model with combined lateral and longitudinal slip. Investigation showed that a non-linear model was required as the crash study induced accelerations outside of a vehicle's linear region. The differences between linear and non-linear models was demonstrated by simulating a linear 2-DOF, non-linear 7-DOF and non-linear 8-DOF model through step-steer and lane change manoeuvres at velocities varying between 10-40m/s to compare their dynamic behaviour. Simulations showed that as velocity was increased results diverged between the linear and non-linear models by up to 12%. This demonstrated the need for a non-linear model for this control study as the post-impact scenarios induced peaks of over 1g of lateral acceleration.

Crash force calculations were carried out based on momentum theory. Speed differentials of 2.5m/s and 5m/s were selected and lateral and longitudinal velocity

Peter Samuel Delves

components were calculated at three different impact angles of 10^0, 20^0 and 30^0. A coefficient of restitution $e = 0.2$, which represents the energy dissipated during the collision, was used within these calculations for the post-impact vehicle velocities, which in turn allowed calculation of the momentum exchange between the two vehicles. With these inputs, the crash model was tested using two crash scenarios, a rear impact and side swipe impact, to assess the behaviour of a vehicle without control intervention and produce a set of benchmark results against which the control system was evaluated. These simulations induced a variety of yaw rates, which resulted in spins covering a full range of final heading angles. The majority of these caused large lateral displacements relative to the vehicle's original positions exposing the side of the vehicle to dangerous secondary impacts.

The control system demonstrated that torque vectoring is a viable option for post-impact control as it was able to stabilise all of the crashes presented at safe heading angles. The control system used a six-phase switching PID controller made up of a set of high gain settling controllers and lower gain holding controllers with the control objective to stabilise the vehicle at heading angles parallel to the initial heading angle. The stabilising controllers were activated when the vehicle was close to heading angles of, 0^0, 180^0 or 360^0. The settling controllers had aggressive high gains that reduced yaw rate rapidly in an attempt to settle the vehicle at the desired heading angle. Once the vehicle passed a certain threshold angle the control objective was switched to the next target angle and the holding controller was activated. These holding controllers held yaw rates until the next threshold close to the desired heading was crossed at which point the next settling controller was activated. This system brought about improvements compared to the benchmark results, with no control action, as it not only re-aligned the vehicle's main crash structures with the carriageway, which was the main control objective, but in doing so it also brought about a dramatic reduction in maximum lateral displacement. In some scenarios, the settling time of the vehicles was increased by the control system by up to 43%. However, given the re-alignment of crash structures and reduction in lateral displacement, this can be considered a reasonable compromise.

Peter Samuel Delves

Chapter Six: Conclusion and Further Work

As post-impact dynamic control is a young area of research little work has been carried out so far. The work carried out by Yang et al. and Kim et al. is the closest and looks at the use of the braking and/or steering systems to control a vehicle. However neither has investigated the potential of drive torque vectoring control, which this study demonstrates is capable of achieving post-impact control.

The work carried out by Yang et al. has primarily been carried out at lower initial speed, commonly using 15 m/s as opposed to 29 m/s, and a higher coefficient of friction of 0.9 compared to 0.7 in this study. This theoretically makes it easier to perform control as larger net forces can be produced and the accidents themselves involve lower levels of dynamic intensity. Yang et al. also do not add any control delay so the system responds quicker. Yang et al. has implemented steer control into their brake control scheme to produce a controller which attempts to minimise lateral displacement. This goes some way to explain why lower levels of lateral displacement and simulation time are seen when compared with this study. However the Yang et al. system sometimes leaves the vehicle's side exposed in relation to the original heading, whereas this study's system stabilises all vehicles at heading angles parallel to the direction of travel. Yang et al. aim to reduce the risk of secondary events but the control system sometimes leaves the side of the vehicle exposed. This could arguably increase the risk if a secondary collision were to occur, whereas this study's control action stops exposure of the vehicle's side, which is safer if another collision were to occur.

Work carried out by Kim et al. is more comparable as it is performed with the same vehicle data, initial velocities, coefficient of friction and the crash force impulses are calculated in a similar manner. Earlier work by Byung-joo Kim and Peng (2012) investigates the use of brake vectoring to control heading angles and lateral deviation. The impact Kim et al. use produces an initial yaw rate of 89^0/s and is directly comparable with the rear impact at velocity difference of 5 m/s and impact angle of 20^0, which produce an initial yaw rate of 87.3^0. Immediately observable is the similarity of the trajectories of these two cases. Kim et al. simulated vehicle moves laterally, which reach the second lane boundary at 5.55 m, just as this study's vehicle does, which just touches this boundary. The vehicle of Kim et al. then travels

Peter Samuel Delves

back towards its original lane finally settling in the adjacent lane at a displacement of around 3m relative to the original position. This study shows similar behaviour, finally stabilising the vehicle on the initial lane boundary at 1.95 m from the original position. Comparing the yaw rate vs heading angle graphs both Kim et al. and this study's vehicles follow a similar path steadily decreasing the yaw rate as it approaches the 180^0 target point. The different phases in the PID switching controller for this study are evident where yaw rates are suddenly altered, whereas in Kim et al. it is smoother until it reaches the desired settling point, where it yaw rate drops steeply.

One advantage observed from this study is that the control system is able to achieve its target angle of 180^0 whereas Kim et al. settled around 190^0. This is because this study's system sustains velocity and is therefore able to keep altering heading angles, as opposed to Kim et al., which reduces velocity to zero by the end of the simulation so the vehicle has no forward velocity to allow any rotate. There are advantages and disadvantages to both systems. This system arguably performs better as it achieves its control objective as it is does not have to balance the decision between reducing lateral displacement and achieving safe heading angles and actually ends up with a lower lateral displacement compared with Kim et al. As the Kim et al. system uses the brakes it is constantly reducing velocity so could be seen as reducing the severity of any potential accident. However as Kim et al. are reducing velocity quickly from a high speed of 29m/s on a road where other vehicles are traveling at high speed it could potentially lead to other impacts at high velocity differentials with other vehicles, whereas this study's use of drive vectoring results in less dramatic reductions in velocity. Therefore, any secondary vehicle-to-vehicle collision will be at a lower velocity differential compared to Kim et al. reducing the severity of any secondary collision. This work has not only proved that drive torque vectoring is capable of controlling a vehicle in a post-impact scenario, in some cases it has outperformed the current braking and or steering systems being investigated.

Peter Samuel Delves

6.2 Further Work

The work in this thesis demonstrates that drive torque vectoring control could be used in post-impact situations. However this work is only in its infancy and could be advanced in the following ways:

1. This system uses an 8-DOF handling model and the simulation is performed on a straight road with no road surface input. Further refinement of this model could be carried out to include suspension travel so that road roughness could be input to the model and assess what effect these vertical disturbances could have on the system.

2. This system uses PID control which uses hard set thresholds for objective and control action switching. This approach works well with a known set of vehicle parameters. However further development of the system could involve the formulation of a set of fuzzy logic rules which would produce a more universal set of controller rules, which would allow this system to work across a range of different vehicle parameter sets.

3. Integration of steering control in the system could bring additional benefits when it comes to controlling a vehicle's trajectory as demonstrated by Yang et al. with their combined brake and steering control research. This would require the implementation of at least a single-output multi-input or possibly a multi-input multi-output system. This could lead to a system that would be able to minimise lateral displacement of the vehicle as well as target safe heading angles. The addition of steering control could also lead to the implementation of pre-crash steering action. The benefits of this, which are shown in Kim et al., are that it could bring about a reduction in peak yaw rates, reduce oscillation about the target settling point, and thus reduce settling times.

4. The system could also have a braking system activation point when stabilisation is detected, where the vehicle is automatically brought to a stop in a controlled manner. This would ideally perform the deceleration in a more progressive manner than applying full braking action, which would allow other drivers around to react safely.

Peter Samuel Delves

5. Consideration of how possible damage sustained to the vehicle during the incident could be investigated. This could be achieved by removing control from one or two motor/s and locking the wheel/s to simulate what would happen if part of the system sustained damage.

Peter Samuel Delves

References

Breitling, T., R. Schöneburg and H. Metzler (2009). "The Mercedes-Benz Experimental Safety Vehicle 2009." Mercedes Car Group (MCG).

Burke, A. F. (2007). "Batteries and Ultracapacitors for Electric, Hybrid, and Fuel Cell Vehicles." Proceedings of the IEEE **95**(4): 806-820.

Byung-joo Kim and H. Peng (2012). Vehicle Stability Control of Heading Angle and Lateral Deviation to Mitigate Sceondary Collisions. AVEC 2012, Seoul, South Korea.

Byung-joo Kim and H. Peng (2014). Collision Strength Estimation and Preemptive Steering Control for Post-Impact Vehicle Motion Control. International Symposium on Advanced Vehicle Control. Tokyo**:** 496-503.

Chan, C. C. (2002). "The state of the art of electric and hybrid vehicles." Proceedings of the IEEE **90**(2): 247-275.

Chan, C. C. (2007). "The State of the Art of Electric, Hybrid, and Fuel Cell Vehicles." Proceedings of the IEEE **95**(4): 704-718.

Chan, C. C., A. Bouscayrol and K. Chen (2010). "Electric, Hybrid, and Fuel-Cell Vehicles: Architectures and Modeling." Vehicular Technology, IEEE Transactions on **59**(2): 589-598.

Chan, C. Y. and H. S. Tan (1999). Lane tracking control in vehicle-following collision situations. American Control Conference, 1999. Proceedings of the 1999.

Ching-Yao, C. and T. Han-Shu (1999). Application of a robust steering controller in emergency situations. Intelligent Transportation Systems, 1999. Proceedings. 1999 IEEE/IEEJ/JSAI International Conference on.

Ching-Yao, C. and T. Han-Shue (2001). "Feasibility analysis of steering control as a driver-assistance function in collision situations." Intelligent Transportation Systems, IEEE Transactions on **2**(1): 1-9.

Peter Samuel Delves

References

De Novellis, L., A. Sorniotti, P. Gruber and L. Shead (2012). Torque Vectoring for Electric Vehicles with Individually Controlled Motors: State-of-the-Art and Future Developments. Electric Vehicle Symposium. Los Angeles.

Digges, K. and G. Bahouth (2003). Frequency of Injuries in Multiple Impact Crashes. The Advancement of Automotive Medicine.

Farmer, C. M. (2004). "Effect of Electronic Stability Control on Automobile Crash Risk." Traffic Injury Prevention **5**.

Genta, G. (1997). Chapter 7 Road Accidents. Motor Vehicle Dynamics Modeling and Simulation, World Scientific Publishing Co.

Hernandez, J. I. and K. Chen Yuan (2004). "Lateral control of higher order nonlinear vehicle model in emergency maneuvers using absolute positioning GPS and magnetic markers." Vehicular Technology, IEEE Transactions on **53**(2): 372-384.

Hogan, I. (2008). The Use of Vehicle Dynamics Control Systems for Automotive Collision Mitigation. PhD, Manchester Metropolitan University.

Hori, S.-I. S. a. Y. (2001). "Advantage of electric motor for anti skid control of electric vehicle " EPE.

Hori, Y. (2004). "Future vehicle driven by electricity and Control-research on four-wheel-motored "UOT electric march II"." Industrial Electronics, IEEE Transactions on **51**(5): 954-962.

Hori, Y., Y. Toyoda and Y. Tsuruoka (1998). "Traction control of electric vehicle: basic experimental results using the test EV “UOT electric march”." Industry Applications, IEEE Transactions on **34**(5): 1131-1138.

Ilic-Spong, M., T. J. E. Miller, S. R. Macminn and J. S. Thorp (1987). "Instantaneous Torque Control of Electric Motor Drives." Power Electronics, IEEE Transactions on **PE-2**(1): 55-61.

Peter Samuel Delves

References

Kondo, K. and M. Makino (2008). "Crash Simulation of Large-Number-of-Elements Car Model by LS-DYNA on Highly Parallel Computers." FUJITSU Sci. Tech **44**(4): 467-474.

Lindgren, A. and C. Chan (2006). State of the Art Analysis: An Overview of Advanced Driver Assistance Systems (ADAS) and Possible Human Factors Issues. Swedish Human Factors Network (HFN).

Manning, W. J. and D. A. Crolla (2007). "A review of yaw rate and sideslip controllers for passenger vehicles." Transactions of the Institute of Measurement and Control **29**(2): 117-135.

McCall, J. C. and M. M. Trivedi (2004). An integrated, robust approach to lane marking detection and lane tracking. Intelligent Vehicles Symposium, 2004 IEEE.

Milehins, M., C. Cheng, T. Chu and R. P. Jones (2010). Handling Behaviour of a TTR Hybrid Electric Vehicle with Independent Rear Wheel Torque Control. AVEC.

Odenthal, D., T. Bünte and A. J. (1999). Nonlinear steering and braking control for vehicle rollover avoidance.

Pacejka, H. B. (2002). Tyre and Vehicle Dynamics, Butterworth-Heinemann.

Pacejka, H. B. and B. I.J.M. (1997). "Magic Formula Tyre Model with Transient Properties." Vehicle System Dynamics **27**.

Peng, X., H. Zhe, G. Guifang, X. Gang, C. Binggang and L. Zengliang (2011). "Driving and control of torque for direct-wheel-driven electric vehicle with motors in serial." Expert Systems with Applications **38**(1): 80-86.

Pietzsch, S., V. Trung Dung, J. Burlet, O. Aycard, T. Hackbarth, N. Appenrodt, J. Dickmann and B. Radig (2009). "Results of a Precrash Application Based on Laser Scanner and Short-Range Radars." Intelligent Transportation Systems, IEEE Transactions on **10**(4): 584-593.

Pomerleau, D. (1995). RALPH: rapidly adapting lateral position handler. Intelligent Vehicles '95 Symposium.

Peter Samuel Delves

References

Sakai, S., H. Sado and Y. Hori (1999). "Motion control in an electric vehicle with four independently driven in-wheel motors." Mechatronics, IEEE/ASME Transactions on **4**(1): 9-16.

Schoeneburg, R. and T. Breitling (2005). "Enhancement of active and passive safety by future PRE-SAFE systems." Mercedes Car Group (MCG)(Paper no:05-0080).

Sharp, R. S. and D. J. N. Limebeer (2001). "A Motorcycle Model for Stability and Control Analysis." Multibody System Dynamics **6**(2): 123-142.

Sugimoto, Y. and C. Sauer (2005). Effectiveness Estimation Method for Advanced Driver Assistance System and its Application to Collision Mitigation Brake System. Proc. 19th Int. Tech. Conf. Enhanced Safety Vehicles.

Tchamna, R. and I. Youn (2013). "Yaw rate and side-slip control considering vehicle longitudinal dynamics." International Journal of Automotive Technology **14**(1): 53-60.

Tideman, M., M. C. van der Voort and B. van Arem (2010). "A new scenario based approach for designing driver support systems applied to the design of a lane change support system." Transportation Research Part C: Emerging Technologies **18**(2): 247-258.

Transport, D. f. (2013). Reported Road Casualties Great Britain: 2013 Annual Report. D. f. Transport. Online**:** 11.

Yang, D., T. J. Gordon, B. Jacobson and M. Jonasson (2011). A Nonlinear Brake-Based Path Controller for Post Impact Vehicle Dynamics. IAVSD.

Yang, D., T. J. Gordon, B. Jacobson and M. Jonasson (2012). "A nonlinear post impact path controller based on optimised brake sequences." Vehicle System Dynamics **50**(sup1): 131-149.

Yang, D., T. J. Gordon, B. Jacobson, M. Jonasson and M. Lidberg (2011). "Optimized brake-based control of path lateral deviation for mitigation of secondary collisions."

Peter Samuel Delves

References

Proceedings of the Institution of Mechanical Engineers, Part D: Journal of Automobile Engineering **225**(12): 1587-1604.

Yang, D., B. Jacobson, M. Jonasson and T. J. Gordon (2014). "MINIMIZING VEHICLE POST IMPACT PATH LATERAL DEVIATION USING OPTIMIZED BRAKING AND STEERING SEQUENCES." International Journal of Automotive Technology **15**(1): 11.

YASA. (2015). "YASA-750 Electric motor." 2015, from http://www.yasamotors.com/products/yasa-750/.

Zhou, J., H. Peng and J. Lu (2008). "Collision model for vehicle motion prediction after light impacts." Vehicle System Dynamics **46**(sup1): 3-15.

Peter Samuel Delves

Appendix 1: Pacejka Tyre Model Parameters

```
%Tyre model params
%%%%%%%%%%%%%%%%%%%%%%%%
%%%Pacejka Parameters%%%
%%%%%%%%%%%%%%%%%%%%%%%%%

%%% From Pacejka Book

%%%Longitudinal Parameters%%%

PCX1 = 1.685;      %Shape factor Cfx for longitudinal force
PDX1 = 1.210;      %Longitudinal friction Mux at Fznom
PDX2 = -0.037;     %Variation of friction Mux with load
PDX3 = 0;          %Variation of friction Mux with camber
PEX1 = 0.344;      %Longitudinal curvature Efx at Fznom
PEX2 = 0.095;      %Variation of curvature Efx with load
PEX3 = -0.020;     %Variation of curvature Efx with load squared
PEX4 = 0.0;        %Factor in curvature Efx while driving
PKX1 = 21.51;      %Longitudinal slip stiffness Kfx/Fz at Fznom
PKX2 = -0.163;     %Variation of slip stiffness Kfx/Fz with load
PKX3 = 0.245;      %Exponent in slip stiffness Kfx/Fz with load
PHX1 = -0.002;     %Horizontal shift Shx at Fznom
PHX2 = 0.002;      %Variation of shift Shx with load
PVX1 = 0.0;        %Vertical shift Svx/Fz at Fznom
PVX2 = 0.0;        %Variation of shift Svx/Fz with load
RBX1 = 12.35;      %Slope factor for combined slip Fx reduction
RBX2 = -10.77;     %Variation of slope Fx reduction with kappa
RCX1 = 1.092;      %Shape factor for combined slip Fx reduction
RHX1 = 0.007;      %Shift factor for

%%%Lateral Parameters%%%

PCY1 = 1.193;      %Shape factor Cfy for lateral forces
PDY1 = -0.990 ;    %Lateral friction Muy
PDY2 = 0.145;      %Variation of friction Muy with load
PDY3 = -11.23;     %Variation of friction Muy with squared camber
PEY1 = -1.003;     %Lateral curvature Efy at Fznom
PEY2 = -0.537;     %Variation of curvature Efy with load
PEY3 = -0.083;     %Zero order camber dependency of curvature Efy
PEY4 = -4.787;     %Variation of curvature Efy with camber
PKY1 = -14.95;     %Maximum value of stiffness Kfy/Fznom
PKY2 = 2.130;      %Load at which Kfy reaches maximum value
PKY3 = -0.028;     %Variation of Kfy/Fznom with camber
PHY1 = 0.003;      %Horizontal shift Shy at Fznom
PHY2 = -0.001;     %Variation of shift Shy with load
PHY3 = 0.075;      %Variation of shift Shy with camber
PVY1 = 0.045;      %Vertical shift in Svy/Fz at Fznom
PVY2 = -0.024;     %Variation of shift Svy/Fz with load
PVY3 = -0.532;     %Variation of shift Svy/Fz with camber
PVY4 = 0.039;      %Variation of shift Svy/Fz with camber and load
RBY1 = 6.461;      %Slope factor for combined Fy reduction
RBY2 = 4.196;      %Variation of slope Fy reduction with alpha
RBY3 = -0.015;     %Shift term for alpha in slope Fy reduction
RCY1 = 1.081;      %Shape factor for combined Fy reduction
RHY1 = 0.009;      %Shift factor for combined Fy reduction
RVY1 = 0.053;      %Kappa induced side force Svyk/Muy*Fz at Fznom
RVY2 = -0.073;     %Variation of Svyk/Muy*Fz with load
```

a

Appendix 1 Pacejka Tyre Model Parameters

```
RVY3 = 0.517;     %Variation of Svyk/Muy*Fz with camber
RVY4 = 35.44;     %Variation of Svyk/Muy*Fz with alpha
RVY5 = 1.9;       %Variation of Svyk/Muy*Fz with kappa
RVY6 = -10.71;    %Variation of Svyk/Muy*Fz with atan(kappa)


%%%Aligning Parameters%%%

QBZ1 = 8.964;     %Trail slope factor for trail Bpt at Fznom
QBZ2 = -1.106;    %Variation of slope Bpt with load
QBZ3 = -0.842;    %Variation of slope Bpt with load squared
QBZ4 = -0.227;    %Variation of slope Bpt with camber
QBZ5 = 0.0;       %Variation of slope Bpt with absolute camber
QBZ9 = 18.47;     %Slope factor Br of residual torque Mzr
QBZ10= 0;         %Slope factor Br of residual torque Mzr
QCZ1 = 1.180;     %Shape factor Cpt for pneumatic trail
QDZ1 = 0.100;     %Peak trail Dpt" = Dpt*(Fz/Fznom*R0)
QDZ2 = -0.001;    %Variation of peak Dpt" with load
QDZ3 = 0.007;     %Variation of peak Dpt" with camber
QDZ4 = 13.05;     %Variation of peak Dpt" with camber squared
QDZ6 = -0.008;    %Peak residual torque Dmr" = Dmr/(Fz*R0)
QDZ7 = 0.0;       %Variation of peak factor Dmr" with load
QDZ8 = -0.296;    %Variation of peak factor Dmr" with camber
QDZ9 = -0.009;    %Variation of peak factor Dmr" with camber and load
QEZ1 = -1.609;    %Trail curvature Ept at Fznom
QEZ2 = -0.359;    %Variation of curvature Ept with load
QEZ3 = 0;         %Variation of curvature Ept with load squared
QEZ4 = 0.174;     %Variation of curvature Ept with sign of Alpha-t
QEZ5 = -0.896;    %Variation of Ept with camber and sign Alpha-t
QHZ1 = 0.007;     %Trail horizontal shift Sht at Fznom
QHZ2 = -0.002;    %Variation of shift Sht with load
QHZ3 = 0.147;     %Variation of shift Sht with camber
QHZ4 = 0.004;     %Variation of shift Sht with camber and load
SSZ1 = 0.043;     %Nominal value of s/R0: effect of Fx on Mz
SSZ2 = 0.001;     %Variation of distance s/R0 with Fy/Fznom
SSZ3 = 0.731;     %Variation of distance s/R0 with camber
SSZ4 = -0.238;    %Variation of distance s/R0 with load and camber
Ro   = 0.313;     %unloaded tyre radius Free tyre radius

%%%Scale Factors%%%

LFZO = 1;         %Scale factor of nominal (rated) load
LCX  = 1;         %Scale factor of Fx shape factor
LMUX = MU;        %Scale factor of Fx peak friction coefficient
LEX  = 1;         %Scale factor of Fx curvature factor
LKX  = 1;         %Scale factor of Fx slip stiffness
LHX  = 1;         %Scale factor of Fx horizontal shift
LVX  = 1;         %Scale factor of Fx vertical shift
LGAX = 1;         %Scale factor of camber for Fx
LCY  = 1;         %Scale factor of Fy shape factor
LMUY = MU;        %Scale factor of Fy peak friction coefficient
LEY  = 1;         %Scale factor of Fy curvature factor
LKY  = 1;         %Scale factor of Fy cornering stiffness
LHY  = 1;         %Scale factor of Fy horizontal shift
LVY  = 1;         %Scale factor of Fy vertical shift
LGAY = 1;         %Scale factor of camber for Fy
LTR  = 1;         %Scale factor of Peak of pneumatic trail
LRES = 1;         %Scale factor for offset of residual torque
LGAZ = 1;         %Scale factor of camber for Mz
LXAL = 1;         %Scale factor of alpha influence on Fx
```

b

Peter Samuel Delves

Appendix 1 Pacejka Tyre Model Parameters

```
LYKA = 1;          %Scale factor of alpha influence on Fx
LVYKA= 1;          %Scale factor of kappa induced Fy
LS   = 1;          %Scale factor of Moment arm of Fx
LSGKP= 1;          %Scale factor of Relaxation length of Fx
LSGAL= 1;          %Scale factor of Relaxation length of Fy
LGYR = 1;          %Scale factor of gyroscopic torque
LMX  = 1;          %Scale factor of overturning couple
LVMX = 1;          %Scale factor of Mx vertical shift
LMY  = 1;          %Scale factor of rolling resistance torque

Fzo  =4000;        %Vertical test load
```

c

Peter Samuel Delves

Appendix 2: Chapter Three Vehicle Parameters

```
%Parameters from Milehins et al. 2010
m   = 1669;             %Vehicle Total mass            (kg)
mb  = 1475;             %Vehicle body mass             (kg)
mf  = 140;              %Front unsprung mass           (kg)
mr  = 100;              %Rear unsprung mass            (kg)
Izz = 3144;             %Vehicle Yaw inertia           (kgm^2)
Ixx = 835.2;            %Vehicle Roll inertia          (kgm^2)
a   = 1.178;            %Distance from CG to front axle (m)
b   = 1.567;            %Distance from CG to rear axle  (m)
l   = a + b;            %Total length of vehicle       (m)
Ixz = 0;               %Vehicle Yaw/roll inertia       (kgm^2)
Iw  = 1.1;              %Spin inertia of wheel          (kgm^2)
Rr  = 0.303;            %Wheel radius                   (m)
Cf  = 59410*2;          %Front tyre stiffness          (N/rad)
Cr  = 50730*2;          %Rear tyre stiffness           (N/rad)
t   = 1.505;            %Track width                    (m)
hcg = 0.52;             %Centre of gravity height       (m)
hr  = 0.483;            %Roll centre height             (m)
kr  = 45187.5;          %Roll stiffness                (Nm/rad)
cr  = 4417;             %Roll damping                   (Nm/(rad/s))
MU  =0.7;               %Co-efficient of friction
g   =9.81;              %Gravity constant               (m/s^2)

%Drag peramiters
Roa =1.23;              %Air density                    (kg/m^3)
Cd  =0.3;               %Drag Co-efficient
S   =2.17;              %Vehicle frontal area           (m^2)

%Calculation of vertical tyre loads
Fzr = (((m/l)*a)*g)/2; %Load on each front tyre        (kg)
Fzf = (((m/l)*b)*g)/2; %Load on each rear tyre         (kg)
```

d

Appendix 3: Chapters Four & Five Vehicle Parameters

```
%Parameters from Kim and Peng 2012
m   = 2450;            %Vehicle Total mass            (kg)
mb  = 2210;            %Vehicle body mass             (kg)
mf  = 140;             %Front unsprung mass           (kg)
mr  = 100;             %Rear unsprung mass            (kg)
Izz = 4946;            %Vehicle Yaw inertia           (kgm^2)
Ixx = 1597;            %Vehicle Roll inertia          (kgm^2)
a   = 1.105;           %Distance from CG to front axle (m)
b   = 1.745;           %Distance from CG to rear axle  (m)
l   = a + b;           %Total length of vehicle       (m)
Ixz = 40;              %Vehicle Yaw/roll inertia      (kgm^2)
Iw  = 1.1;             %Spin inertia of wheel         (kgm^2)
Rr  = 0.303;           %Wheel radius                  (m)
t   = 1.505;           %Track width                   (m)
hcg = 0.66;            %Centre of gravity height      (m)
hr  = 0.40;            %Roll centre height            (m)
kr  = 94000;           %Roll stiffness                (Nm/rad)
cr  = 8000;            %Roll damping                  (Nm/(rad/s))
MU  = 0.7;             %Co-efficient of friction
g   = 9.81;            %Gravity constant              (m/s^2)

%Drag peramiters
Roa =1.225;            %Air density                   (kg/m^3)
Cd  =0.3;              %Drag Co-efficient
S   =2.17;             %Vehicle frontal area          (m^2)

%Calculation of vertical tyre loads
Fzr = (((m/l)*a)*g)/2; %Load on each front tyre       (kg)
Fzf = (((m/l)*b)*g)/2; %Load on each rear tyre        (kg)
```

e

Appendix 4: Full 8-DOF Simulink Model

Peter Samuel Delves